UNIVERSITÀ DEGLI STUDI DI ROMA "TOR VERGATA"

FACOLTA' DI INGEGNERIA

DOTTORATO DI RICERCA IN
SISTEMI E TECNOLOGIE PER LO SPAZIO

XXII CICLO

A GLOVE-BASED SYSTEM EQUIPPED WITH HOME-MADE PIEZORESISTIVE BEND SENSORS

GIUSEPPE LATESSA

A.A. 2008/2009

Docenti Guida:

Dr. Giovanni Saggio

Dr. Andrea Reale

Dr.ssa Francesca Brunetti

Coordinatore: Prof. Giancarlo Cardarilli

A MAMMA E PAPA'.
Grazie per avermi insegnato
il rispetto, la dignità, l'amicizia, l'amore.
Grazie per avermi donato il senso del dovere.
Grazie per avermi fatto capire che una vita
senza obiettivi è una vita vuota.

Abstract

In the last three decades, after the first discovery of conductive polymers made by Shirakawa et al.[1], a great deal of interest has been devoted to the use of those materials because of their flexibility, the low cost processability, the light weight, the easiness of tailoring their properties in order to obtain the needed characteristics.

There are different types of conductive polymers, such as polyacetylene, polypyrrole, polythiophene, polyphenylene, polyaniline, etc. Polythiophenes, in particular, represent an important class of conducting polymers due to their solubility, processability, and environmental stability, beside possessing excellent electrical conductivity, electroluminescent property, and non-linear optical activity.

This activity is based on the Poly(3,4-ethylenedioxythiophene)/Poly (Sodium 4-Styrene Sulphonate) (PEDOT:PSS) that shows high conductivity, transparency and possesses great environmental stability [2]. PEDOT:PSS have been used successfully in different types of applications, including various types of sensors.

This work is focused on the realization of piezoresistive sensor based on PEDOT:PSS. These devices change their electrical resistance when they are bent. The substrate is totally flexible, low cost, customizable, based on Poly (Trimellitic-

anhydride-chloride copolymerized with 4,4-methylenedianiline) in *N*-methylpyrrolidone.

An ad-hoc measurement was realized in order to obtain an electrical resistance sensor measure. The idea is to replicate as really as possible the human finger flexion/extension movements. The set-up consists of three hinges controlled by three step-by-step motor to measure an array up to three different sensors. All the system is remotely controlled by Labview NI Interface and the resistive response of the sensor is read by a 5.5 digits 34405A Agilent digital multimeter.

Among several possibilities to adopt these sensor, my first aim is a glove-based system realization. An instrumented-glove (called *Hiteg Glove*) is the ensemble of mechanical to electrical transducers, a support (usually Lycra based), conditioning electronics plus power supply, transmission system, all useful to measure the 23 degree of freedom [3] of finger joint movements. Thanks to their lightness, cheapness and the fact that I experienced a novel way of their application which, the bend sensors was utilized ad transducers. Each sensor was mounted on the glove in correspondence of one human hand joint so to permit the flexion/extension movements registering. Moreover ad-hoc projected sensors were utilized for the abduction/adduction movements.

The last step of this works provides to realize a 3D Virtual Model of the glove. The basic model of the virtual hand was realized starting from *Blender*, which is an open source multiplatform software for 3D graphical applications. It has a robust feature set and has the interesting capabilities of texturing, skinning, animating, rendering. Virtual Hand permits a real-time replay of the hand movements obtained with the glove.

The instrumental glove including virtual reality represents a lot of opportunity for several significant fields: social, as sign language recognition and as alternative support to actual general purpose pc input devices; medical, for functional analysis, for rehabilitation follow up on patients with damaged upper/lower limbs and for medical staff training; working, for staff training in dangerous conditions or gesture recognition; sport, in order to recording movement and posture monitoring during activity or effect of external parameters evaluation on physical performances; entertainment, as games, multimedia or music.

Contents

Chapter 1

Home-made Piezoresistive Bent Sensors

1. 1 Introduction

Human motion capture suggested several developed systems based on different physical principles, such as optic [4], magnetic [5], pneumatic [6], mechanic [7], electric [8], and so on. In this work, I focused my attention on the realization of piezoresistive bent sensors because they show several advantages first of all the cost.

The sensors are realized in PEDOT:PSS using a low cost technique [9]. The substrate is totally flexible, low cost, customizable, based on Poly (Trimellitic-anhydride-chloride copolymerized with 4,4-methylenedianiline) in *N*-methylpyrrolidone. When the substrate is bent towards the printed side (outward bend) the resistive part increases its resistance value, while in opposed mode ths electrical resistance goes down at the same entity.

The use of PEDOT:PSS ranges from antistatic coating applications (cathode ray tube screens, electronic packaging, photographic films, LCD polarizers), electronic and optoelectronic applications (all organic field effect transistors, organic light emitting diodes, capacitors, photovoltaic, photodetectors), sensors. In particular, in the field of sensors, it has been demonstrated the use of this material in artificial noses [10], in humidity and glucose sensors [11] and in strain sensors realized with coated fibers and fabrics [12]. Usually this polymer that is insoluble, is available in its oxidized form in combination with a water soluble polymer, the polystyrene sulfonic acid (PSS).

The introduction of PSS in the polymerization process has two main benefits: on one side it balances the cationic charge of PEDOT, on the other side it allows the dispersion of the PEDOT in water generating a complex where the oligomeric PEDOT segments are attached to the long chains of the PSS.

In order to improve the sensors performances, Carbon NanoTubes (CNTs) were added into polymeric solution. Most of the interest about this material is due to their really exciting properties: they have both a high electrical and thermal conductivity, they show a ballistic conduction behavior on their axis, they can be either semiconductor or metallic, they are extremely mechanically strong, their dimension scale down to diameters of around 1nm, they are good field emitters.

So I obtained low-cost devices to track human fingers movements. They are flexible, light, customizable, repeatable and usable for an array of significant applications.

1.2 Sample preparation

Figure

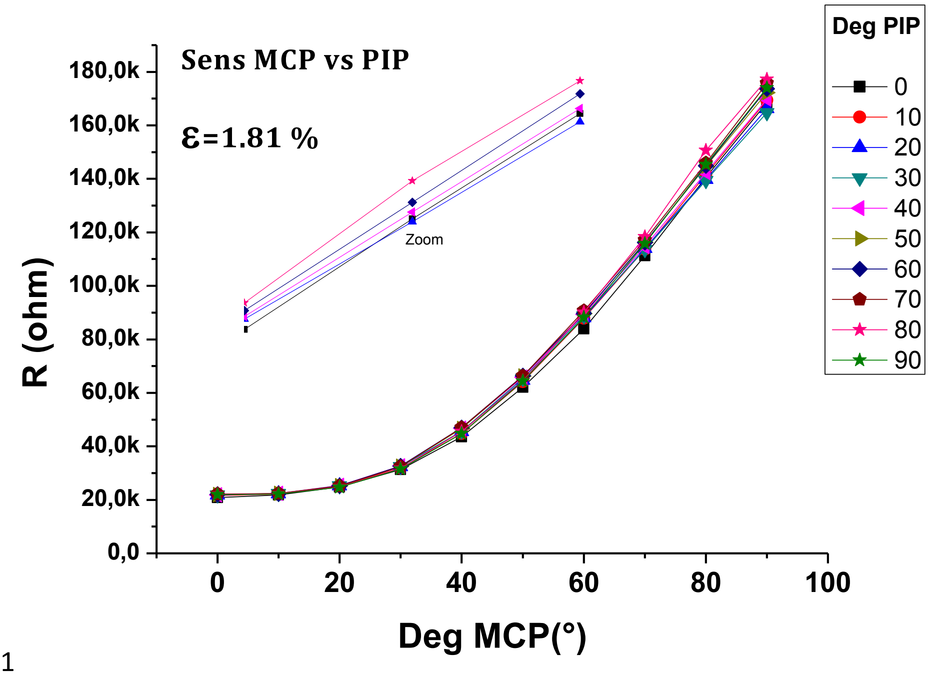

1

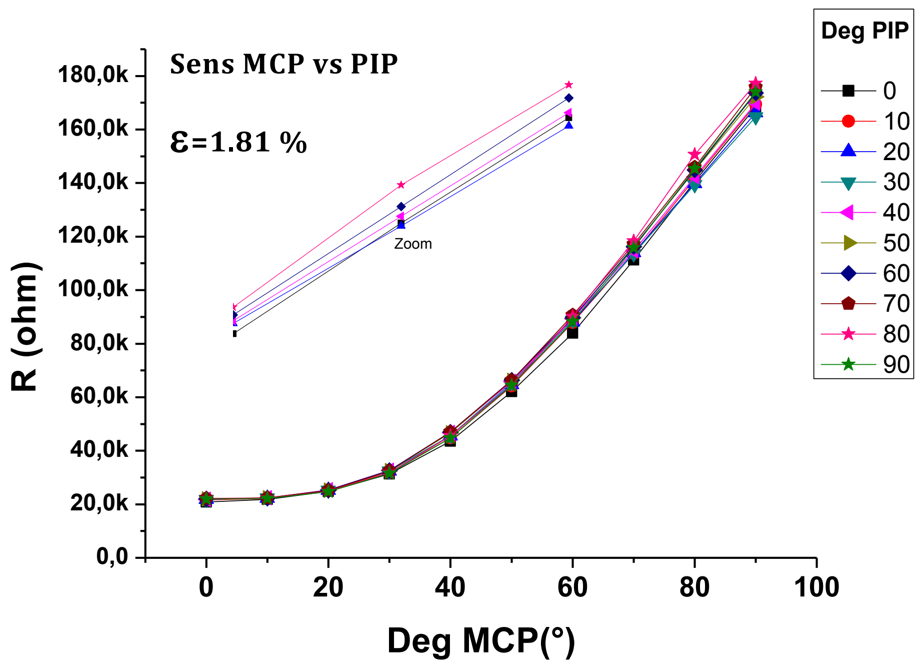

shows the fabrication process for the realization of the flexible piezoresistive sensor, starting from a silicon/silicon oxide wafer. The device is initially made on a rigid substrate and then the piezoresistive film is transferred on a plastic one.

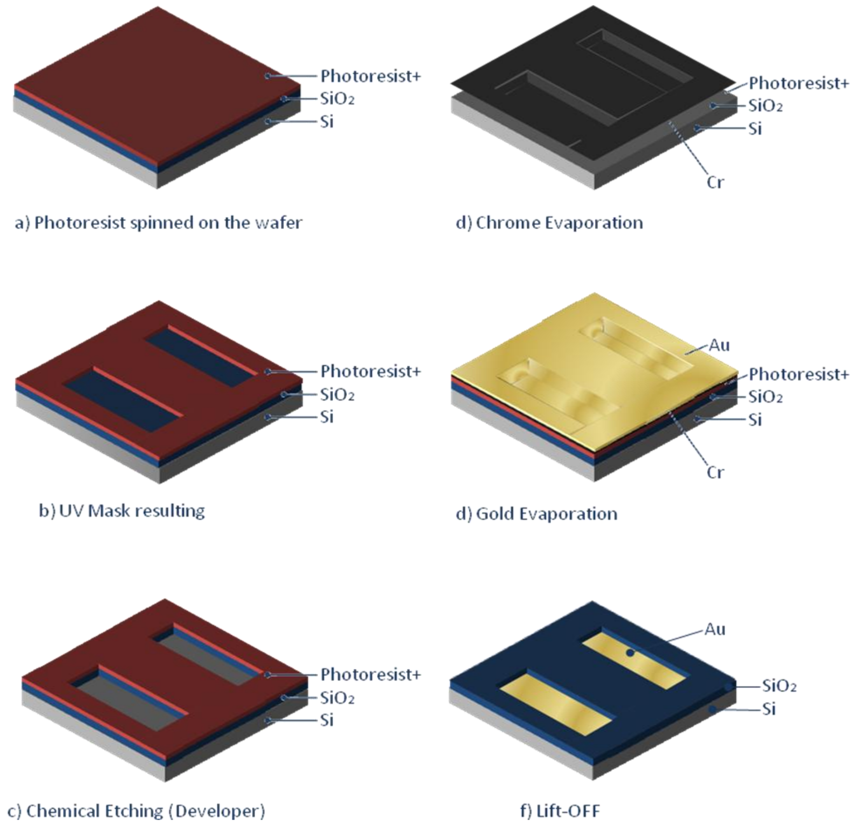

Figure 1. *Standard lithography process for the growth of the piezoresistive film on conductive material*

1.2.1 Photolithography

The fabrication starts with a 2 in. highly doped p+ silicon wafer (500 μm thick) covered with a 250nm of thermal grown silicon oxide. A pattern with lines of 2cm * 1cm dimension is defined on top of the oxide using a standard lithography process.

A photoresist changes its property when it is exposed at the light. The used photo-material, the AZ5214, was deposed with a spin coating technique. The result is a perfectly homogeneous red layer. The UV exposition permits to remove the not wanted areas and to define the sensor shape. The procedure is reported in the next Figure 2.

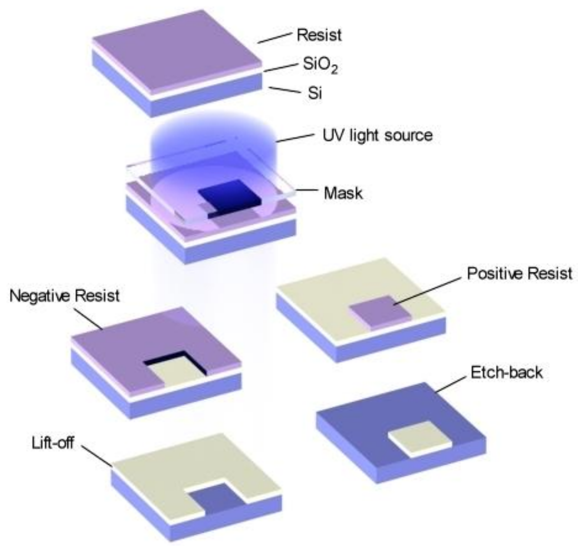

Figure 2. *Mask design is transferred on the pattern using a positive/negative photoresist material*

A typical device measures about 2cm * 1 cm, but the dimensions are customizable up to 5cm * 5cm. Among the three principal exposition techniques (contact, proximity, projection), the proximity choice was taken, for the simplicity adding to the minor risk to break the pattern and to low costs. The space between mask and sample is about tenth of micron, while the final thickness resolution is less of 10 µm.

An ad-hoc developer was used to remove the red layer where the light didn't touch the pattern. Afterwards, a wet etching in a buffered hydrofluoric acid solution (HF+NH4+water) is performed in order to remove the oxide and expose the contact areas.

In the next step, a 10 nm layer of chromium and 90nm gold are evaporated and subsequently lifted-off. The resulting patterned electrode represents the template that can be used for the realization of the piezoresistive sensors. The Figure 3 shows two sample representations with a top view of the Au pads.

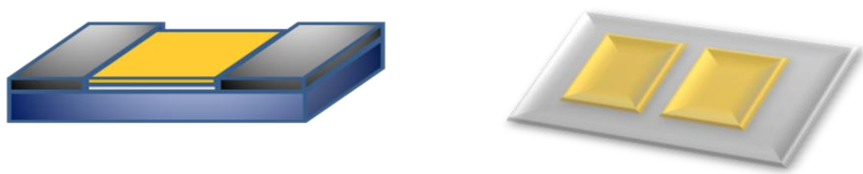

Figure 3. *Chrome/gold contacts.*

1.2.2 Polymeric Organic Composites

A composite can be defined as the material created when two or more distinct components are combined. A composite material can provide superior and unique mechanical, electrical and physical properties because, with its preparation, we try to combine the most desiderable properties of its constituents while trying to suppress their least desiderable ones. In this contest, the possibility of combining the properties of organic and inorganic compounds in an unique material is an old challenge for the materials science researchers. Moreover, the possibility to prepare systems made of dissimilar components mixed at the nanometer scale has recently produced significant efforts to investigate innovative synthetic approaches for the preparation of such a kind of materials, called "nanocomposites", feeding the possibility to have new properties which can result even unknown in the parent constituent materials.

The goal is to improve the mechanical, thermal and electrical properties but especially to create a material which could be more easily processed from a technological application's point of view and which could have a more controlled manufacturing cost.

Since the amazing discovery of highly conducting polyacetylene marking the birth of a new field and resulting in the award of the Nobel Prize for chemistry in 2000 [1], very diverse applications of organic conductive polymers have emerged owing to their remarkable electronic and photonic properties.

There are different types of conductive polymers, such as polyacetylene, polypyrrole, polythiophene, polyphenylene, polyaniline, etc. Among these types, polypyrrole and polythiophene and their derivatives show conductivities that are stable at room temperature and above for years 117[13]117. Polythiophenes, in particular, represent an important class of conducting polymers due to their solubility, processability, and environmental stability, beside possessing excellent electrical conductivity, electroluminescent property, and non-linear optical activity [14].

In the next Figure 4 it's showed a graphical representation of a thiophen molecule.

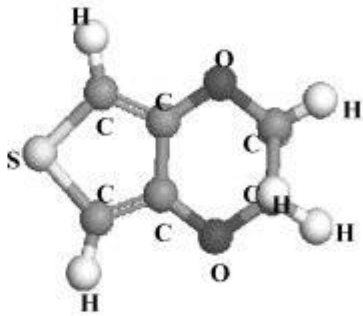

Figure 4. *Graphical representation of tiophen molecule*

1.2.3 Electrochemical Polymerization Synthesis

The PEDOT:PSS polymer matrix is deposited on the patterned electrode by electrochemical polymerization [15]. This is a known procedure that permits to obtain a polymer starting by precursor monomers.

The electropolymerization is carried out at a constant potential of 3V (versus Ag/AgCl reference electrode). The polymer grows only in the conductive areas where the metallic films were deposited (gold areas); this gives the possibility of realizing sensors of different shapes and aspect ratio in order to optimize their piezoresistive response.

The solution was realized using the monomer EDOT as received from Bayer AG and poly(sodium 4-styrene sulfonate) (NaPSS, average Mw 1,000,000); a mixture of acetonitrile and distilled water (solution 1:1 v/v%) was used as a solvent. The deposition of the PEDOT:PSS was carried out using the chronoamperometry; the concentration of EDOT was 0.1M and the NaPSS concentration was 0.02M. Platinum is used as the counter electrode.

The chemical representation of the resulted polymer is reported in the next Figure 5. The negative charges are delocalized along the macro-molecule and so the internal current is established thanks to these free electrons.

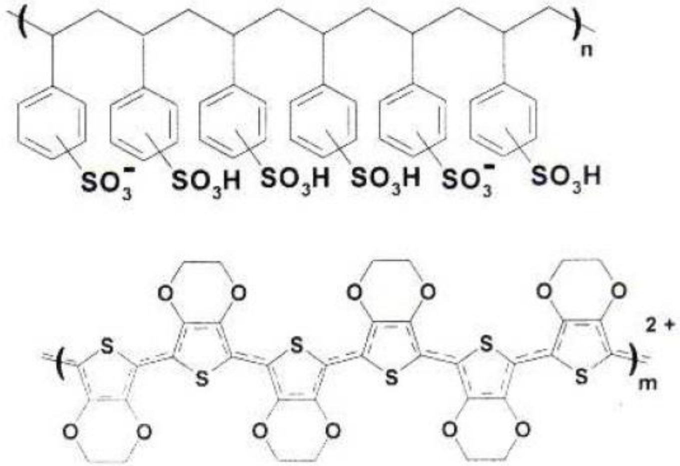

Figure 5. *Pedot:PSS in the chemical representation*

As a first advantage, PEDOT is an enviromentally "friendly" system, that is in the synthesis process are not formed oncogene derivatives. Moreover, using water-soluble polyelectrolite [poly(styrene sulfonic salt (PSS)] as the charge-balancing dopant, there are good possibility to obtain a water-soluble system with good film-forming properties, high conductivity (~10 S/cm), high visible light transmissivity and excellent stability. Conducting PEDOT films are currently being investigated for use as antistatic material, supercapacitors, electrochromic devices and biosensors.

1.2.4 Flexible Substrate

The patterned electrodes are finally transferred to a polyimide support. This support can be obtained depositing a solution of a poly(trimellitic-anhydride-chloride copolymerized with 4,4- methylenedianiline) in *N*-methylpyrrolidone onto the anode. It is possible to use both a casting technique that allows us to obtain substrates with a thickness of about 500 μm and a spin coating technique that allows us to obtain a substrate ranging from 100 μm to 300 μm. In our case we spin coated the solution at 1000 rpm.

After curing at 130 ∘C for 90 min, a flexible and tough polyamide film with 100 μm thickness is peeled off from the anode surface. The spin coating process can be tailored to obtain the desired thickness of the flexible substrate. Different thicknesses can be used for specific ranges of sample elongation.

A four part representation for the realized substrate is reported in the Figure 6.

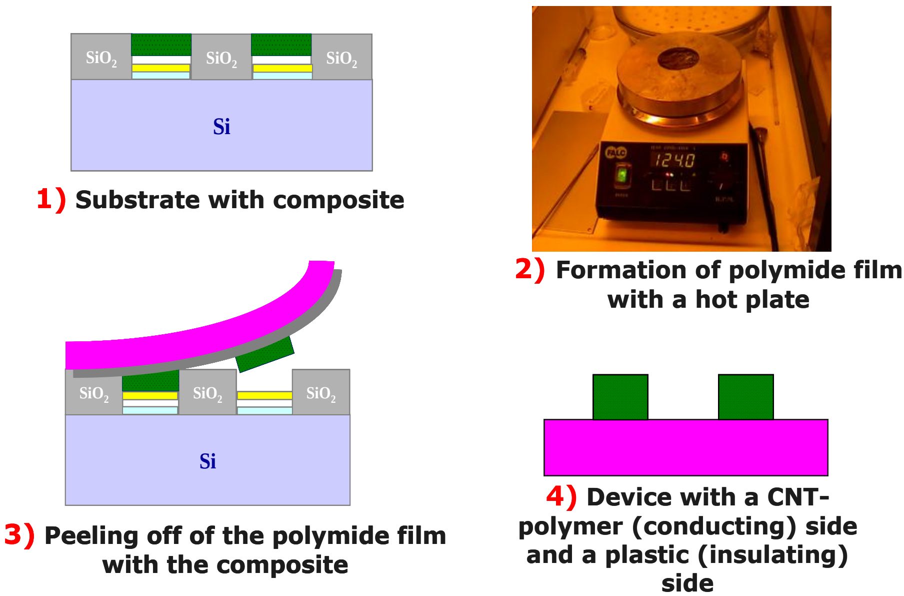

Figure 6. *Principal steps in the realization of the flexible sensor.*

The obtained flexible sensor is shown in Figure 7 , the PEDOT:PSS film is represented by the black pattern.

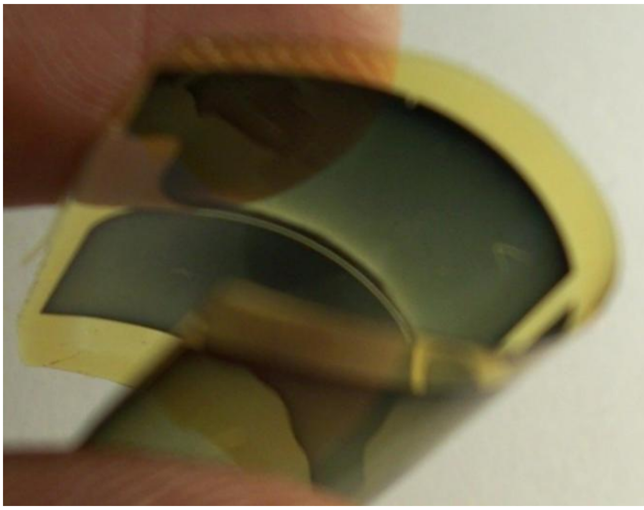

Figure 7. *The realized flexible piezoresistive sensor*

1.3 CNTs Based Sensors

Carbon nanotubes (CNTs) were discovered accidentally by Suijo Iijima in 1991 observing with a TEM a sample of synthesized fullerenes. The nanotubes consisted of up to several tens of graphitic shells (so-called multi-walled carbon nanotubes (MWNTs)) with adjacent shell separation of ~0.34 nm, diameters of ~1 nm and large length/diameter ratio. Their peculiar properties have obtained them the rank on new allotrophic form of the carbon, after graphite, diamond and the fullerenes.

The main reason for the really fast popularity of the CNTs is their unique properties:

- they are mechanically very strong, with a high Young modulus and a high aspect ratio;
- they have interesting conducting properties, behaving either as metals or as semiconductors and also showing ballistic conduction on their axis;
- they show a significant thermal conductivity;
- a lot of factors like chemical species adsorption, mechanical deformation and magnetic fields can cause detectable changes in their resistivity or band gaps, affecting the conductance of CNTs and providing very good sensing properties.

The extreme versatility of CNTs and their enormous mechanical, electrical, thermal and chemical properties made this material very interesting in the development of a new class of electronic devices.

1.3.1 CNTs Structure

Carbon nanotubes are tube-like structures obtained synthetically in non thermodynamic equilibrium conditions as a result of a special arrangement of carbon atoms.

There are two main types of carbon nanotubes: single wall carbon nanotubes (SWNTs, Figure 8) consist of a single graphite sheet seamless wrapped into a cylindrical tube. Multiwalled nanotubes (MWNTs, Figure 9) comprise an array of such nanotubes that are concentrically nested like rings of a tree trunk.

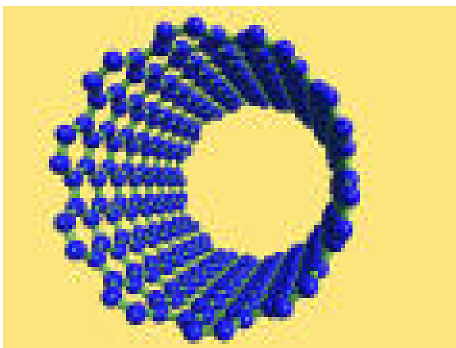

Figure 8 *Transversal section of an opened SWNT*

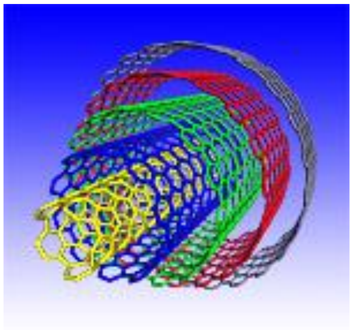

Figure 9. ***Transversal section of a MWNT***

The cylinder are made of hexagonal rings and are closed at both ends with two hemispheric surfaces containing also pentagonal rings, usually half fullerene molecules. Real nanotubes present many structural defects in the structure, like octagonal or pentagonal rings on the surface. The diameters of SWNTs vary in a range between a minimum corresponding to the double of the interplanar distance of the graphite (~0,7 nm) to a maximum of 10 nm. Due to the high ratio between length and diameter they can be considered mono-dimensional structures. It's however very difficult to obtain a single tube, since they usually tend to bond in bundles, usually of 10-20 units.

Every SWNT is characterized from its diameter and from its roll-up vector r that represents the direction of rolling the graphite on the axis of the nanotube. This roll-up vector, also called chiral vector, can be defined as a linear combination of base vectors a_1 and a_2 of the basic hexagon:

$$r = na_1 + ma_2$$

with m, n integers. The vector is orthogonal to the axis of the tube. Different kinds of nanotubes are defined by the vales of m and n, and it is possible to distinguish three major categories:

- m = n, armchair
- m = 0 or n = 0, zig-zag
- any other m or n, chiral

1.3.2 PEDOT: PSS/CNTs based Sensors

Because all of their excellent properties, I tried to utilized carbon nanotubes as piezorestive material. So about 5 mg of CNTs was added in the presented solution of Edot/Pss (see 1.2.3).

The polymerization voltage was the same (about 3 volts) and the same are the organic material solutions. The CNTs are furnished by Chemical Department of "Tor Vergata" University in Rome. CNTs were inserted in ultrasonic bath for several hours first of their utilization.

The presented result are obtained thanks to the microscopic setup. An insulting tip permits to strain the samples, in order to obtain a microscopic deformation; the tip is controlled by a waveform generator. One volt correspond to 8 μm of strain (***Δ***Vpiezo).

The next reported graphic permits to obtain an analysis between a typical PEDOT:PSS sensor (Figure 10) and a selected PEDOT/PSS/CNTs based sensor (Figure 11). The carbon nanotubes sensor show an improvement of the performances in terms of piezoresistivity. In opposite, the CNTs based sensors are difficulty reproducible because it's very complex to obtain a perfect dispersion of the tubes in the polymeric matrix.

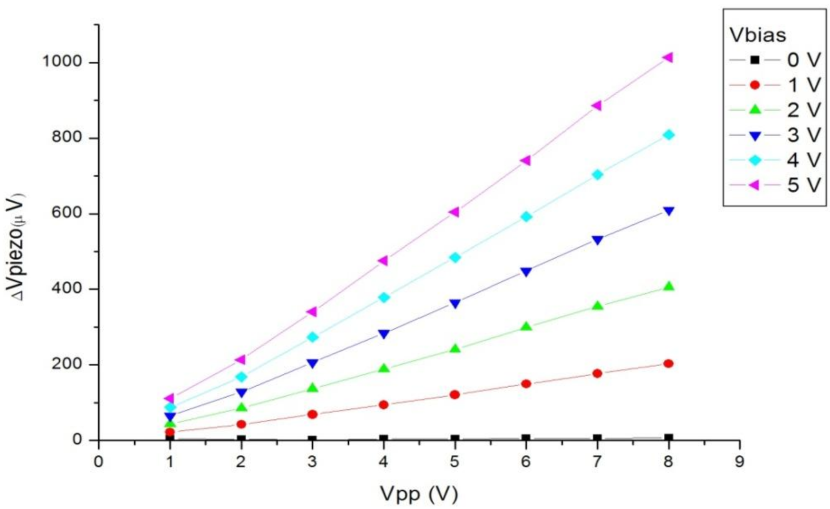

Figure 10. *Piezoresistive response of a Pedot:PSS sensor vs the applied strain*

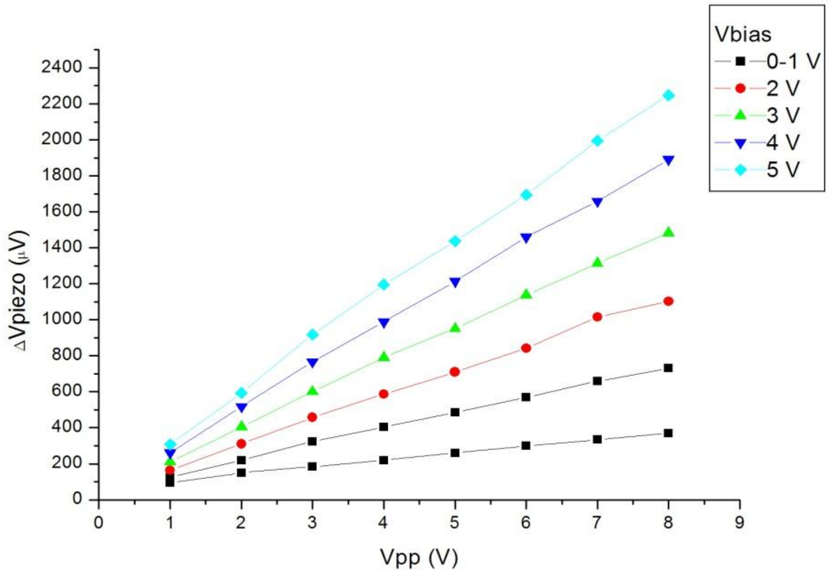

Figure 11. *Piezoresistive response of a Pedot:PS/CNTs sensor vs the applied strain*

1.4 Organic Thin Film Transistors (OTFTs)

OTFTs were realized with two principal aims: flexible transistors as strain sensors and on the other side devices for sensor signal amplification.

The typical structure is based on pentacene as semiconductor material and Poly(vinyl-alcool) (PV-OH) as dielectric material. Pentacene is obtained thanks to an evaporation technique, while the insulting layer is spinning with coater. Source, drain and gate contacts are realized in PEDOT:PSS. The substrate is composed by Poly (Trimellitic Anhydride Chloride – CO 4,4' –Methylene Dieniline)) (PMMA). The device is totally flexible.

The used transistor is 1cm * 0.75 cm and it is built in an array as in Figure 12.

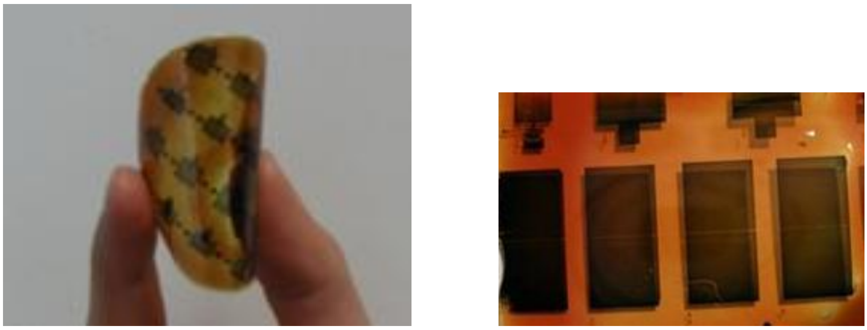

Figure 12 *Realized OTFTS in different views*

The output properties were obtained for a V_{DS} from 0V to -45V and for a V_{GS} from 3V to -9V. The measured I_{DMAX} is about -20 μA.

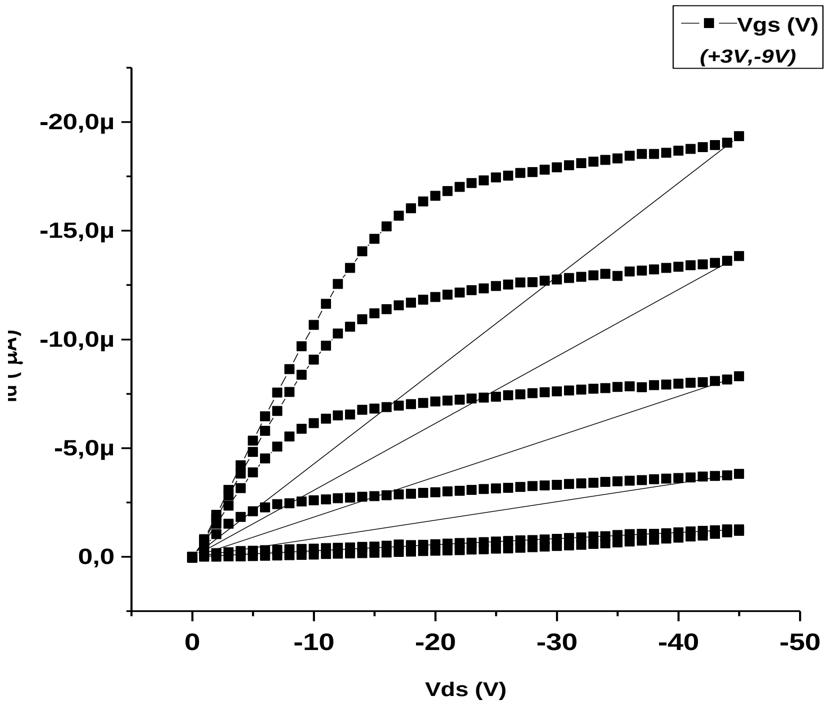

Figure 13. *OTFT output characteristics at the end of the process*

Lifetime is about 3 months. In the Figure 14 it's reported the output properties after 1 month and it shows that the drain current is decreased. This effect is more evident after 3 months, as in Figure 15.

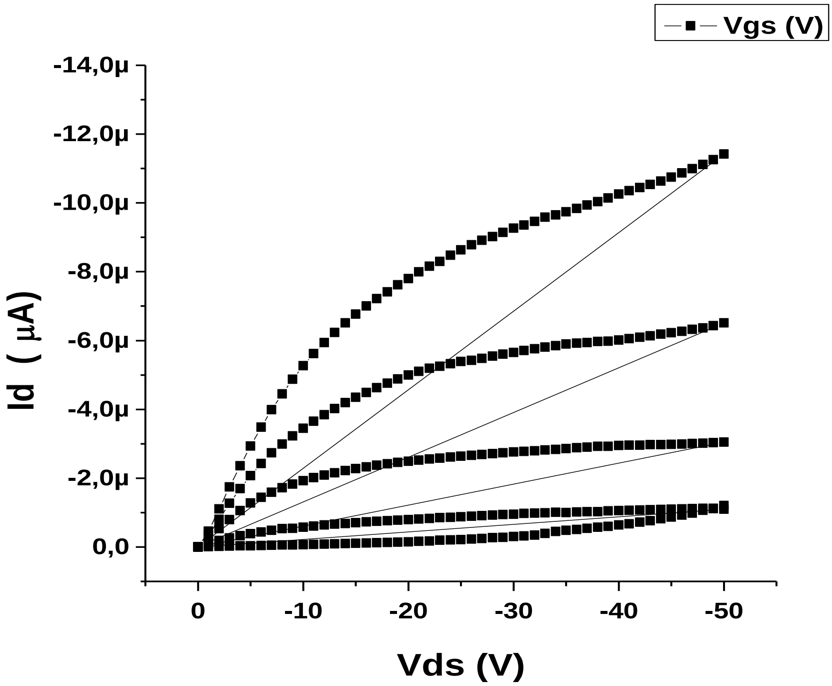

Figure 14 *OTFT output characteristics after 2 months*

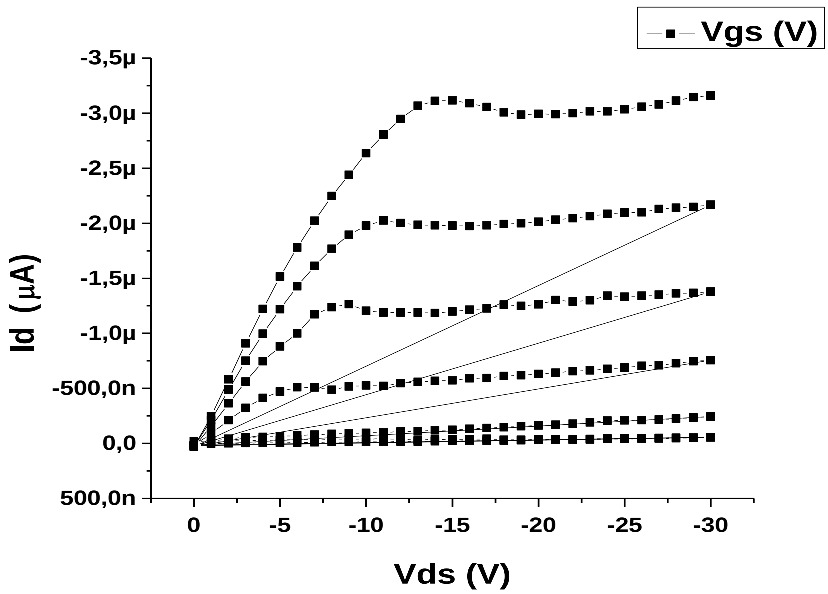

Figure 15. *OTFT output characteristics after 3 months*

Chapter 2

Instrumental Measurement Setup

2.1 Introduction

A sensor is any electronic device able to convert a measurable quantity (physical, chemical, biological) in an electronic signal. In the case of deformation sensors, the electrical quantity involved is the electrical resistance: strain sensors are sensing devices that change their resistance value when stretched or compressed. Strain is a dimensionless unit, defined as a change in length for unity length [16]. Strain sensors are typically bonded to the surface of a solid material to measure its minute dimensional changes when put into compression or tension:

one such device is called strain gauge (SG). Strain gauges and their underlying principles are often used in devices for measuring acceleration, pressure, tension, and force. To evaluate the performance of such a device, it is used the gauge factor, defined as the fractional change in resistance due to the deformation divided by the strain.

In this step, it’s reported the description about two ad-hoc setups: microscopic and macroscopic measurements. The first setup is based on an insulating tip for strain the sensors and it is possible to apply both a static and a dynamic deformation controlled by a piezoelectric actuator.

Macroscopic setup is composed by an hinge mounted on a stepper motor; the applied strain is a bending deformation, in order to replicate the human fingers movements.

For each measurement system an opportune mechanical model was developed. So two different Gauge Factors are obtained so to obtain the sensor sensitivity and establish the sensor performances.

2.2 Gauge Factor (GF)

GF is the electrical quantity involved in strain detection measurements is the resistance. Therefore the device used should be ohmic to achieve the best performance, i.e. it should follow the first Ohm’s law:

$$V = R * I$$

where V is the bias across the device, I is the current flowing in it and R is the resistance. The law states that the ratio between these two quantities is not dependent on them: for such a device, we can be sure that any change in resistance is not due to any electrical modulation.

Resistance is a property of a whole device. Concerning the microscopic effect of the carrier conduction ant its scaling at macroscopic dimensions, the second Ohm’s law states that the overall resistance of a material depends from its intrinsic resistivity ϱ (which describes the scattering the electrons undergo in the material) and its geometrical dimensions (length l and section S) according to the following relation:

R = (ϱ * l)/ S

The fractional change of the resistance is thus depending on these three parameters. By differentiation, we obtain:

$$\frac{DR}{R} = \frac{Dr}{r} + \frac{DL}{L} - \frac{DS}{S}$$

ΔL/L is the axial deformation, called axial strain and it is usually identified with ε; ΔS/S is the strain along the other two orthogonal dimensions, which both are related to ε by the Poisson coefficient ν (Δy/y = Δz/z = - νε) [87]. Gathering together ΔL/L and ΔS/S, we obtain that the fractional change of the resistance is due to both an intrinsic and a geometrical factor:

$$\frac{dR}{R} = \frac{dr}{r} + e + 2ne = \frac{dr}{r} + e(1 + 2n) \quad \textit{(intrinsic factor + geometrical factor)}$$

Eq 1

The sensitivity of the resistance change with respect to the applied strain is thus:

$S_{R\text{-}\varepsilon} = \Delta R / \varepsilon$ **Eq 2**

To evaluate the performance of a strain sensor, it is used to define the Gauge Factor as the ratio between the electrical measurable response (the resistance fractional change) and the mechanical interesting quantity (the axial strain) which induces the change of resistance:

$$GF = \frac{DR}{R}\frac{L}{DL} \qquad GF = \frac{1}{e}\frac{DR}{R} = \frac{1}{e}\frac{Dr}{r} + (1 + 2n)$$

Eq 3

A high gauge factor is desirable because it indicates a larger change in resistance for a given strain and it is easier to measure: in this sense, GF represents how large is the response of a given sensor [17].

For most of the metals, no resistivity changes under deformation are observed (the intrinsic factor is equal to zero) and ν is about 0.5 (no volume changes under deformation), so they have a GF of 2: their strain sensitivity depends only on the geometrical dimensions, so they are built in a patterned way in order to achieve the higher possible length; for some special alloys and carbon gauges, the GF may be as large as 10. On the other hand, metals are perfectly ohmic, so they provide a linear response on all the range: the usual commercial strain gauge are metallic ones.

In the case of a semiconductor, the resistivity also changes with strain, along with the physical dimensions. This is due to changes in electron and hole mobility with changes in crystal structure as strain is applied. The net result is a much larger gauge factor than is possible with metal gauges. The value of the semiconductor gauge factor varies between -50 and -200. The resistance can be change nonlinear with respect to strain. To use the semiconductor strain gauge to measure strain, we must have a curve or table of values of gauge factor versus resistance: usually, they cover a deformation range much narrower than the metallic ones, and thus they are very specific.

2.3 Microscopic Measurement Setup

To induce mechanical deformation on the sample in a controlled way, we built up a sample holder placed on an optical bench: the sample can be suspended between two aluminum plates at different distances, and deformed by an insulating tip. Three axial and one angular micropositioners are used to place the tip orthogonally to the axis of the sample and directly above the centre of its span, as you see in Figure 16. The tip is pulled up and down by a piezoelectric ceramic controlled by a voltage amplifier: the force applied by the tip is proportional to a voltage control signal V_{pp}. 1V of modulation via V_{pp} corresponds to an elongation of 8 μm of the tip: in this way it is possible to control the deformation induced on the samples.

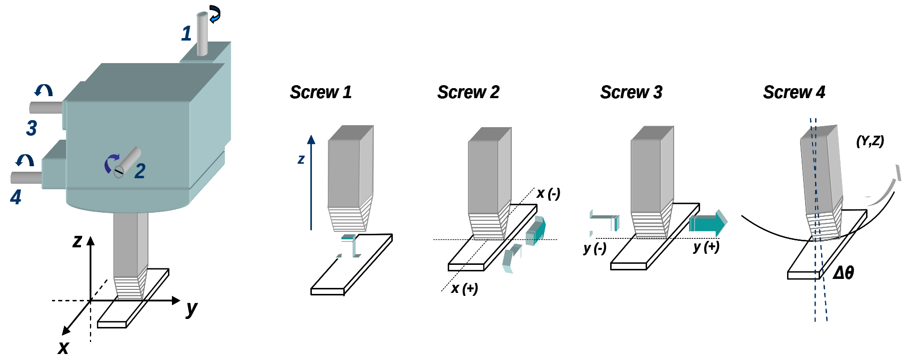

Figure 16. *Three axial and one angular micropositioners*

The microscopic setup is shown in Figure 17. The DUT (Device Under Test) is deformed by an insulating tip. It is possible to apply both a static and a dynamic deformation controlled by a piezoelectric actuator (Physyk Instrument) acting on the sample [18]. The piezo actuator through an insulating rigid tip applies a vertical force at the centre of the flexible film proportionally to a control voltage. Even if the piezo actuator is provided with a feedback monitor signal, the effective displacement can be known only after setup calibration.

The setup allows the detection of the piezoresistive signal through coherent detection techniques to guarantee a better noise control via a lock-in amplifier, by modulation of the control voltage of the actuator, i. e. modulation of the displacement induced at the contact point on the sample. Cautions must be taken while choosing modulation frequency in order to do not occur into low-pass behaviour of the piezoelectric actuator. Such behaviour becomes more and more evident while increasing the resistance load to which the actuator is applied. The experimental data indicate that the deformation of the polymeric films increases the resistance. This effect, for the considered deformation range, is additive (further deformation produces further increase of the resistance) and reversible, meaning that no plastic changes are involved in this process.

The deformation induces a variation of a resistance that is evaluated measuring the bias of a Wheatstone bridge formed by the sample itself, a reference sample, a trimmer and a fixed resistance.

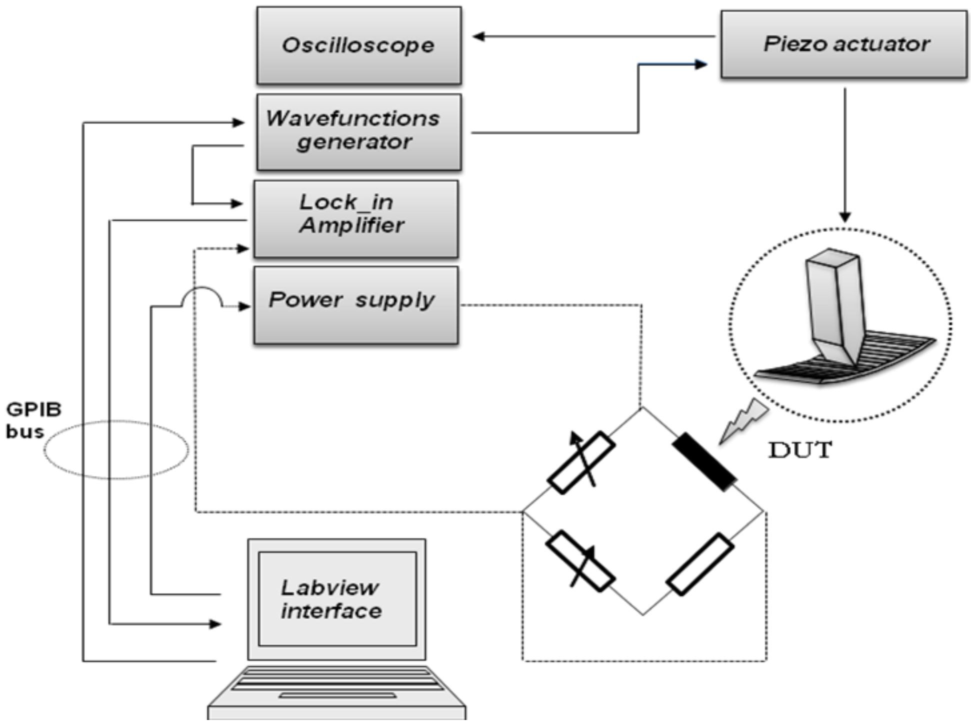

Figure 17. *Microscopic setup for strain measurements*

2.3.1 Microscopic Gauge Factor

The microscopic set-up allows us to measure the GF as the ratio between the electrical measurable response $\frac{\Delta R}{R}$ (resistance fractional change) and the strain $\boldsymbol{\varepsilon}$ applied to the sensor. In a schematic representation where the distance between the contacts (equal to the distance between the suspension points) is 2L, all the deformation is applied at the center of the sample in L where is applied the actuator elongation equal to $\boldsymbol{\Delta}$L, the GF results as

$$\mathbf{GF} = \frac{\Delta R}{R} * \frac{1}{\varepsilon} = \frac{\Delta R}{R} * \frac{2L^2}{\Delta L^2} \qquad \textbf{Eq 4}$$

The definition of the GF parameter in this form can be used for the estimation of the quality of a piezoresistor provided that the very delicate and complicated set-up calibration procedure is clarified. The effective elongation of the sensor has to be known exactly, and the feedback signal on the piezo actuator is insufficient for determining the exact amount of deformation induced in the sensor, since the sample itself can offer enough mechanical resistance to the actuator, especially when coherent detection is used. Often to overcome this problem reference strain gauges are used for setup calibration, however we have verified that for the microscopic range of deformation considered in this section, the rigidity of the setup can be considered infinite with respect to the mechanical resistance of our samples. This is not obvious since even if polyimide can be considered a soft elastic substrate, for the range of thicknesses obtained by spin coating process, the rigidity of the sample becomes quickly comparable to the rigidity of the setup when large macroscopic deformations are considered.

Typical measured GF for a polyimide substrate with thickness of 100 μm is around 17.8 +/- 4. The reason for the relatively large error is given by the difficulties of the calibration procedure, which is performed through micropositioners that presents an hysteresis of the order of 1 μm. This hysteresis affects the determination of effective microscopic sample bending and consequently the effective induced strain.

2.4 Macroscopic Measurement Setup

The idea is to replicate as really as possible the human finger flexion/extension movements (Figure 18).

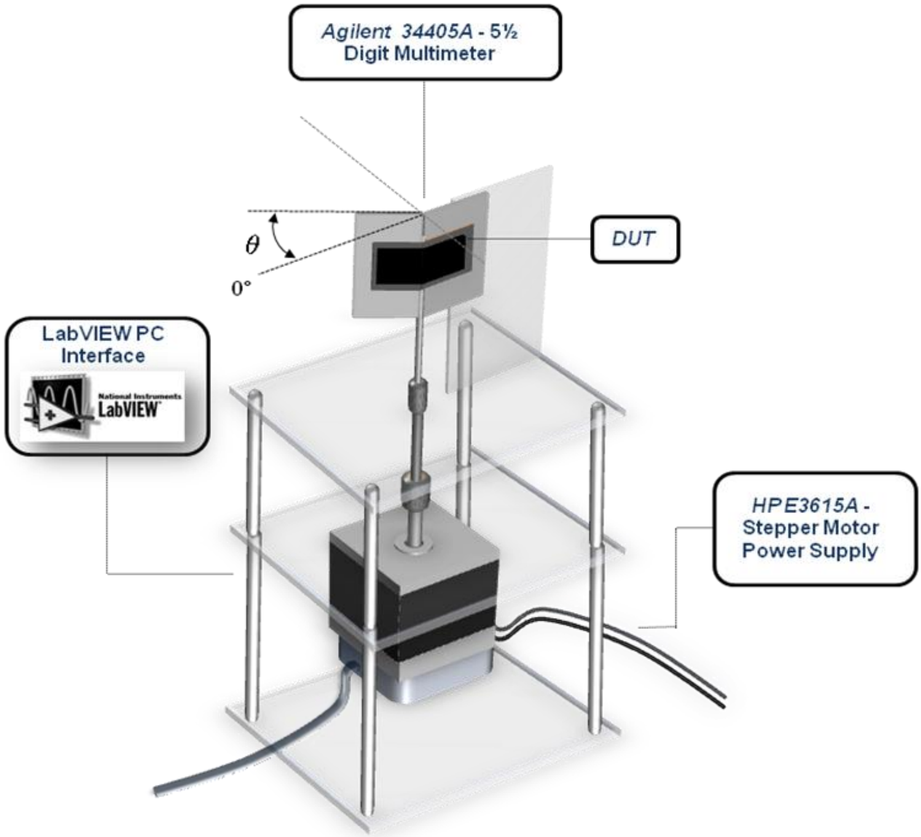

Figure 18. *Macroscopic bending measurement setup*

The set-up consists of three hinges controlled by three step-by-step motor (PD-109-57 Trinamic mechatronic drive with NEMA23) that allow to discriminate angles with an error less than few tenth of degree. The PD-109-57 comes with the PC based software development environment TMCL-IDE for the Trinamic Motion Control Language (TMCL). Using predefined TMCL commands it is possible to determine starting and final angle assumed by the hinge and to impose timing for each step movement of the motor. The whole system is controlled with a LABVIEW interface.

Every hinge is connected to the 6.35mm motor axis through an elastic joint in order to minimize friction torque. A rigid frame provides the necessary stability to the system.

A key issue of the measurement is represented by the possibility to discriminate between the bending and the stretching effect induced by the hinge on the sample. We developed an ad hoc support system that allows to obtain a correct deformation angle without any stretching effect on the sample: one end of the sensor is taped, while the other end it is in strict contact to the hinge but free of slipping.

Another advantage of this set-up is the possibility to control only one motor for a single strain sensor and up to three motors for arrays of sensors. Each hinge can reach a bending of 120°. All the system is performed as the human finger movement suggests: the bending of the methacarpo-falangeal joint involves the shift of the other two joints; the bending of the proximal interfalangeal joint shifts the distal interfalangeal joint.

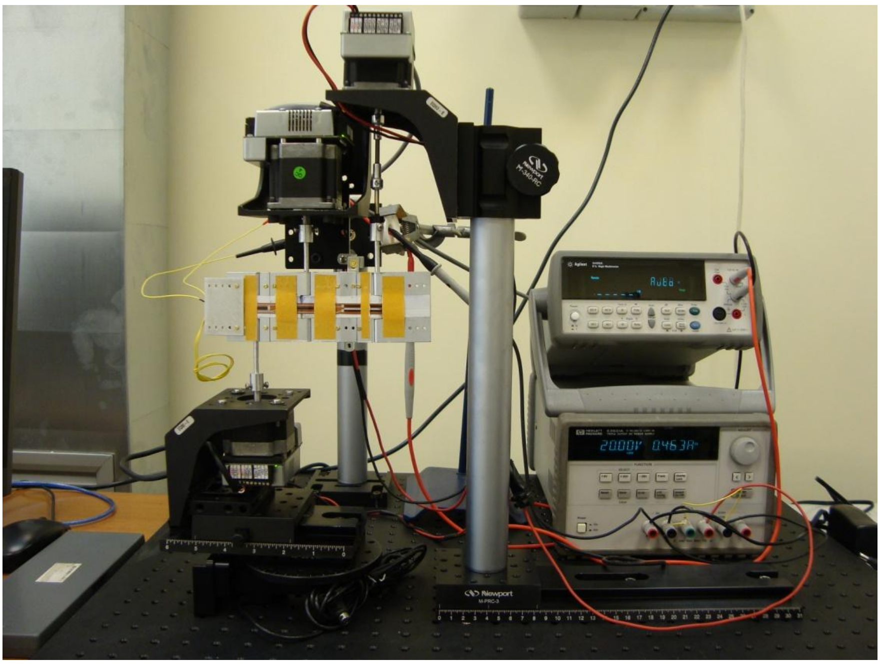

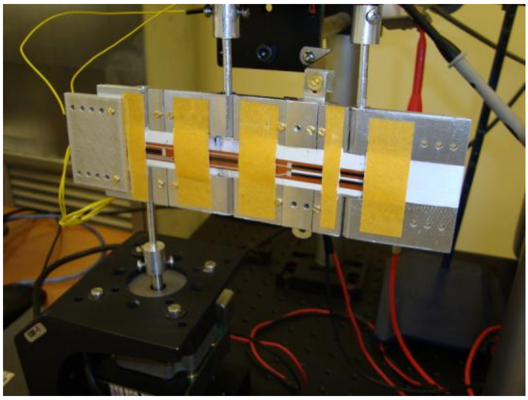

Figure 19. *Totally automated bending measurement setup with three different motors and for the characterization of three different sensors*

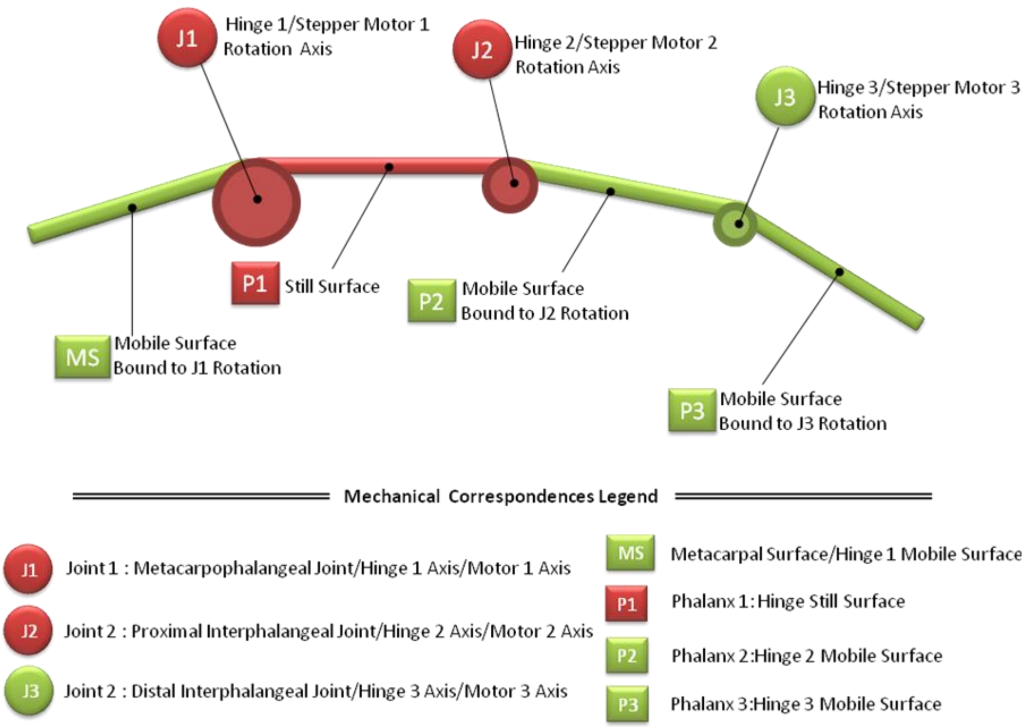

Figure 20. Schematic operations for three motors

The setup is remotely controlled by a personal computer to automate the measurement procedure and the resistive response of the sensor is read by a 5.5 digits 34405A Agilent digital multimeter.

I want to emphasize the great importance of an ad-hoc measurement set-up for the sensor characterization. So I tried to start three different measurements with two different modalities: manual goniometer and automatic measurement with our dedicated set-up. The result is that the error mean in terms of standard deviation is 2.5% for the manual measurements and only 0,5% for the automatic set-up.

2.4.1 Buttonhole Choice

The buttonhole's choice is fundamental to obtain repeatable measures. The buttonhole is applied into one hinge wing and it permits to slide the inserted sensor. Three are the principal adopted solution, that are reported in the next.

(1) Flexible Buttonhole (Figure 21(a))

Buttonhole is realized with a special bi-adhesive scotch. It's typical the use of particular pinchers in order to obtain the wanted binary flow. It's simple to built, it's low cost solution, it's very quick. There are several utilizing materials. Against, this solution is simply perishable in the same single measure.

(2) Rigid Buttonhole (Figure 21 (b))

Buttonholes is realized in a rigid material, such as plexiglass for example. Then it is used Teflon in order to improve the sensor flow. A screw microcontroller is realized for an excellent regulation of the space between the wing and the buttonhole. The problem is just to regulate this critical distance.

(3) Roll On Buttonhole (Figure 21 (c))

This is more complex system: it's realized with two or three flow pads. The inter-distance is regulated tank to one spring for each pad. The system realization is not simple and all the structure is not perfectly stable. But on the other side this solution represents a unique system adoptable for all the sensors and all the dimensions. It's perfectly regolable.

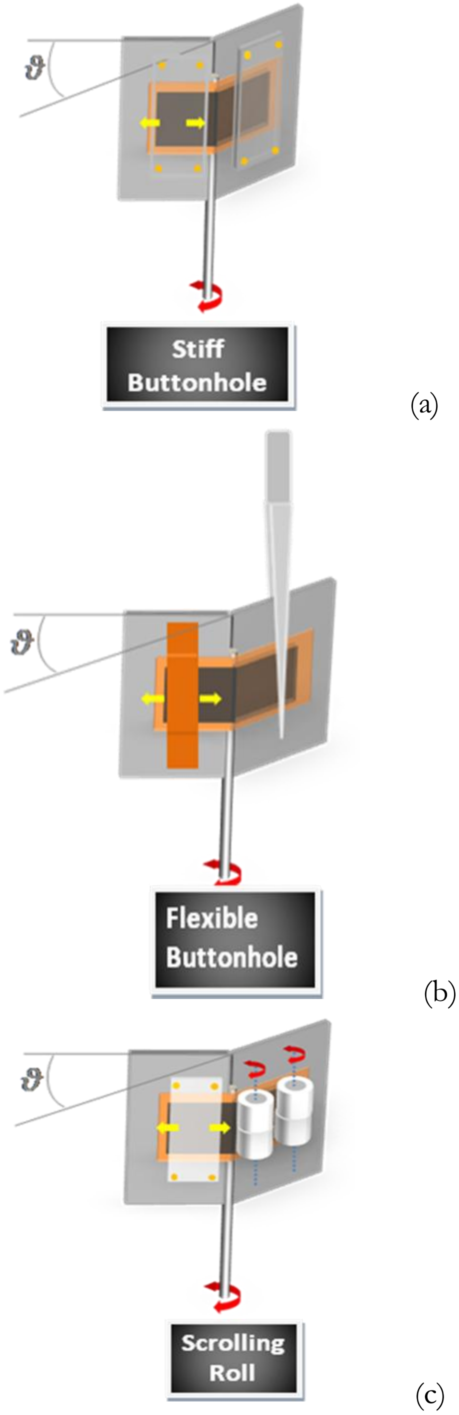

Figure 21. *All realized types of buttonholes*

2.5 Mechanical Model

In order to validate the obtained measurement results justifying them by means of a specific mechanical model for the bend sensor. To develop the model let's start with the fundamental parameter regarding the sensor's strain sensitivity, i.e. its gauge factor (*GF*), defined as the fractional change in resistance *R* due to an applied strain ε: $GF = dR/R\varepsilon$. Various gauge factors exist, dependent on the direction of the applied strain ε. In this work, the longitudinal gauge factor GF_L is considered, relevant to the change in resistance when a strain ε is applied across the length of the resistor, parallel to the current flow. It is known to depend on the piezoresistivity coefficient of the film and on the mechanical properties of the carrier substrate, as shown by Papakostas and White [19].

My analysis assumes the mostly verified event that the film is very thin compared to the substrate (so that it does not affect the stresses in the substrate) and conforms to the strains of the substrate in the planar directions.

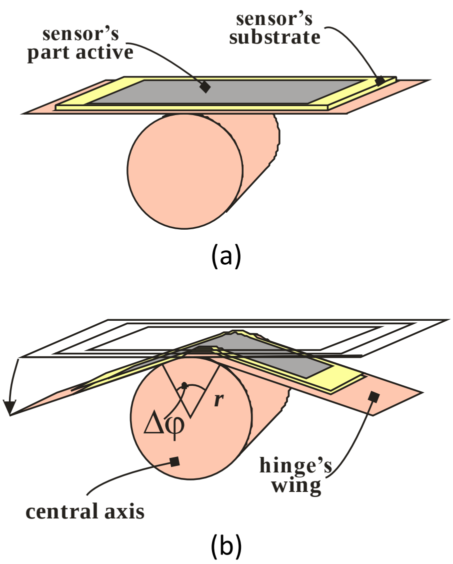

Figure 22. *Sensor lying on the hinge's wings in (a) flat and (b) angled position*

Moreover, it is assumed that the substrate remains tight fitting to the hinge.

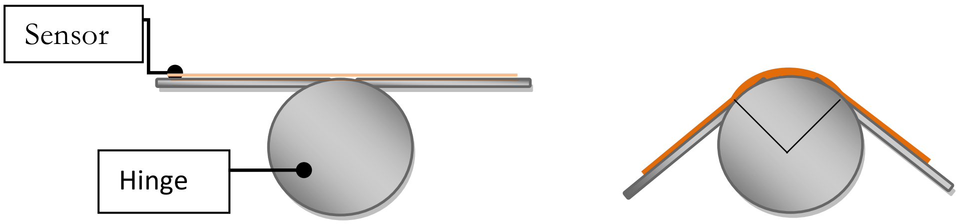

Figure 23

Let $\Delta\varphi$ be the rotation of one wing of the hinge with respect to the other one. As depicted in Figure 22 and in Figure 23, a portion of the piezoelectric sensor is bent on the hinge pivot. The sensor can slip over the hinge, so that reference is made to the neutral plane of the substrate, which do not undergo strains. It is located on the middle of the substrate, and hence its distance from the pin centre is $r+h/2$, where r denotes the pin radius and h is the thickness of the substrate. As a consequence, the length of the bent portion of the substrate is:

$$l_b = \left(r + \frac{h}{2} \right) \Delta\varphi$$

Eq 5

and its curvature is:

$$\chi = \frac{1}{r + h/2}$$

Eq 6

In turn, the piezoresistor film bonded to the substrate turns out to be strained by the substrate bending over the same span length l_b, and the induced longitudinal strain is:

$$\varepsilon = \frac{h}{2}\chi$$

Eq 7

The relevant fractional change in resistance turns out to be:

$$\frac{\Delta R_b}{R_b} = GF_L \varepsilon$$

Eq 8

where GF_L is the longitudinal gauge factor, and R_b is the unstrained resistance of the span length l_b. The latter is a fraction of the unstrained resistance R measured between the electrodes, enclosing a length l of the piezoresistor film:

$$R_b = \frac{l_b}{l} R$$

Eq 9

By observing that ΔR_b coincides with the total resistance increase ΔR since the remaining portions of the film remains unstrained, by the previous equations it easily follows that:

$$\frac{\Delta R}{R} = \frac{R_b}{R}\frac{\Delta R_b}{R_b} = \frac{l_b}{l} GF_L \varepsilon = GF_L \frac{h}{2l} \Delta\varphi$$

Eq 10

This important relationship shows that the output signal $\Delta R/R$ is expected to be independent of the pin radius r, and to be linearly proportional to the input signal $\Delta\varphi$. Moreover, the sensitivity of the transducer is directly proportional to the longitudinal gauge factor GF_L and to the substrate thickness h, whereas it is inversely proportional to the distance l between the electrodes. Of course, for the present analysis to hold true, the latter quantity cannot be chosen less than the maximum value attained by l_b, given by the maximum rotation angle $\Delta\varphi$ times $r+h/2$.

Then, a refined mechanical model is proposed. For easiness of notation, the position $r^*=r+h/2$ is made. Moreover, the following well known result from beam theory is used: given a clamped-clamped linear elastic beam with length a and one clamp subject to an imposed rotation θ, the curvature at the rotating clamp is $4\theta/a$ (Figure 24).

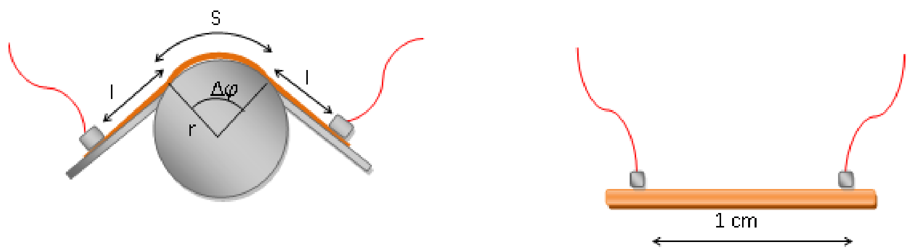

Figure 24. *Schematic curvature for a sensor*

As stated above, the previous mechanical model assumes that the substrate remains tight fitting to the hinge. In practice, two restraints are applied to the substrate, with the aim of pulling it on the wings. Their distance is denoted by l^*. One of them is sliding, in order to prevent any axial stretch of the substrate. Each one of these constraints, together with the wing reaction, constitutes a couple of forces, which is however unable to keep the substrate entirely in contact with the wings. As a matter of fact, two different cases can be distinguished, respectively depicted in Figure Y and Z.

When $\Delta\varphi < l^*/4r^*$, the substrate touches the hinge pin only at point *O*, and remains detached from the wings until point *B*. pin.

When $\Delta\varphi > l^*/4r^*$ the substrate touches the hinge pin along the zone *OA*, where the curvature is equal to $1/r^*$. In particular, the relative rotation of the cross section *A* with respect to *B* is clearly given by $\Delta\varphi/2 - l_c/2r^*$. Then, imposing that the curvature at *A* is $1/r^*$, the following equation is obtained:

$$4\left(\frac{\Delta\varphi}{2} - \frac{l_c}{2r^*}\right)\frac{1}{(l^* - l_c)/2} = \frac{1}{r^*}$$
Eq 11

which yields:

$$l_c = \frac{4r^*}{3}\left(\Delta\varphi - \frac{l^*}{4r^*}\right)$$
Eq 12

The above quantity is positive, provided that $\Delta\varphi > l^*/4r^*$, and vanishes when $\Delta\varphi = l^*/4r^*$, which is the limiting cutoff between the considered cases.

In both of them, the curvature χ is not uniform along the substrate: indeed, it is a function $\chi(s)$ of the curvilinear abscissa *s* along the substrate axis. As a consequence, the strain ε in the piezoresistor film, given by equation 7, does depend on *s*, i.e., $\varepsilon = \varepsilon(s)$, and equation 10 generalizes into:

$$\frac{\Delta R}{R} = \frac{1}{l} GF_L \int_{-l^*/2}^{l^*/2} \varepsilon(s)ds = \frac{1}{l} GF_L \int_{-l^*/2}^{l^*/2} \chi(s)\frac{h}{2}ds = GF_L \frac{h}{2l}\Delta\varphi$$
Eq 13

where the obvious relation

$$\int_{-l^*/2}^{l^*/2} \chi(s)ds = \Delta\varphi$$
Eq 14

has been used.

It is interesting to note that equation 13 governing the sensor response in the latter refined model coincides with equation 10, obtained after introducing the simplifying assumption of tight contact between the substrate and the wings. In fact, it can be shown that it governs the sensor response as far as the assumption of vanishing axial strains in the substrate is appropriate.

2.6 Labview Interface

All instrumental interfaces are driven by NI Labview Interface. In particular, the hinge's motion is automated in order to obtain a variable deformation of the pressure sensors. At the same time, the program permits to control the multimeter, such as the number of acquisition.

As example, I report a front panel for the electrical resistance acquisition when the sensor is bending (Figure 25).

.

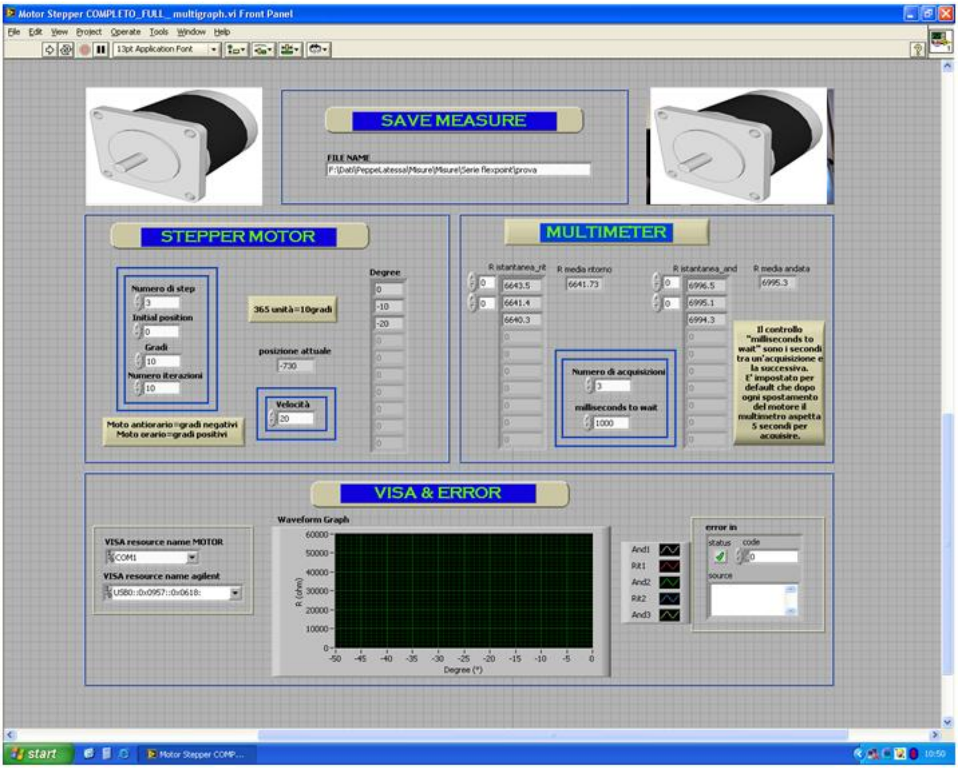

Figure 25. *Labview Interface.*

There are four principal sections:

1) Save Measure;
2) Stepper Motor;
3) Multimeter;
4) Visa&Error.

"Save measure" section permits to select the name of measure file and the appropriate directory.

"Stepper Motor" section permits the motor stepper control. This part contains the principal controls for the program.

In detail:

- *Step Number*: this control permits to select how many steps the hinge have to move;
- *Inizial position*: this box sets the motor initial position. The default value is zero;
- *Degree*: this control sets the amplitude of the single step;

- *Iterations number*: this number permits to establish how many times the measure is repeated;
- *Velocity*: this control sets the motor velocity (typically it is about 20).

"Multimeter" section is about the measure of the sensors resistance ad so about the data capture.

There are two fundamental controls in this box:

- *Acquisition numbers*: it permits to establish the measure precision. In particular, we can set how many acquisitions the multimeter have to do in every step. The single value that we see at the end is the mean about all the measured resistances.
- *Milliseconds to wait*: this box contains the time between a measure and the next.

The last section, titled " Visa & Error", is about the GPIB addresses of the instrumentation and it contains the information about an occurred error. There are only indicators, ma no controls. In particular, there is the possibility for a graphical preview of the measure.

Chapter 3

Results

3.1 Introduction

This work represents a experimental research and the measures are its fulcrum. So it's very difficult for me the choice of most significant graphic and how they have to arranged. In fine I have divided all the measures in few categories, such as outward bending, inward bending, microscopic measurements, macroscopic measurements, temperature coefficient calculation, time response measures.

Not all measures are performed with home-made sensors. In this section I present two other alternate sensors bought by Flexpoint Sensor System and Images SI.

3.2 Commercial Bending Sensor

In the Chapter I home-made strain sensors are presented. But t isn’t possible to realize continuously in all my research these devices. Then it is shown a repeatability problem to obtain them.

So I tried to discover alternative bending sensors with similar or best properties with respect my devices. Two principal interesting solutions are represent by Flexpoint bending sensors and Images SI sensors.

3.2.1 Flexpoint Sensors

They are thin film bending sensors. A sensor is composed, as home-made devices, by two different layer: a piezoresistive proprietary material and a flexible substrate composed by polyimide.

The adopted realization technique is an inkjet printing. When the sensor is bending, the piezoresistive material suffers a lot of micro-strain that improve its electrical resistance. This is schematized in the Figure 26.

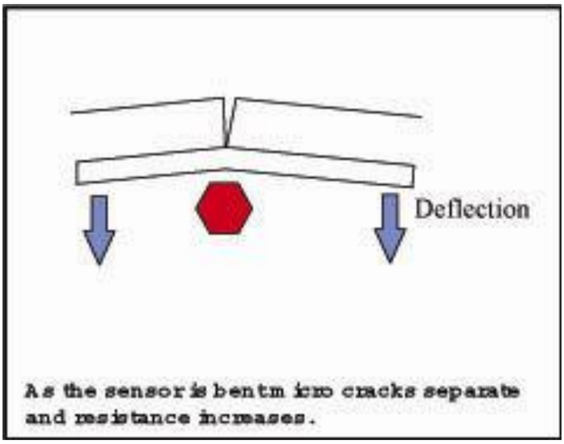

Figure 26. *Electrical resistance increase*

The contacts are similar to home-made sensors and they are realized in a special paste based on a silver component. The furnished sensors are of three different dimensions(1”, 2”, 3”) and three different encapsulations: polyimide, polyester and no encapsulation.

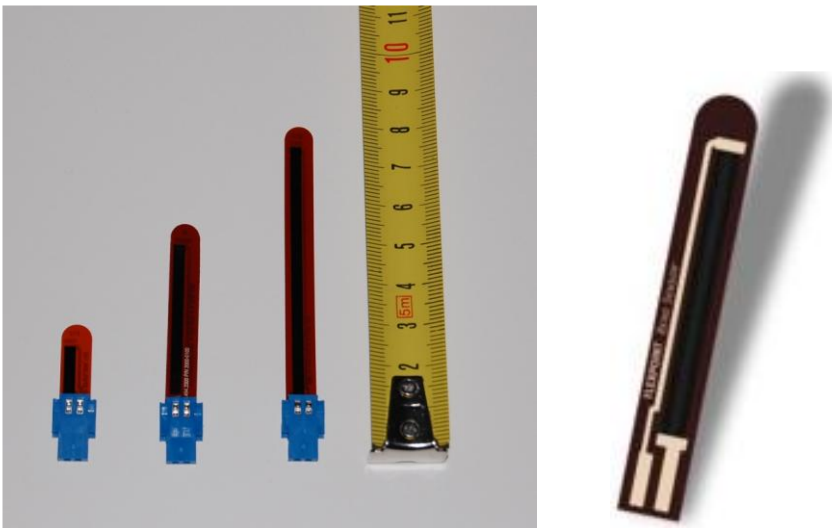

Figure 27. *Flexpoint commercial sensors*

The interaction with Flexpoint is no limited to commercial devices. An important collaboration permits to realize the first case of bending array sensors. The novel concept is that 3 sensors are sited on the same substrate so to improve the repeatability for several applications.

Array sensors are projected with Autocad by me and my research group and they are realized by Flexpoint. The overall result is an esoskeleton mountable on the human hand, as you see in Figure 28.

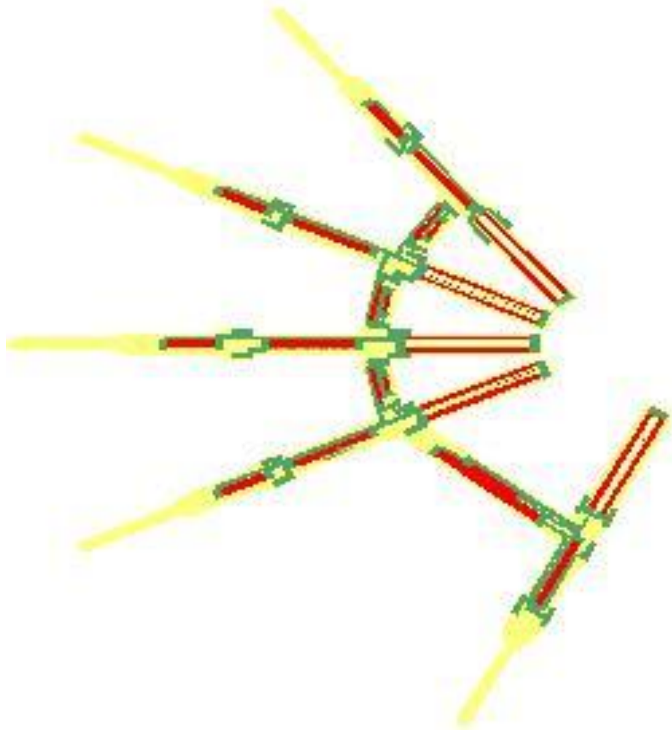

Figure 28. *Architecture of the sensors*

In Figure 29 it's reported a single array sensor. There are several obtained advantages, such as the number wires reduction or a binary for a right sensor flow.

Figure 29. *Our customized array sensor realized by Flexpoint*

3.2.2 Images SI Sensors

Images SI sensors represent another possible solution. Sensors are realized with a multilayer technique: a copper foil, an acetate film, the resistive material, probably Pedot based, and an heat shrink tubing.

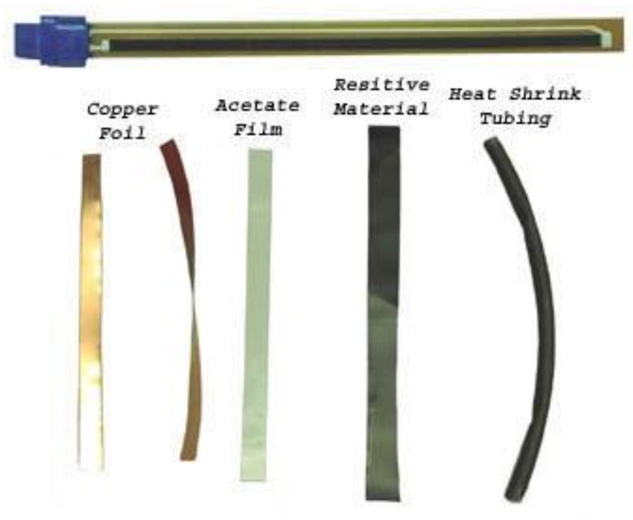

Figure 30. *Images bending sensors with specific layers*

The thickness is greater than the Flexpoint sensor and so it shows an improvement of mechanical resistance.

4 Piezoresistive Behavior in Microscopic Measurements

The utilized setup is shown in Figure 17. The DUT (Device Under Test) is deformed by an insulating tip. It is possible to apply both a static and a dynamic deformation controlled by a piezoelectric actuator (Physyk Instrument) acting on the sample. The piezo actuator through an insulating rigid tip applies a vertical force at the centre of the flexible film proportionally to a control voltage. 8 μm of nominal displacement are obtained for 1 V applied to the control input.

The deformation induces a variation of a resistance that is evaluated measuring the bias of a Wheatstone bridge formed by the sample itself, a reference sample, a trimmer and a fixed resistance. The response of the sensor to microscopic deformations is shown in Figure 31. The relative resistance variations extracted by the coherent detection raises linearly to the applied deformation i.e to the control voltage V_{pp} applied to the piezo actuator until a saturation value.

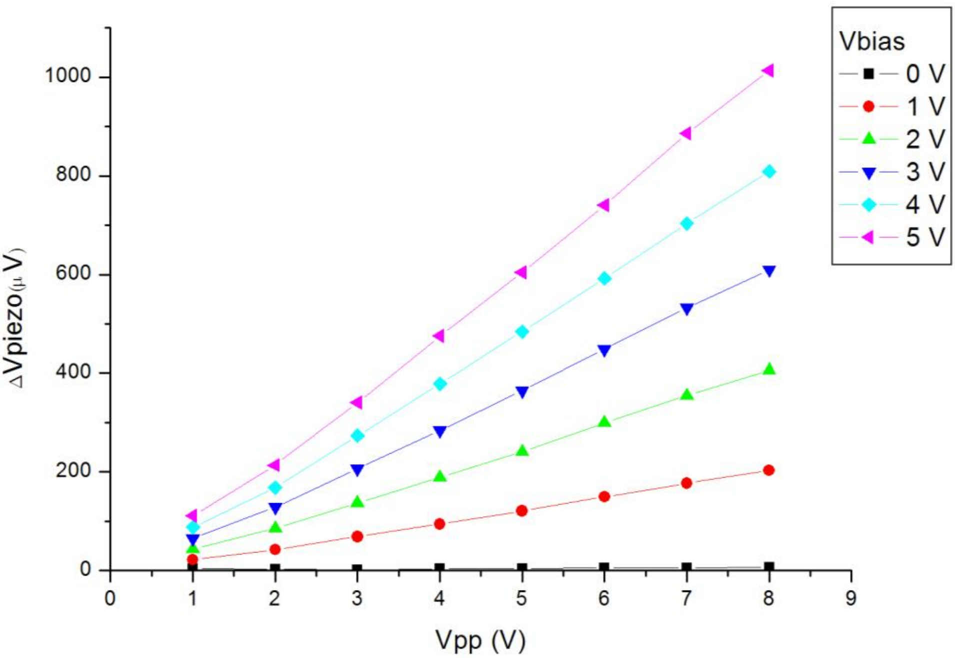

Figure 31. *Microscopic measurements for a home-made strain sensor*

These measures permit to obtain the GF of the sensor as the ratio between the electrical measurable response $\boldsymbol{\Delta}$R/R $\frac{\Delta R}{R}$(resistance fractional change) and the strain $\boldsymbol{\varepsilon}$ applied to the sensor. GF is the sensitivity parameter. Greater is GF, better is the piezoresistive sensor.

$$GF = \frac{\Delta R}{R} * \frac{1}{\varepsilon} = \frac{\Delta R}{R} * \frac{2L^2}{\Delta L^2}$$

For GF count, the rigidity of the setup can be considered infinite with respect to the mechanical resistance of our samples. This is not obvious since even if polyimide can be considered a soft elastic substrate, for the range of thicknesses obtained by spin coating process, the rigidity of the sample becomes quickly comparable to the rigidity of the setup when large macroscopic deformations are considered.

A GF measure is reported in Figure 32. It's a linear behavior, with a principle of saturation showed for higher ΔL/L.

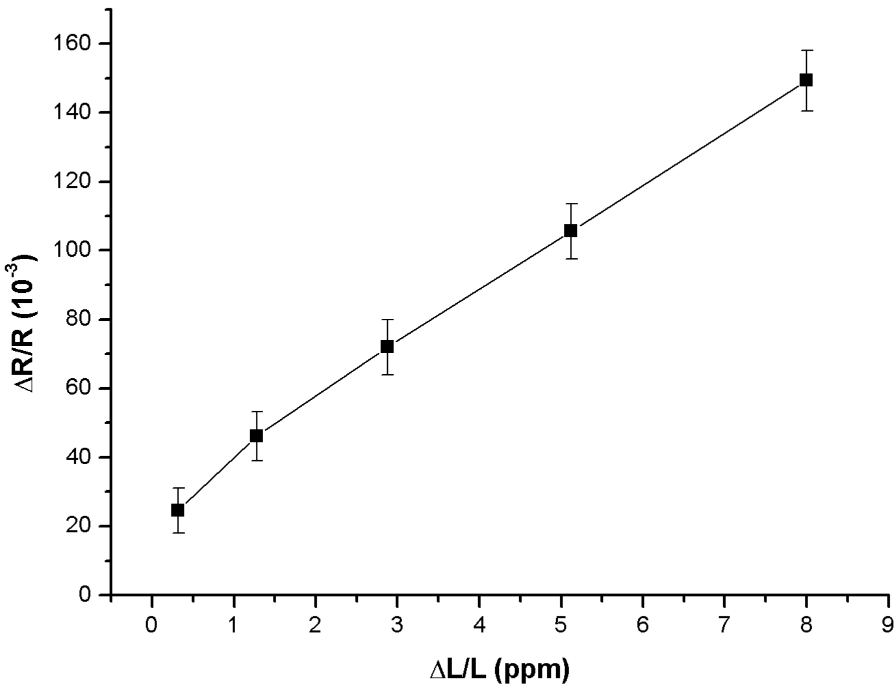

Figure 32. *GF behavior for an home-made sensor*

Typical measured GF for a polyimide substrate with thickness of 100 μm is around 17.8 +/- 4. The reason for the relatively large error is given by the difficulties of the calibration procedure, which is performed through micropositioners that presents an hysteresis of the order of 1 μm. This hysteresis affects the determination of effective microscopic sample bending and consequently the effective induced strain.

3.3 Piezoresistive Behavior in Macroscopic Measurements

Macroscopic measurement setup is shown in Figure 18. This set-up consists of an hinge controlled by a step-by-step motor that allows to discriminate angles with an error less than few tenth of degree. The idea is to replicate human finger movements. Different types of measures are done thanks to the system versatility.

A key issue of the measurement is represented by the possibility to discriminate between the bending and the stretching effect induced by the hinge on the sample. We developed an ad hoc support system that allows to obtain a correct deformation angle without any stretching effect on the sample: one end of the sensor is taped, while the other end it is in strict contact to the hinge but free of slipping .

3.3.1 Outward measures

An outward measure consists into the bending of the sensor so that the piezoresistive film is extended. For the outward bending, the sensors can be bent in a range of 0°- 120°.

The average relative variation of the resistance for each bending angles $\Delta R/R$ (%) is reported on the vertical axes. The horizontal axes represents the bending angle (degree).

All sensor types are performed in macroscopic outward behaviour. In Figure 33 is reported the electrical resistance variation of an home-made sensor. The angle is variable from 0° to 60°, with a step of 10° and with an hold-time of 10 secs. The measure is repeated for ten turns.

The resultant average data demonstrate a linear response of the sensor in the range of the measured angles. This is a very interesting aspect in the design of specific tools based on the macroscopic behaviour of our samples, since a linear sensor response simplifies the design of control and monitoring software for recognition and control of 3D movements.

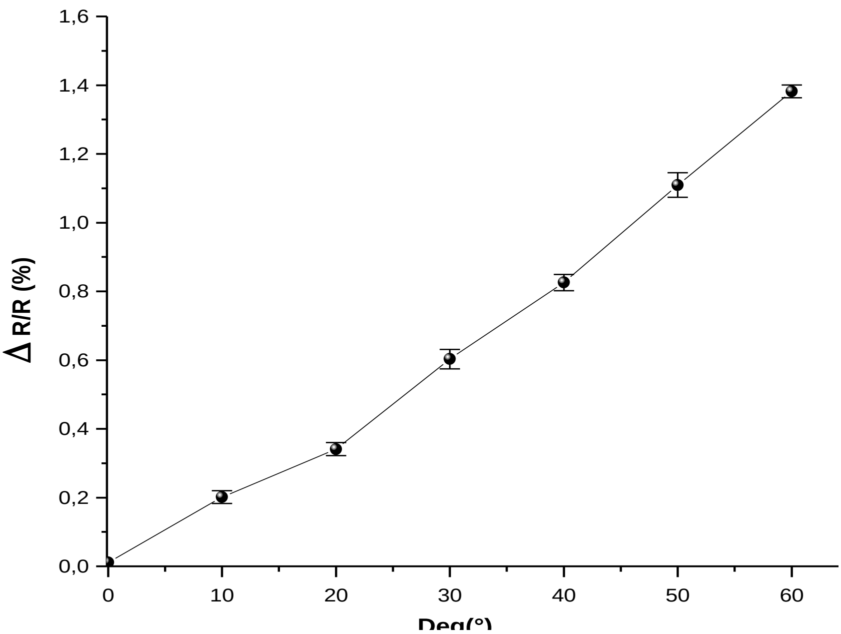

Figure 33. *Macroscopic measurement of an home-made sensor*

Flexpoint no encapsulated sensors macroscopic behavior is reported in Figure 34. The bending angle is up to 120°. The sensor shows fantastic performances in terms of piezoresistivity, but the behavior is not linear. Flexpoint sensors have an optimal repeatability (the standard deviation, reported in the **Figure 36** as Y error, is less than 1%).

The Figure 35 shows the comparison between three several sensors types designed by Flexpoint. The measure is repeated on two different specimen for sensor type. No encapsulation sensors indicates the greatest electrical resistance variation.

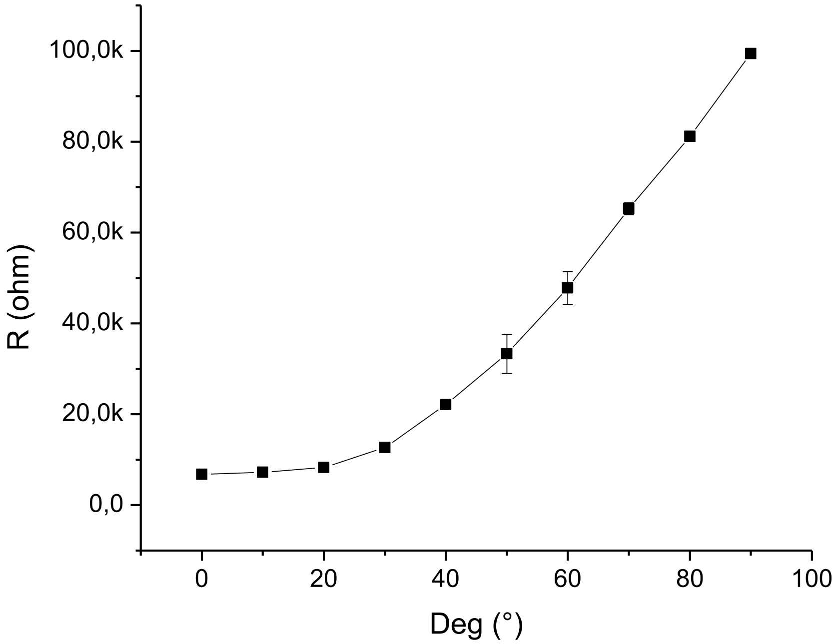

Figure 34. *Flexpoint no encapsulated sensors macroscopic behavior*

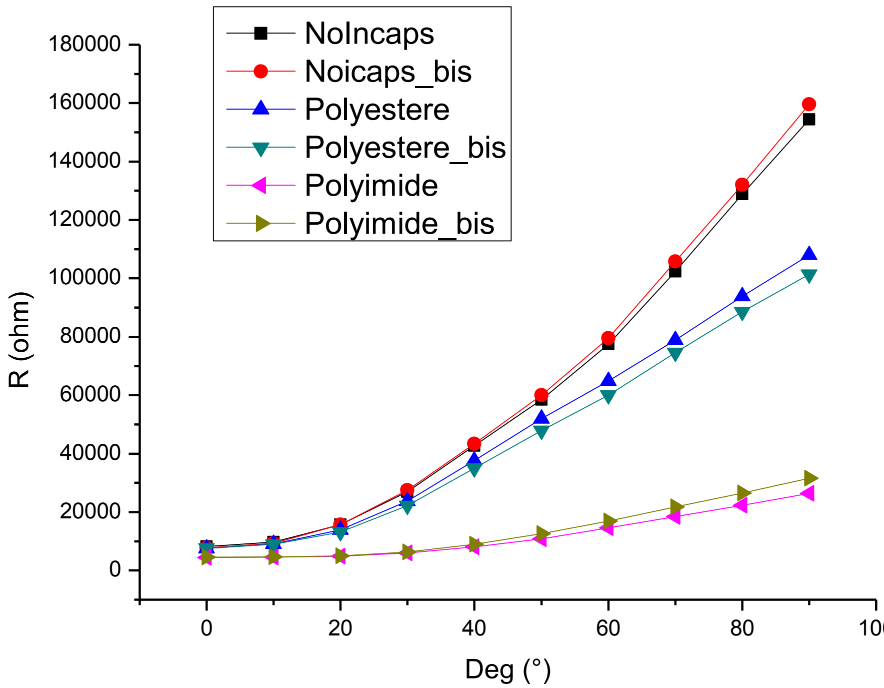

Figure 35. *Comparison of the resistance variation between all types of commercial Flexpoint bending sensors*

Images SI sensors has a quite good electrical resistance variation. The GF is smaller than Flexpoint sensor, but the behavior is linear. The error in terms of standard deviation is about 1.7 %. In the next Figure 36 is reported the electrical resistance variation versus the bending angle referred to an Image SI sensor.

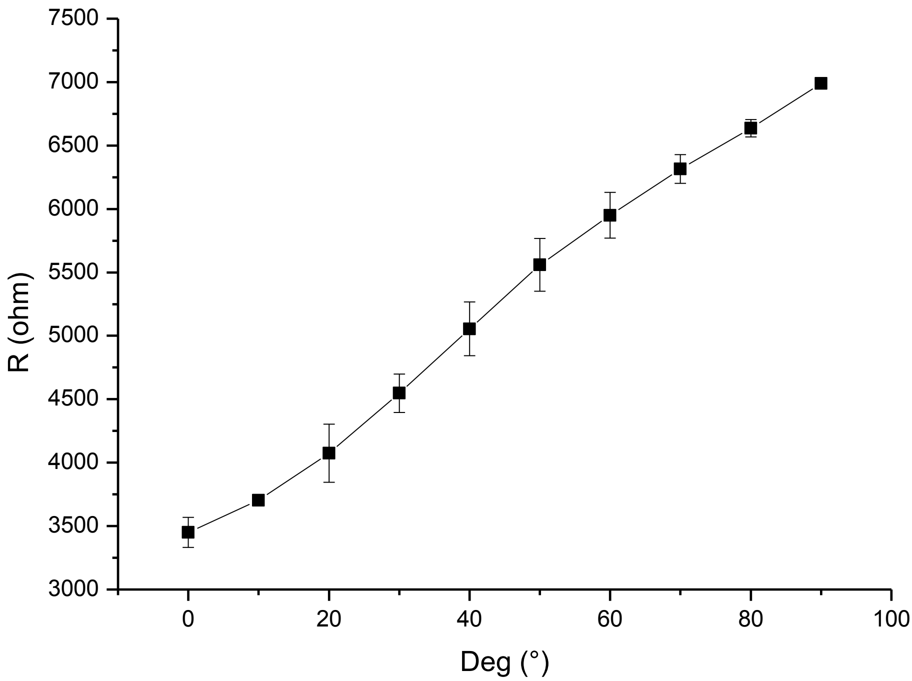

Figure 36. *Outward Image sensor behavior*

3.3.2 Inward measures

An inward measure consists into the bending of the sensor so that the piezoresistive film is compressed. Bending angle is from -120° up to 120° or less.

Not all the strain sensors shows a bidirectional behavior, but this is a significant property for different applications. In the next are reported inward and outward responses of all three type of used sensors:

Home-made sensor (**Figure 37.** *Bidirectional behavior of an home-made sensor*

-

-). The bidirectional behavior is almost symmetric for outward and inward, but the electrical resistance variation is poor.
- Flexpoint sensor (Figure 38). There is no inward resistance variation, but the resistance variation is excellent.
- Images sensor (Figure 39). The inward behavior is less than the outward and the electrical resistance variation is good.

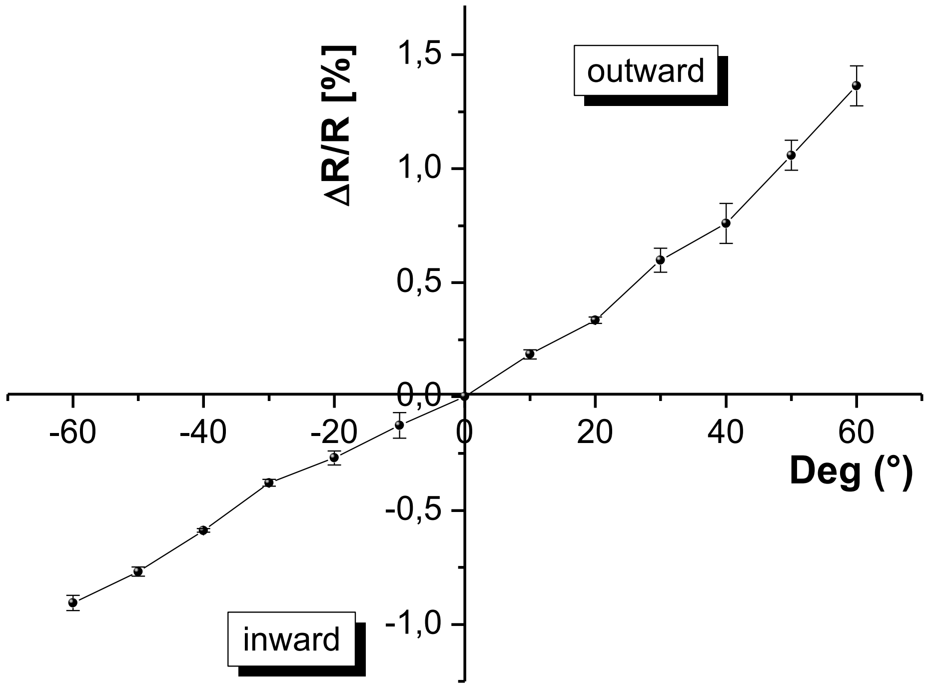

Figure 37. *Bidirectional behavior of an home-made sensor*

-

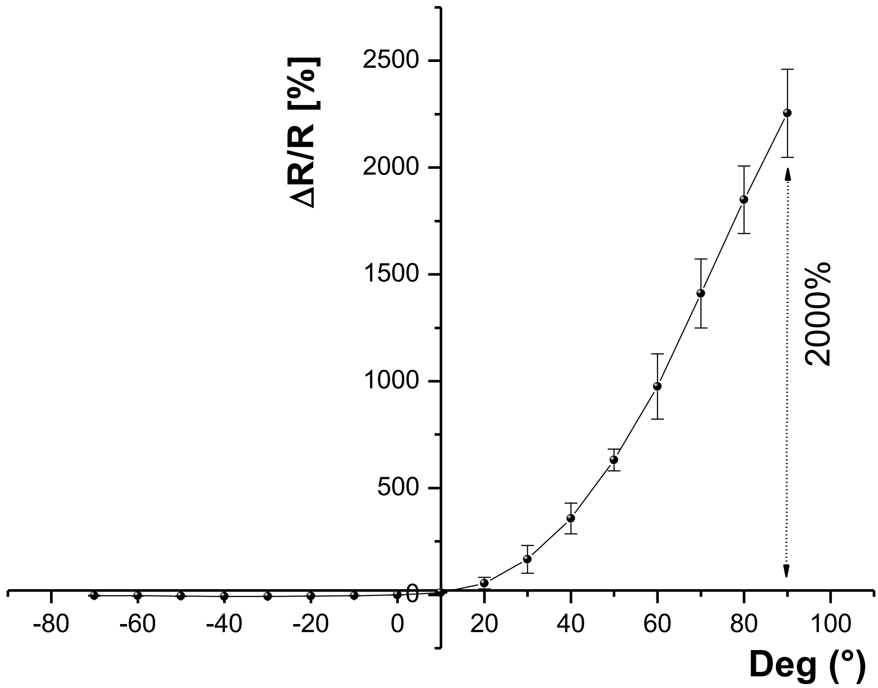

Figure 38. *Bidirectional behavior of an Image sensor*

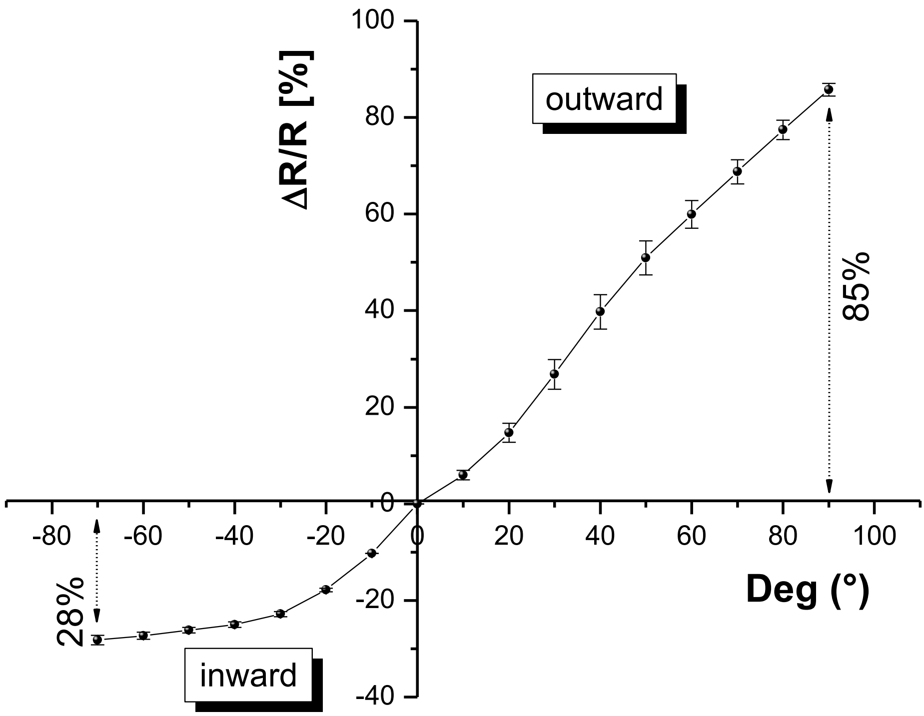

Figure 39. *Bidirectional behavior of a Flexpoint sensor*

3.3.3 Time Response Measures

The home-made sensor was also characterized in terms of its time response (Figure 40) . It can be underlined as the measures are highly repeatable and both rising and falling time are practically the same.

To assure reproducibility attention was paid to reversibility, hysteresis and recovery performance.

The recovery performance was satisfactory demonstrated with several bending procedure of the sensor ranging every time from an angle of 0° to an angle of 60° with a step of 10° and going back from 60° to 0° with the same step. No hysteresis effects and the good recovery performance have been evidenced .

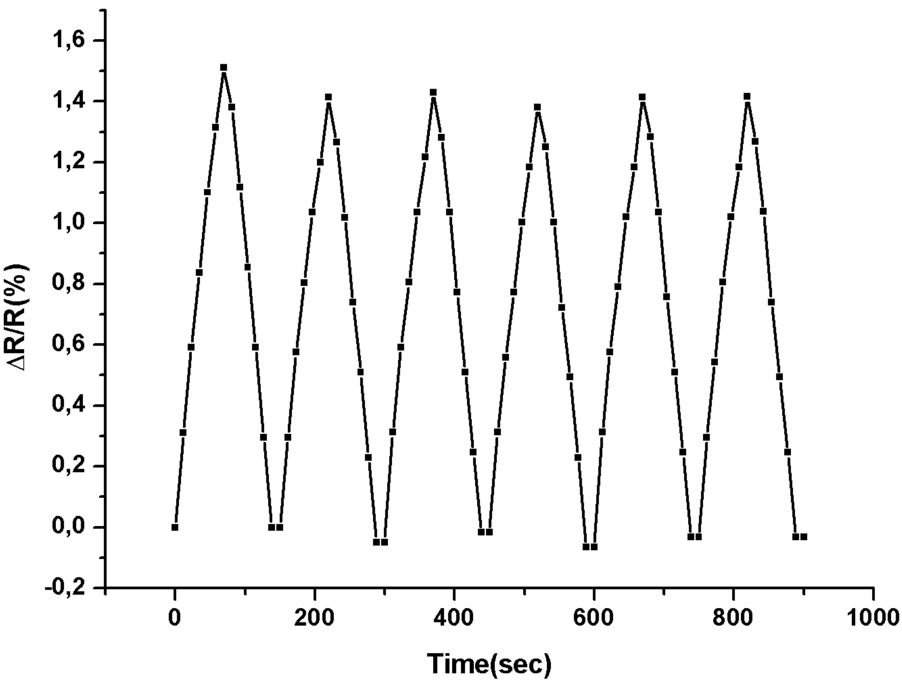

Figure 40. *Time response of an home-made sensor*

3.3.4 Macroscopic GF

In the Figure 41 is shown the sensitivity behavior of Flexpoint and Images sensors. The second one is almost stable after 30°of bending. In the other case, the GF is linear and it is very high.

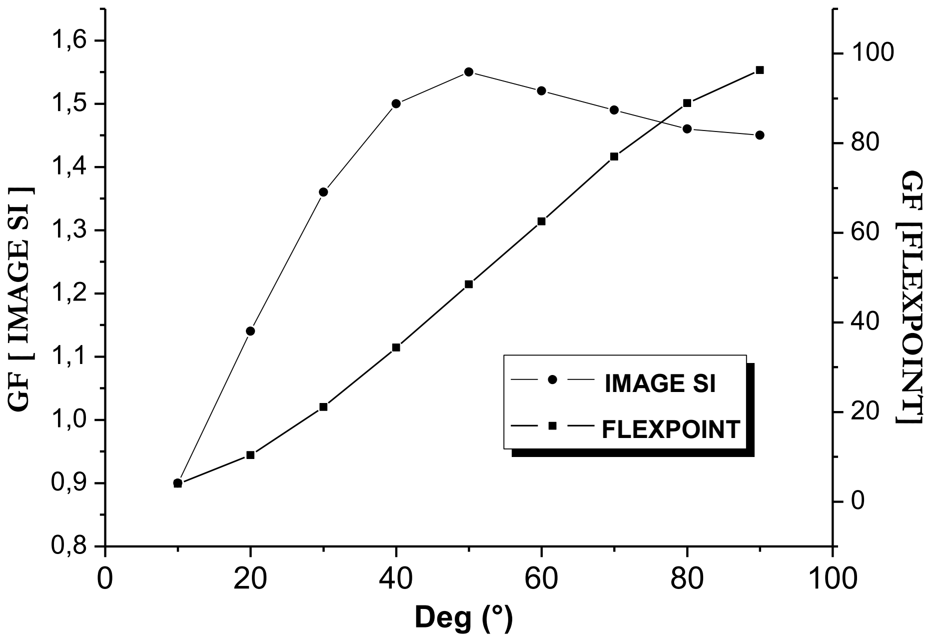

Figure 41. *GF behavior of Flexpoint and Images sensors*

3.4 Temperature Coefficient of Resistance

Strain sensors have to estimate the applied strain. External parameters as humidity and in particular temperature mustn't interesting the electrical resistance variation.

In order to establish the temperature influence on the electrical resistance variation, it exists an opportune coefficient, reported in the next:

$$TCR = \frac{R(T) - R(T_0)}{R(T_0)} \cdot \frac{1}{T - T_0} \qquad \textbf{Eq 15}$$

A probe station was used for electrical resistance variation on the home-made strain sensors. The imposed temperature is form 30°C to 80°C. It's evident a resistance decreasing when the temperature raises. The behavior remains linear.

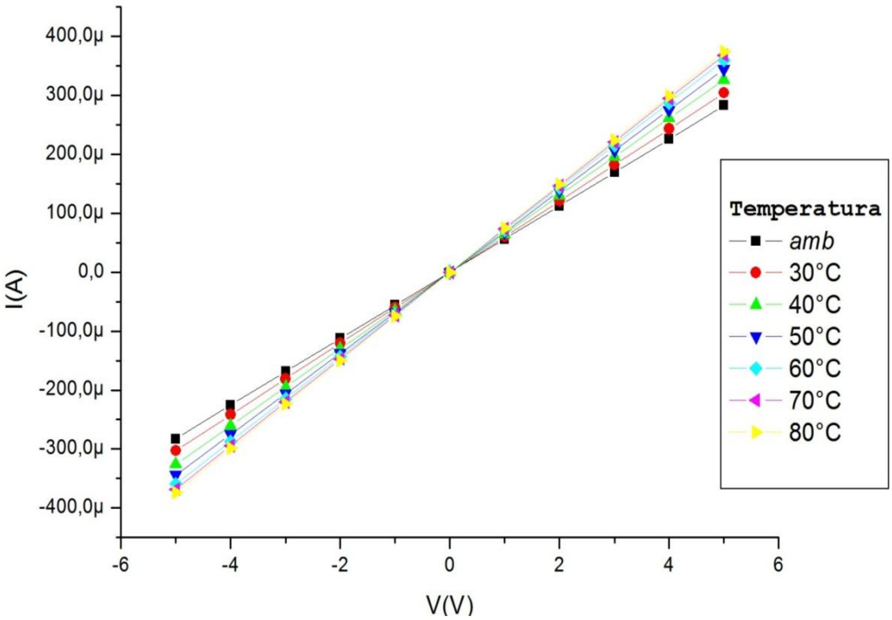

Figure 42. *Temperature dependence of I-V characteristics.*

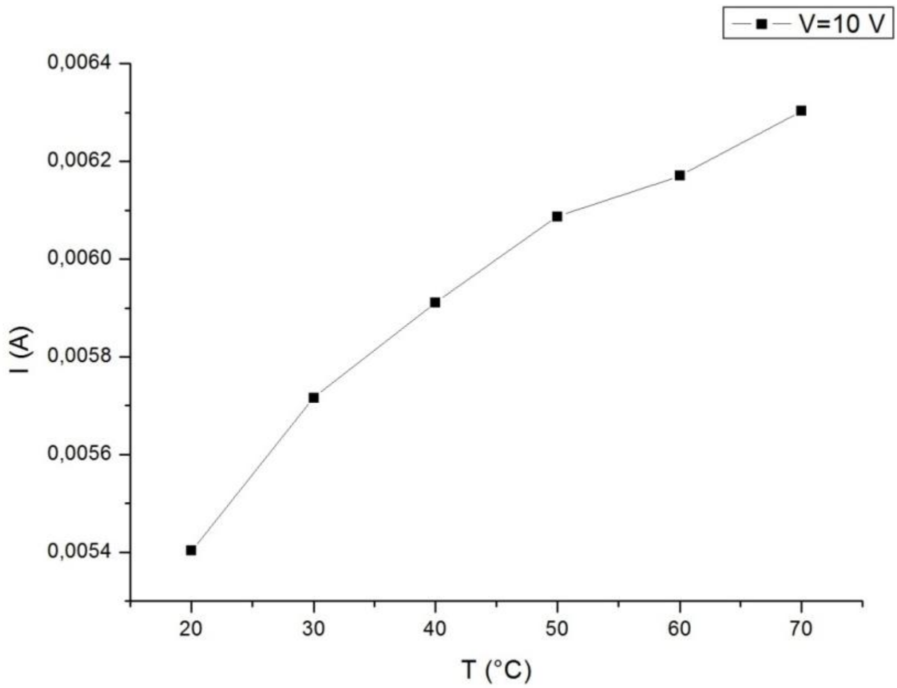

Figure 43. *Current vs Temperature referred to an home-made sensor*

From the Eq 1551, it's obtained a TCR=0.0038. This result is encouraging and it is possible to estimate the influence of temperature on the electrical resistance as 2% with respect the strain.

3.5 Array Sensors Characterization

An array sensor is composed by three different sensors on the same flexible substrate. An electro-mechanical characterization is due, because when each sensor is deformed, all the substrate could be strained so to influence the others.

In the second, these array sensors are realized in order to obtain an excellent instrumental glove. The mounting on the glove is performed so to bind only one array sensor end (PIP joint end), while the other is free of run. So it is evident a translation of the array with respect the human joint.

MCP joint sensor suffers a translation when the other two sensors are deformed. Its electrical resistance variation is reported in Figure 44 compared to the PIP joint sensor and in Figure 45 respect the DIP joint sensor. In both cases there is a resistance variation due to this mechanical translation, so when the array is mounted on the glove, a software correction is brought.

A really good thing is that the reported overall error (in terms of SD) is about 2% - 3%.

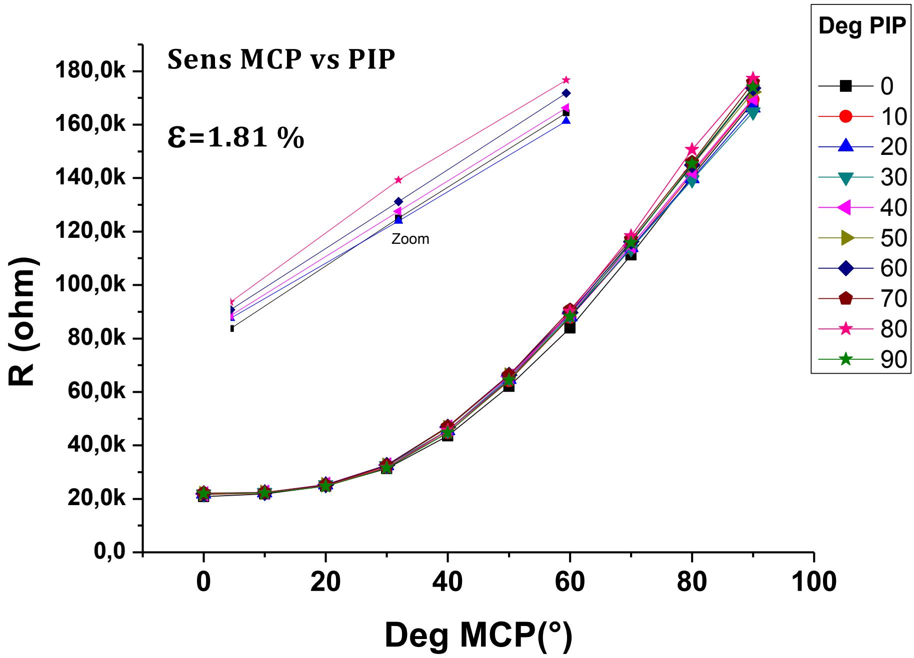

Figure 44. *MCP sensor for PIP bending*

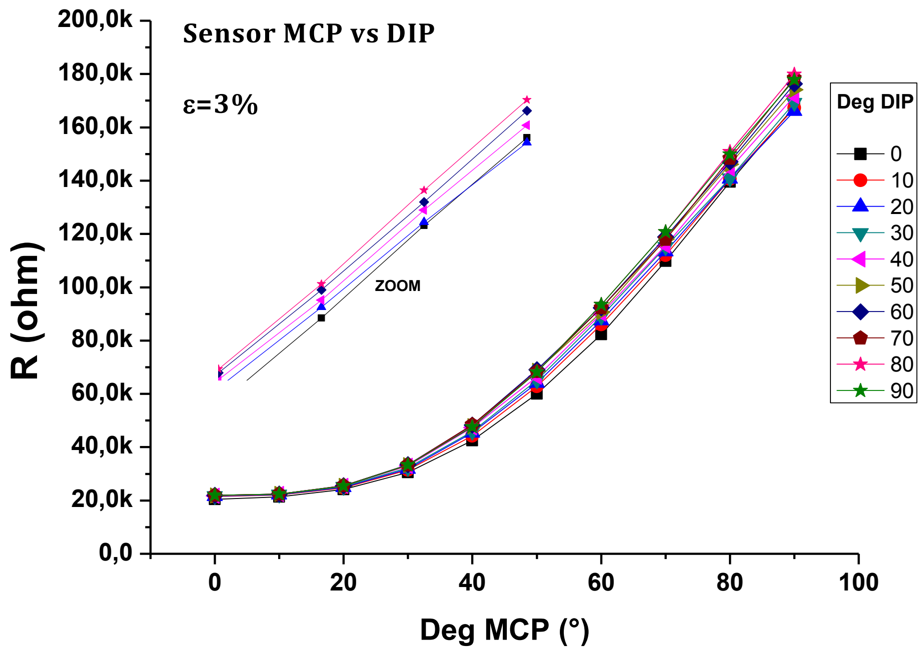

Figure 45. *MCP sensor for DIP bending*

The same analysis is done about the PIP joint sensor. The mentioned sensor suffers a translation with respect DIP joint sensor (Figure 46) and none versus MCP sensor (Figure 47).

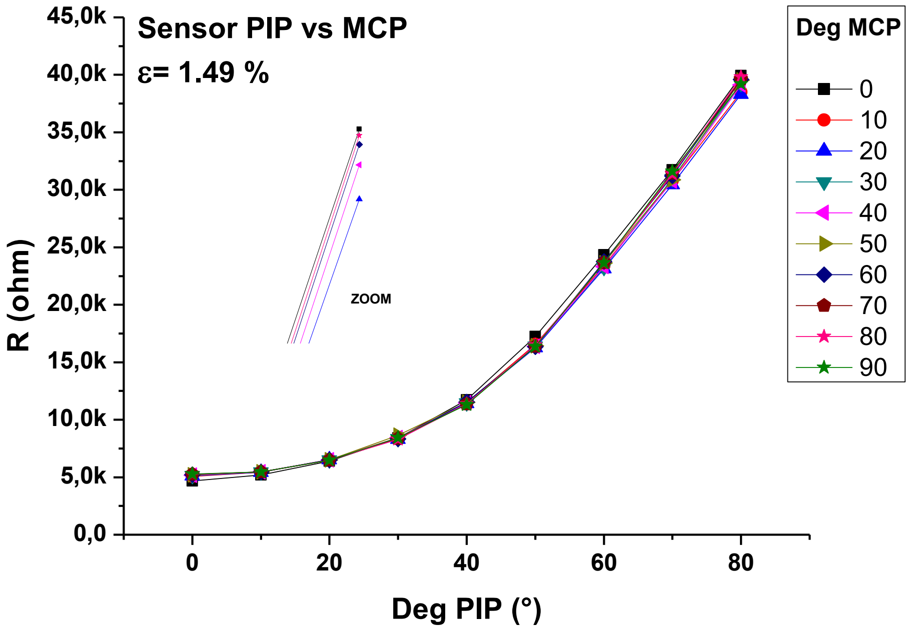

Figure 46. *PIP sensor for MCP bending*

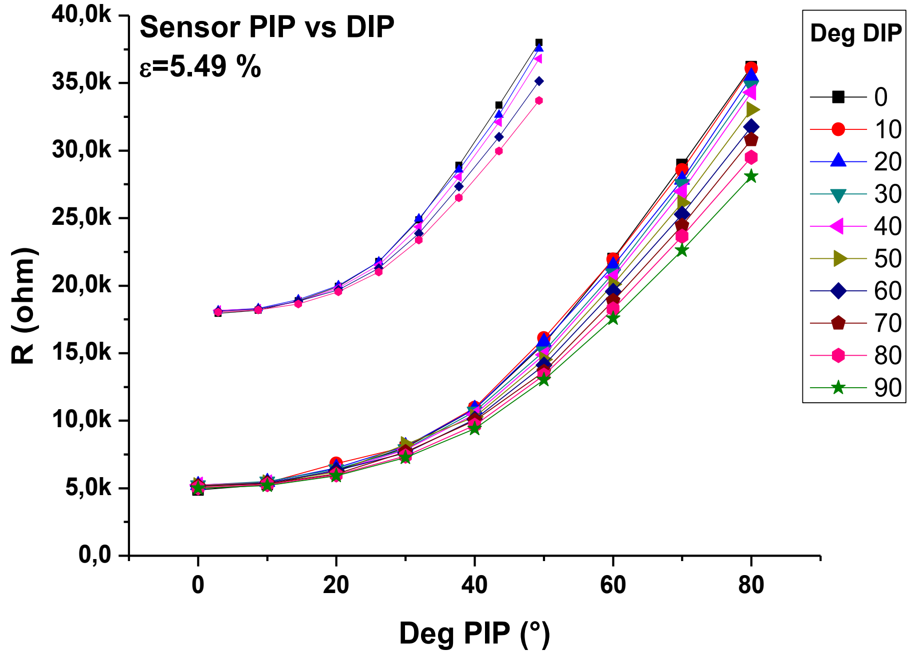

Figure 47. *PIP sensor for DIP bending*

At the end the DIP joint sensor's behavior was investigated. It not suffer of any translations. The properties are reported in Figure 48 with respect the MCP sensor and in the Figure 49 with respect the PIP sensor.

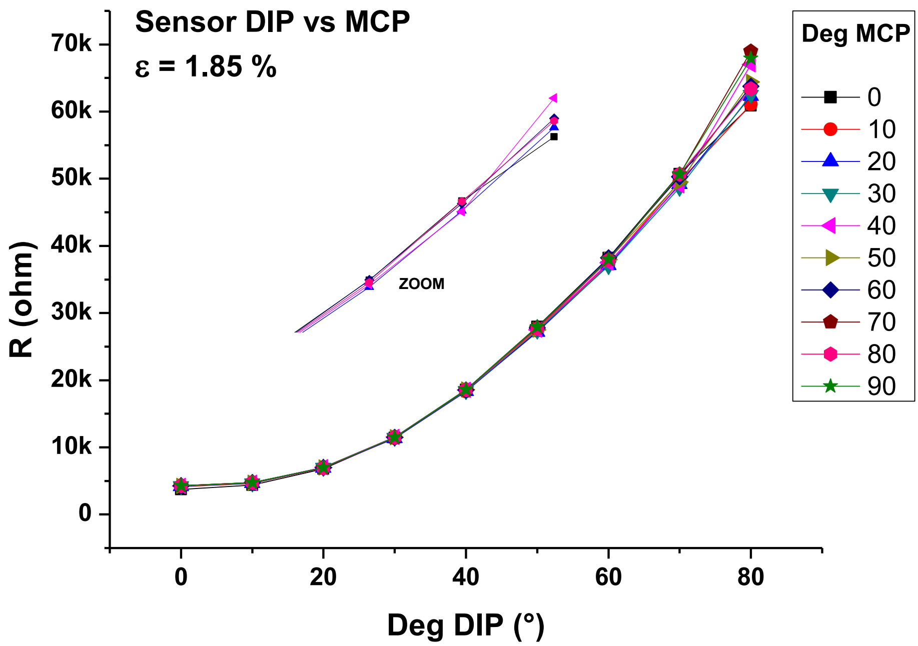

Figure 48. *DIP sensor for MCD bending*

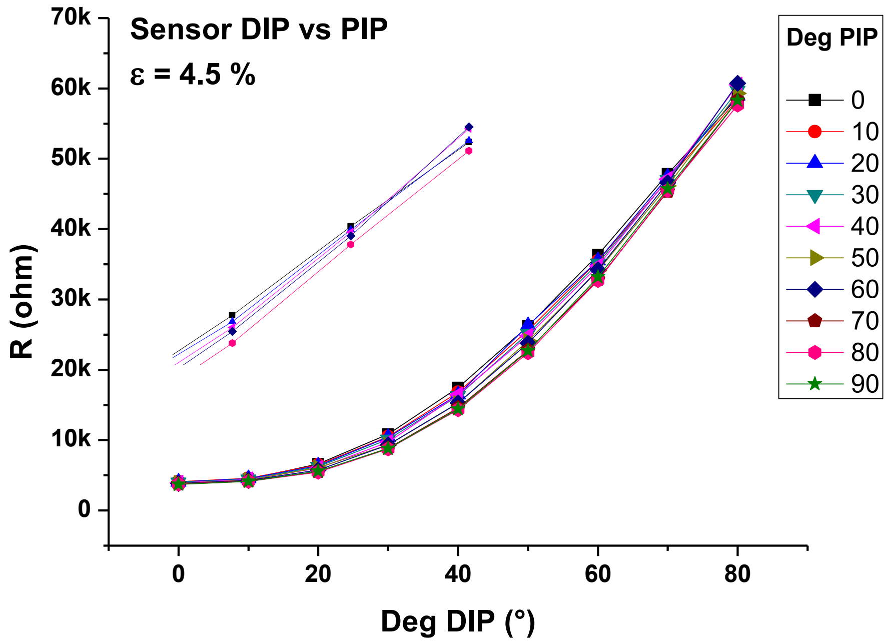

Figure 49. *DIP sensor for PIP bending*

5.3.2 Thickness Film Characterization

The “not-wanted” electrical resistance variation caused by mechanical sensors translation is probably due to not homogeneous sensor film. This explanation is supported by the reported measurements obtained with a profilometer.

Figure 50 was obtained in the centre of the sensor. The other peak is due to the silver paste applied beside the piezo material. The Figure 51 represents an enlargement in the centre.

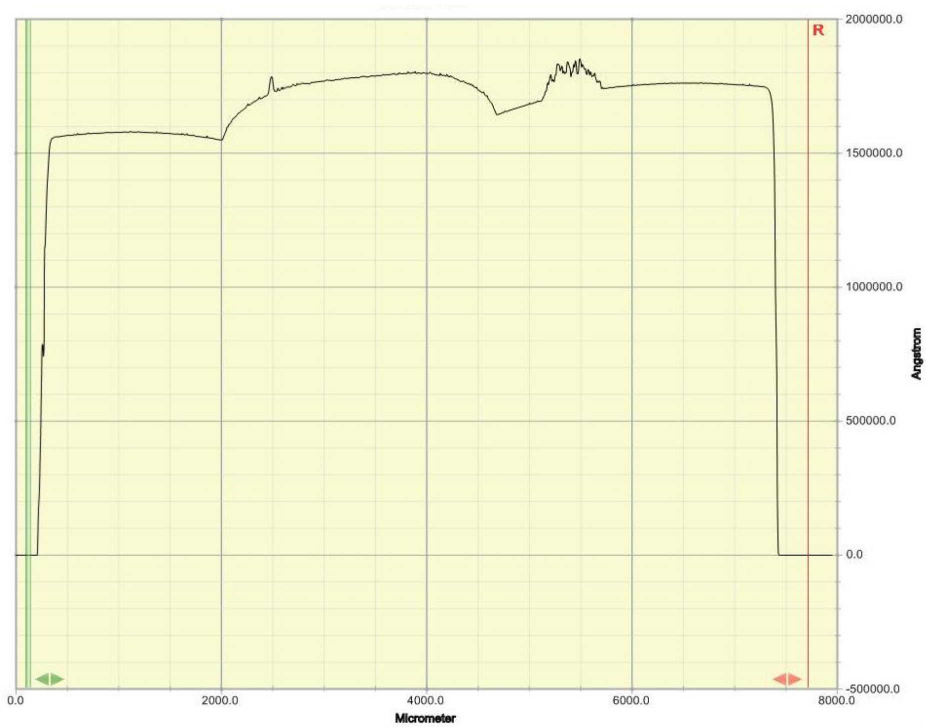

Figure 50. *Profilometer characterization*

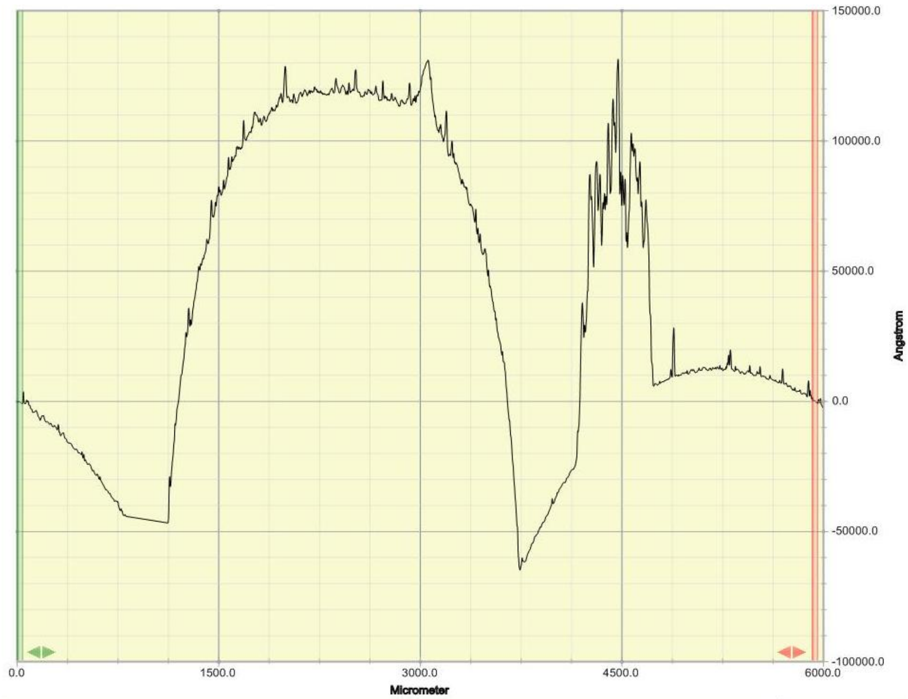

Figure 51. *Zoomed profilometer characterization*

3.6 Electrical characterization

Time-domain sensor characterization, performed with a Agilent TDS210 digital oscilloscope controlled from a PC with Labview through a GPIB link, was based on the auto-balanced bridge. The electrical schematic is shown in Figure 52.

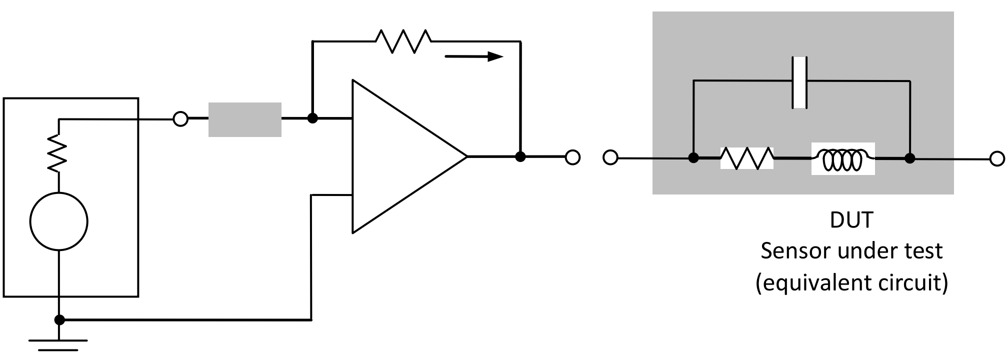

Figure 52. *Schematic of DC and RF sensor characterization with a digital oscilloscope trough a auto-balanced bridge*

3.7 Transition analysis

Stimulating the bridge with a DC voltage, it was possible to extract the sensor resistance variation with bending angle under 2-step motor rotation, from 0° to ±60° and return to 0° degrees.

From the auto-balanced bridge circuit, the sensor resistance can be easily obtained from dc voltage levels

$$I_F = -\frac{V_{CH2}}{R_F} \qquad R_{SENS} = \frac{V_{CH1}}{I_F} = -R_F\,\frac{V_{CH1}}{V_{CH2}}$$

To evaluate the resistance overshoot and the relaxation time, the resting resistance in flat position was monitored, after which the sensor was bent to a specified angle (60°), with the maximum speed rate, and the sensor resistance was monitored until the new resting resistance was established. At that point, the sensor was bent at the same rate to 0° and resistance was monitored until the measured value returned to that of the initial resting resistance. In this way, motion typical of both flexion and extension was captured, to measure the resistance overshoot and the relaxation time, in both cases, respectively.

On relaxation, however, when the original angular displacement is recovered, given the elasticity of the support substrate, the original resistance is restored. It was noticed that the resistance recovery time with increasing and decreasing rotation is independent on the speed rate.

Figure 53 figure exhibits an overshoot in the sensor resistance when the sensor is abruptly bent, and a decrease with relaxation, when the original flat position is restored.

Specifically, the peak value of the resistance was measured, along with the time required to reach this voltage peak. This time is much greater (~100 ms) than the duration over which the material was in motion. Using these two values, calibration curves, could be generated to predict bending rates and angles.

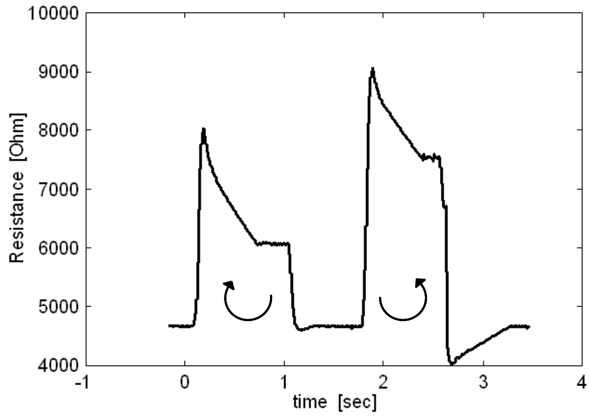

3.7.1 Steady-state equivalent circuit extraction

To investigate also as parasitic elements are correlated to bending angle, an RF characterization was performed. Stimulating the bridge with a carrier wave (CW), it was possible to yield the magnitude and phase of sensor impedance, from the auto-balanced bridge, as

$$|Y_{SENS}| = \frac{1}{R_F}\frac{|V_{CH2}|}{|V_{CH1}|} \qquad \langle Y_{SENS}\rangle = \pi + 2\pi \cdot freq \cdot t_d$$

where t_d is the time delay between the input and output scope channels.
From the sensor equivalent circuit results:

$$Y_{SENS} = Y_r + jY_i = j\omega C + \frac{1}{R + j\omega L} = j\omega C + \frac{R - j\omega L}{R^2 + \omega^2 L^2}$$

$$Y_r = \frac{R}{R^2 + \omega^2 L^2}$$

$$Y_i = \omega C - \frac{\omega L}{R^2 + \omega^2 L^2}$$

Extracting the resistance value at low frequencies, series inductance L and shunt capacitance C can be obtained from

$$L = \frac{1}{\omega}\sqrt{\frac{R}{Y_r} - R^2}$$

$$C = \frac{1}{\omega}\left(Y_i + \frac{\omega L}{R^2 + \omega^2 L^2}\right)$$

In this way, plots of resistance along with parasitic capacitance and inductance vs. bending angle can be obtained, as reported in Figure 53.

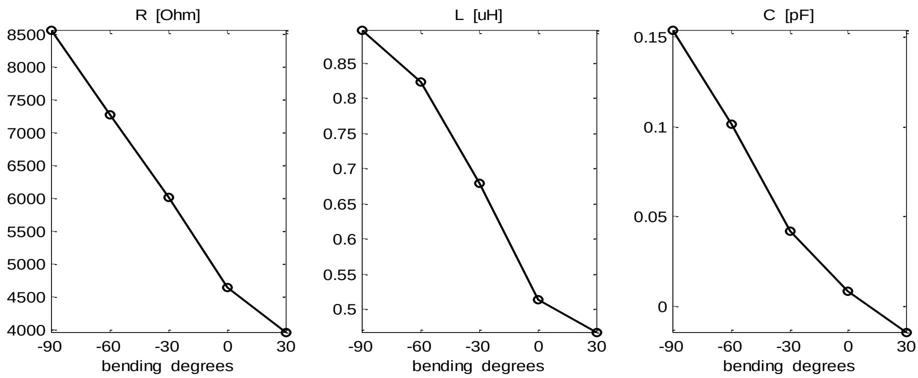

Figure 53. *Equivalent circuit parameter variations for different sensor bending under quasi-static rotations.*

Chapter 4

Glove-Based System

4.1 Introduction

Hand movement data acquisition is used in many engineering applications ranging from the analysis of gestures to the biomedical sciences. Glove-based systems represent one of the most important efforts aimed at acquiring hand movement data. While they have been around for over three decades, they keep attracting the interest of researchers from increasingly diverse fields.

In this contest my work intends to obtain an instrumental glove that permits to acquire all the human fingers movements. The architecture glove represents a real novelty with respect the others glove.

A glove-based system is defined as a system composed of an array of sensors, electronics for data acquisition/processing and power supply, and a support for the sensors that can be worn on the user's hand [20]. Therefore this section is divided into three principal parts: architecture glove, hardware signals acquisition and virtual 3D model glove.

At the start an overall discussion about the state of art is proposed. A testing procedure is utilized in order to obtain the glove repeatability, that is the fundamental parameter for several significant applications.

4.2 Technology Overview

Hands are used for interacting with and manipulating our environment in a huge number of tasks in our everyday life. It is then not surprising that a considerable amount of research effort has been devoted to developing technologies for studying interaction and manipulation and for augmenting our abilities to perform such tasks. The development of the most popular devices for hand movement acquisition started about 30 years ago and continues to engage a growing number of researchers.

In order to measure human motion, several system can be developed based on different physical principles, such as optic [20]-[21], magnetic [23], pneumatic [6], mechanic [24], electric [25], and so on. All of them have advantages and disadvantages with respect the others.

A magnetic tracker uses a magnetic field produced by a stationary transmitter to determine the position of amoving receiver element [26]. Advantages include the low-cost, reasonable accuracy, and no requirement of direct line of sight transmitter–receiver. Disadvantages include sensitivity to magnetic fields and ferromagnetic materials that may be in the workspace. Metallic objects need to be removed from the area close to the transmitter or receiver.

Ultrasonic technique is based on an ultrasonic signal produced by a stationary transmitter to determine the position of a moving receiver [24]. Ultrasonic trackers do not suffer from metallic interference. However, they suffer from echoes from hard surfaces and require direct line of sight from transmitter to receiver. If an object obstructs the line of sight between an ultrasound transmitter and receiver, the tracker signal is lost. Update rate is approximately 50 datasets/s, less than half that of magnetic trackers.

Optical technology uses optical sensing to determine the real-time position/orientation of an object [26]. This is no invasive technique and it is based on cameras and markers to acquire movements. In the other side there are several limits, such as the visibility (i.e. hand's palm), it needs large rooms, it's expensive and it occurs an intensive training for the subject.

An inertial tracker is a self-contained sensor that measures the rate of change of an object's orientation or the rate of change of an object's translation velocity [26]. Advantages include sourceless operation with theoretically unlimited range, no line-of-sight constraints, and very low sensor noise. A major disadvantage is that to derive position or orientation, the output of inertial trackers must be integrated and the result is sensitive to drift and bias of the sensors.

In this complex scenario, my work is based on piezoresistive bend sensors. because our aim was to realize long term measures taking into basic consideration the realization costs, and one bend sensor's commercial cost can be as low as few dollars. These sensors act as analog resistors since are made of carbon resistive elements printed on a thin flexible substrate. When the substrate is bent towards the printed side (outward bend) the resistive part increases its resistance value. With a backwards (inward) bend commercial sensors usually give no meaningful results since a really poor decreasing resistance variation is reported. In any case this latter undesirable (for some applications) result can be avoided if devices with piezoresistive sensor elements are smartly developed and adopted.

4.3 State of art

The first glove-based systems were designed in the 1970s, and since then, a number of different designs have been proposed. In the precedent paragraph a technology overview is proposed: fiber optic, Hall-effect sensors and piezoresistive sensors (my choice) is the principal utilized possibilities.

Here an explanation about most significant parameters is summarized in Figure 54.

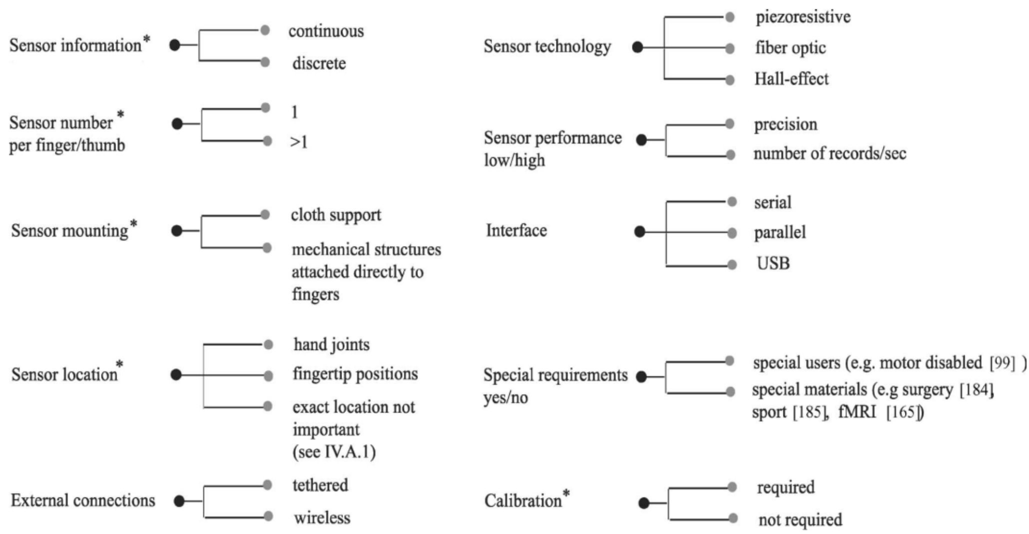

Figure 54. *Most significant parameters in order to realize an electrical glove*

In particular, my experience suggested that the sensor mounting and the sensor location on the glove are the possible parameters to obtain an improvement respect the others research group. Is it possible to bind both the ends of the sensors? What is the exact sensor number for each finger in order to obtain an excellent repeatability? What is the best glove material? These and other significant choices have been led to different glove-based system developed by business companies or research group. So I located the best ideas in the glove-based system realization.

The first glove prototype included the Sayre Glove. The Sayre Glove was developed in 1977 by Thomas de Fanti and Daniel Sandin based on the idea of Rich Sayre. It used flexible tubes with a light source at one end and a photocell at the other, which were mounted along each finger of the glove. As each tube was bent, the amount of light passing between its source and photocell decreased. Thus, voltage from each photocell could be correlated with finger bending [27].

Designed to be a multipurpose device, the Data Glove quickly gained the attention of researchers in different fields and a number of devices similar to it were proposed. A low-cost version of the Data Glove, the Power Glove [28][29], was commercialized by Mattel Intellivision as a control device for the Nintendo video game console in 1989 and became well known among video games players. It used resistive ink printed on flexible plastic bends that followed movements of each finger to measure the overall flexion of the thumb, index, middle, and ring finger.

Developed by James Kramer at the Virtual Exploration Laboratory of the Center for Design Research (CDR) at Stanford University, it was commercialized by a CDR spin-off, Virtual Technologies, Inc. (Palo Alto, CA) in 1992. It comes equipped with 18 or 22 piezo-resistive sensors. The 18-sensor model features two bend sensors on each finger, and four abduction/adduction sensors, plus sensors measuring thumb crossover, palm arch, wrist flexion, and wrist abduction/adduction. The 22-sensor model features four additional sensors for measuring DIP joints flexion. Calibration is needed to make glove measurements insensitive to differences in users' hands, finger length, and thickness and convert sensor voltages to joint angles. It is performed with the VirtualHand calibration software by having the user flex their hand a few times and editing the gain and offset parameter value for each sensor to best match the motion of the virtual hand to the physical hand. A wireless version of the CyberGlove (CyberGlove II) was commercialized in 2005. It today represents perhaps the best possible solution, but the problem is about the excessive cost. The software tool is very expensive too.

The Humanglove (1997) is commercialized by Humanware Srl (Pisa, Italy) [23]. It is equipped with 20 Hall-effect sensors that measure flexion/extension of the four fingers MCP, PIP, and DIP joints and flexion/extension of the thumb TMCP, metacarpal phalangeal (MP), and interphalangeal (IP) joints, as well as fingers and thumb abduction/adduction; two additional sensors measure wrist flexion and abduction/adduction [23]. Glove calibration is similar to that of the CyberGlove and is performed through a software package called Graphical Virtual Hand, which displays an animated hand that mirrors movements of the user's hand.

Gentner et at. [30] developed in 2009 a low cost sensor glove. Flexpoint sensors are utilized and modified in order to obtain a linear response and to optimize measurement accuracy. The low material costs (<US$ 500) and easy manufacturing make this solution interesting for widespread use in research, clinical and rehabilitative settings.

4.4 Architecture Glove I: Arched Sensors Configuration

Here we adopted bend sensors as transducers. This is because of their lightness, cheapness and the fact that we experienced a new way of application which, differing from the usual literature way of usage [7][20], prevents these sensors from being stressed by elongation and torsion forces. In such a way it is potentially avoided the problem that some unwanted forces may prejudice the sensor from returning to its initial state because of its non perfect elasticity, so to lead to a drift in the sensor characteristics during its life of utilization. Moreover, in this way we potentially prevented the "force of the hand grip" from leading to the so defined "source of noise in the sensor output" [32]. In this configuration the sensors are applied on the glove in correspondence to the dorsal part of the hand, in a way that, in order to measure flex/extension movements, the sensors themselves assume an arched form when the fingers joints are in flat position, and follow the fingers profiles with closed fist, as Figure 55 schematized. The sensor arched form is also utilized for measuring addu/abduction movements as in Figure 55.

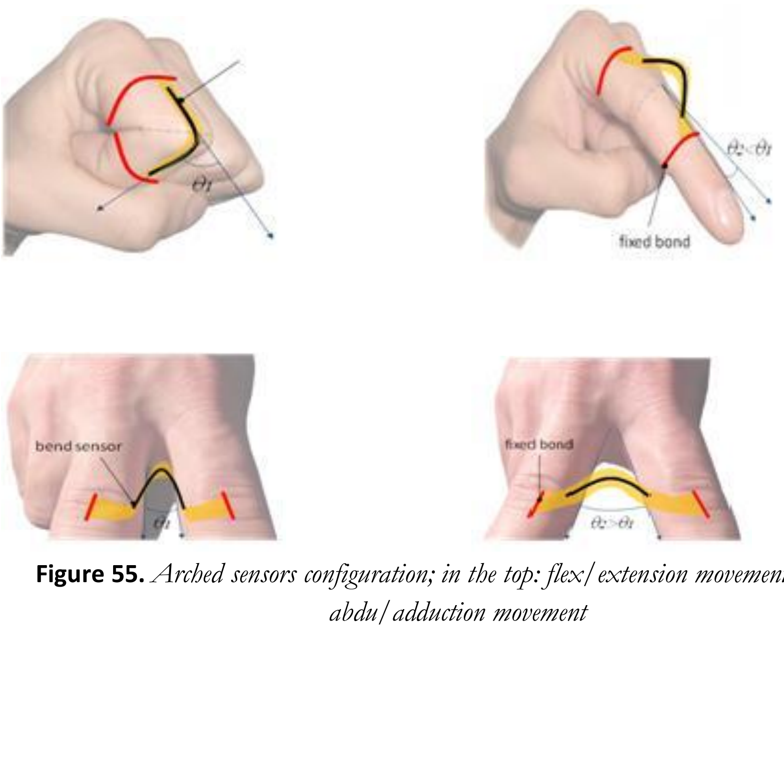

Figure 55. *Arched sensors configuration; in the top: flex/extension movement; in the bottom: abdu/adduction movement*

Since overall measurement performances of the bend sensors can be influenced by support onto which they are mounted I preferred to adopt a glove with a reduced degree of elasticity. In such a manner the sensor responses depend for the most part on their arched form and in a minimum way on the change, with joint movements in the inter-distance between sensor ends due to the glove elastic behavior.

4.4.1 Arched Sensors Considerations

Bending measurement set-up reported in Figure 18 is utilized.

In order to characterize the sensor behavior, the proposed arched configuration was replied on the set-up with the sensor ends both taped on the hinge wings, assuming a hump figure. The two sensor bonds were obtained with two rectangular hard plates which allowed to vary the distance between the sensor ends from 0.5 to 8 cms. The two bonds permit to fix the sensors in a way that, when the hinge is flat, the sensor is positioned at its maximum bending, while it lies adherent to the hinge profile with the hinge on its maximum predetermined angle.

The instrumented glove was developed on the basis of commercial piezoresistive sensors provided by Flexpoint. Depending on which was the finger joint to be measured, i.e. distal- proximal- metacarpo- phalangeal, it was used a specific commercial available flexible sensor: 2.5cms, 5.1cms and 7.6cms long respectively.

In order to investigate how these commercial sensors can be adopted for different hand size, we measured their behavior when the inter-distance between the taped ends is reduced as in Figure 56.

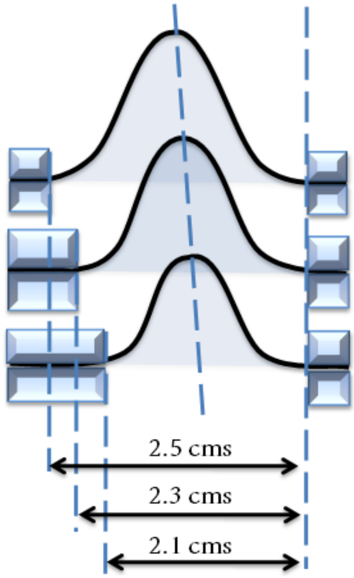

Figure 56. *Inter-distance reduction between fixed ends.*

Figure 57 reports the results obtained in the resistance value variations investigating, as an example, the inter-distance reduction of the sensor of 5.1cms in length.

It can be noticed how the variation in resistance values is increased with reducing the inter-distance from 2.5cms to 2.1cms. This particular and uncommon aspect that we examined revealed an interesting sensor behavior since the reduction of the inter-distance correspond to a decrease of the curve radii of the carbon sensitive part of the sensors.

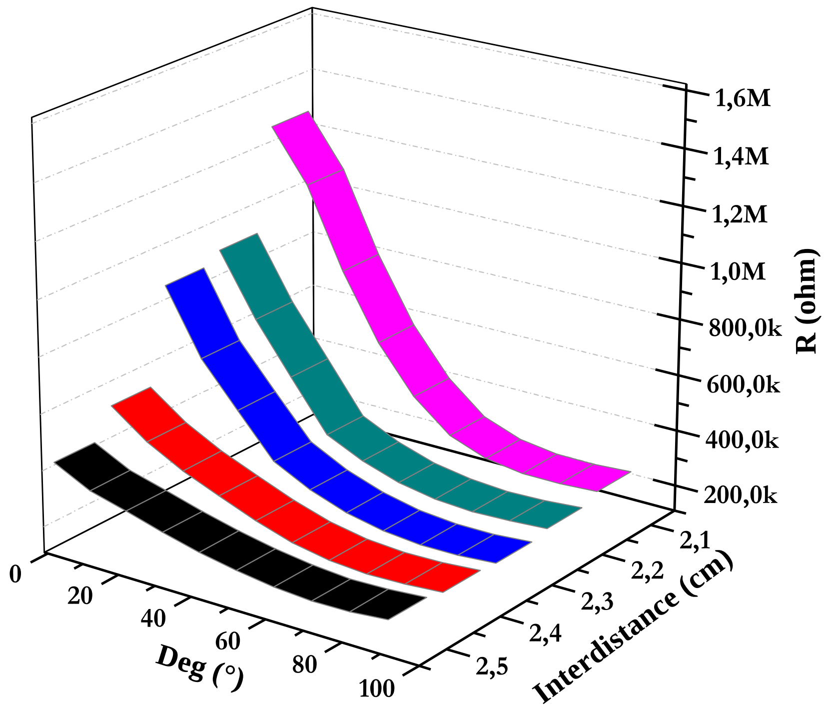

Figure 57. *Resistance variation vs bending angle and vs inter-distance between sensor taped ends.*

The most interesting consideration is that the more the investigated distance is reduced, the more the resistance variation is increased, leading to evident advantages. Anyway, it must be considered that there is a limit to the distance reduction, in the sense that it cannot become shorter than the joint being measured.

Being the curve relative to the 2.1cms the most interesting one, error values relative to the measured resistance were analyzed. Figure 58 regards this error evaluation. This was obtained starting from 0° up to 90° of bending angle with a step of 10°. The standard deviation increases for higher bending angles, while it is unimportant for lower ones.

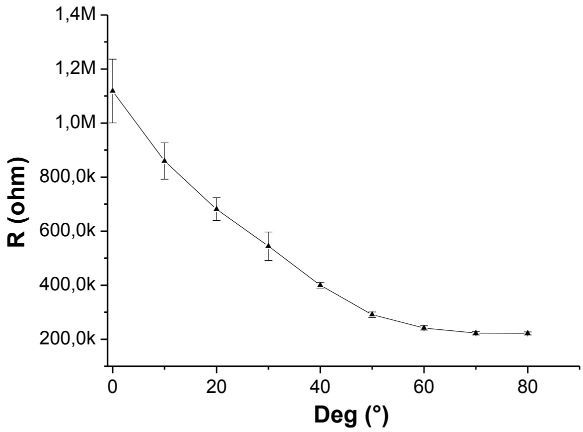

Figure 58. *Error evaluation for measures of the 5.1 cms long sensor, taped ends at a inter-distance of 2.1 cms*

For a comparison purpose, in Figure 59 are reported the relative resistance variation versus bending angle for the 7.6cms, 5.1cms, 2.5cms length sensors with the inter-distances end taped respectively reduced to 3.5cms, 2.5cms and 1.2cms. Again the measured results are obtained when the bending angle is varied from 0° to 90° with a 10°step.

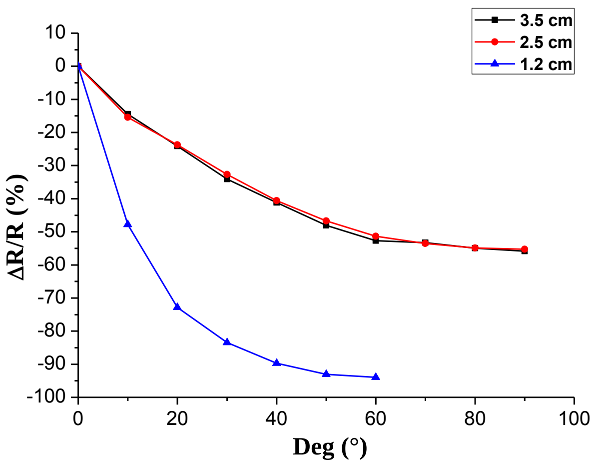

Figure 59. *Relative resistance changes vs bending angles for three different sensors*

The sensor behavior shows a saturation aspect at higher bending angles. This behavior was not a problem for two main reasons: our system was able to discriminate bending values even when in the range of 80°-90°, thanks to the conditioning electronic circuitry, in addiction the thickness of the glove precludes the possibility of reaching physiological angles which fingers can arrive when out of the glove.

4.4.2 Conclusions

Arched sensors configuration is a real novel possibility. Typing both the sensors ends is the principal cause of a limited glove lifetime. My aim is to avoid all of this. The proposed architecture is really simple to obtain; the sensors are stopped thanks to a commercial flexible adhesive paste.

Two are the found problems: the greater glove encumbrance and the minor electrical resistance variation. So the preference is on the next presented architecture solution.

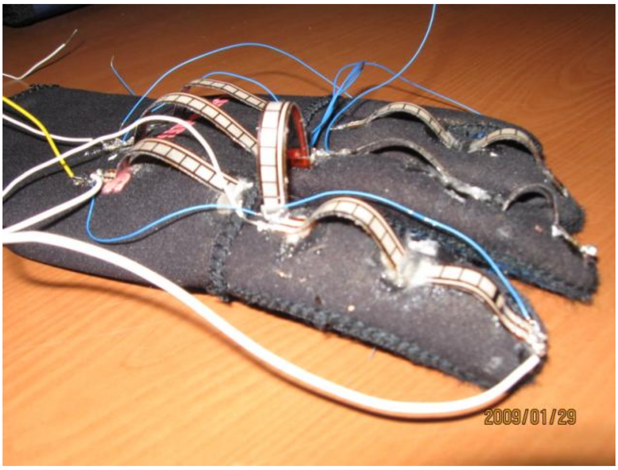

Figure 60. *First home-made prototype of the arched form configuration equipped with commercial bending sensors*

4.5 Architecture Glove II: Array Sensors

The sensors mounting on the glove is a fundamental step for a good-done glove repeatability. In the field of piezoresistive materials there are different solutions proposed by some people. It is typical that the strain sensors are mounted on the dorsal part of the glove with two different blinds at the sensor ends[25]. This solution can represent a problem due to the not perfectly elasticity of the sensors that suffer of an electrical resistance increase not wanted. Other people utilized an architecture without a real glove [31], but this is a problem in order to obtain a good accuracy when the structure is take off and wear.

Our research starts with the aim to find an ad-hoc piezoresistive sensor for the glove. So we investigated different type of sensors, such as home-made sensors [15], elastic sensors, capacitive sensors and different types of commercial bend sensors. Flexpoint sensors today represent the best solution for strain measurements showing an excellent electrical resistance variation and a good repeatability. All these mentioned sensor exploitations as literature reports are interesting from different points of views. Anyway all of them have as minimum common denominator the fact that each sensor is fully independent and act separately from each other. This aspect presents some advantages but some drawbacks too.

Here we propose a different architecture with sensors disposed in an array configuration. The design has been made in collaboration with the Flexpoint Sensor Systems Inc. (www.flexpoint.com). In our design three sensors are placed adjacent on the same substrate, as depicted in Figure 61. The array sensors were modified with the aim to give an improvement of their mechanical resistance. So it was inserted a flexible rubber substrate on the bottom of the array with a thickness of 1.2 mm. The obtained result permits to strike out the undesired micro-strains on the sensors.

Figure 61. *Array sensors realized in collaboration with the Flexpoint*

We placed each array onto the dorsal part of each finger, every sensor on every joint, to realize our complete data glove, named Hiteg-glove, stands Hiteg (Health Involved Technical Engineering Group) our group name.

The array were mounted on a commercial glove made by a mix of lycra and cotton materials with a reduced elasticity. The glove was enough comfortable during donning, doffing and use, as reported by users.

The array was designed in a way that sensors which measure the proximal interphalangeal (PIP in Figure 62) and the metacarpophalangeal (MCP) joints have the same resistance value when unbent (finger flat position) while the sensor on the distal interphalangeal joint has the half of that resistance value. This was an helpful expedient in designing the conditioning electronic circuitry. Regarding the sensor utilized to measure postures of the metacarpophalangeal joint, a sort of slot was realized in the central part of its longest dimension (see array Figure 63), so to insert in it a tip previously fixed to the glove (see Figure 63) and to obtain an array sliding movement constrained into a predefined rail.

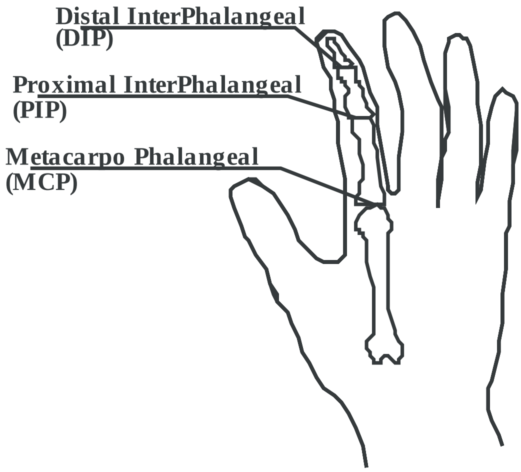

Figure 62. *Human hand joints*

The array's edge, in correspondence with the finger nail, was fixed to the glove. The array was then not inserted in a closed sleeve but in a open pocket a bit wider but not longer than the array itself. When finger flexed, the pocket's open end allowed free sliding movements for the array maintained aligned with the finger thanks to the tip inserted into the slot of the array.

Because of the sliding mechanism, the part of the sensor being flexed changes according to the amount of bending, as schematized in Figure 63. This can become an interesting fundamental aspect to trade on in next future in order to realize sensors with non uniform geometries so to obtain a desired pre-imposed electrical resistance variation vs flexion force function. For example it was possible to obtain a linear variation of electrical resistance vs bending deformation for the Flexpoint sensors.

(a)

(b)

(c)

Figure 63. *Sliding mechanism of the array sensors in different views depending on the bending*

4.5.1 Array Advantages

I experienced some advantages in utilizing sensors in array configuration, meaning three sensors on a single substrate, used to measure the three joints of the same finger:

- One single substrate assures sensors to be kept always aligned with each other; otherwise sensors with the usual physical separation can produce inter misalignment during the glove usage
- The array is guaranteed to remains always aligned with the respective finger thanks to the predesigned rail configuration
- All the electrical contacts can be grouped in one tip of the array, so greatly reducing the problem of the tangle of all the electrical wires to be connected to the external circuitry
- The array assures a single electrical mass for three different sensors, so the reference potential is exactly the same for all and electrical potential shifts from the reference value are avoided
- One array design can be easily adopted for all the fingers since it is sufficient to scale the design according to the finger sizes.

4.6 Testing Glove

I validated my novel array configurations by mean of the standard measure procedure. As a reference test method we adopted the generally accepted one proposed by Wise et al. [32] (1990) and expanded by Dipietro et al. [23] (2003), as further re-arranged by Simone et al. [25] (2007), but with some minor differences to overcome recognized problems.

The tests were performed on six healthy individuals, four men and two women. All of them were right-handed as determined by the Edinburgh Handedness Inventory (Oldfield, 1971) and had normal hand function. We used only a single version of the glove for all subjects, that is a *M* size which fitted well for each subject, except for subject 3 having a hand size slightly larger and subject 6 with a hand size slightly smaller respect to size *M*. The glove was placed on the dominant right hand for all. Before performing the predetermined tasks, all people were asked to execute some random movements for minutes so to become confident with the data glove, with the advantage of a visual feedback of a hand avatar reproducing the same movements on a pc screen.

Customized plaster molds (Figure 64) were created individually for each subject, in a way that the hand joints could bent forming from 10° to 60° angles, depending on the particular joint and subject.

(a) (b)

Figure 64. *Realized plaster mold (a) two different molds (b) hand positioned on the mold*

Test steps can be summarized as:

Test A - Mold grip and glove on between data acquisition: The subjects, previously trained, were asked to hold (not to clench) the mold for 6 s and to release the mold placing the hand in a pre-imposed flat position on a desk for additional 6 s (this corresponds to 1 trial, for which the X-th data is acquired, averaging at least 130 measures), cycling 10 times (the average $\bar{X}$ of all the ten X data forms 1 *data block*) without removing the glove. The forearm was in a prone-supine and the wrist in a neutral position. The procedures were repeated 10 times till obtaining 10 *data blocks* in total.

Test B - Mold grip and glove off between data acquisition: differing from *test A* the subjects were asked to take the glove off between each cycle, so to evaluate donning and doffing effects on the measurement process

Test C - Hand flat and glove on between data acquisition: The subjects were asked to put the hand flat on a desk with the wrist fixed in a neutral position while the forearm pronated. Then the subjects had to clench the hand lightly in maximum flexion and to return it to the flat position. Every actions for the standard duration of 6 s (1 trial) and cycling 10 times to form 1 *data block* always without removing the glove. The procedures were again repeated 10 times till obtaining 10 *data blocks* in total.

Test D - Hand flat and glove off between data acquisition: differing from *test C* the subjects were asked to take the glove off between each cycle

During the tests we voluntarily utilized for the conditioning electronic circuitry a wired arrangement to be confident to do not add eventual errors due to the wireless transmission system.

4.6.1 Proposed Differences from the Standard Test Method

Differing from the reference test method, we realized the form of the molds with the aim to assure a comfortable closing hand position (see fig. 4) rather than arrange a roughly cylindrical aspect. In such a way we could avoid the Dipietro et al.'s (2003) observed problem that changes in grip force affected measured values, since no force is necessary to keep the hand on the position imposed by the mold. In such a manner it was also not necessary to compensate recommending the subjects to grip the mold with as low of a force as possible (Simone et al., 2007).

Again as a minor difference with the reference test method, the subjects had feedbacks of their movements via a virtual hand avatar on a computer screen reproducing the same movements, and an automatic beep informed when to change the hand position.

4.6.2 Results and Comments

For the *j*-th data block and the *k*-th sensor, we calculated the range $R_K = max_j(\overline{X_{jk}}) - min_j(\overline{X_{jk}})$, its average value $\overline{R_k}$ and the X_{jk} standard deviation *SD* values. The results were automatically obtained thanks to an acquisition software. In Figure 65 is reported an example of a typical data block in terms of Digital Volts (*DV*) vs number of samples. There are 14 degrees of freedom corresponding to hand joints interested in the flex-extension movements.

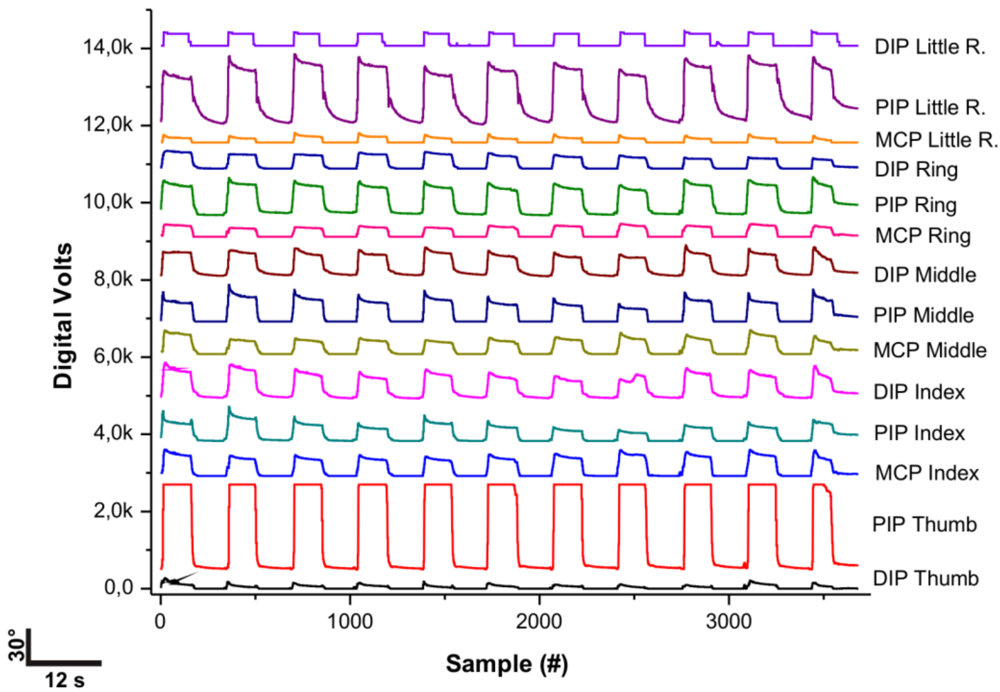

Figure 65. *Typical obtained data block. On the axis, digital volts vs samples number are reported for all the hand joints*

The acquired data block were then automatically converted in the values defined in order to evaluate the glove repeatability.

To overcome the problem of no meaningful measures acquired during the transition times, we eliminated with an automatic filtering procedure the 5% of values at the very begin and the very end of each trial. Indeed this choice was less stringent with respect to others reported in literature (Simone et al., 2007).

Subject	Test A		Test B		Test C		Test D		Total	
	Rk	**SD**	**Rk**	**SD**	**Rk**	**SD**	**Rk**	**SD**	**Rk**	**SD**
(Man) 1	3.77	1.41	5.04	1.55	2.49	0.42	1.02	0.34	3.07	0.93
(Man) 2	2.49	1.17	6.47	1.29	2.30	0.50	2.06	0.50	3.33	0.86
(Man) 3	4.29	1.42	6.74	1.88	2.48	0.45	2.18	0.51	3.92	1.06
(Man) 4	3.75	1.51	4.40	1.54	2.09	0.53	1.12	0.68	2.84	1.06
Male Mean	3.58	1.38	5.66	1.56	2.34	0.48	1.60	0.51	3.29	0.98
(Female) 5	4.16	1.66	5.05	1.88	2.27	0.78	2.07	0.48	3.39	1.2
(Female) 6	4.98	1.73	6.99	2.15	2.80	0.83	2.16	0.78	4.23	1.37
Female Mean	4.57	1.69	6.02	2.02	2.54	0.80	2.13	0.63	3.81	1.28
Overall Mean	**3.91**	**1.48**	**5.78**	**1.72**	**2.40**	**0.58**	**1.77**	**0.55**	**3.46**	**1.08**
Wise '90	6.5	1.94	6.8	2.6	4.4	2.2	4.5	1.6	5.55	2.08
Dipietro '03	7.47	2.6	9.38	2.96	5.88	1.92	3.84	1.23	6.64	2.17
Simone '07	5.22	2.44	-	-	1.49	0.5	-	-	-	-
Gentner '09	6.09	1.61	7.16	2.26	3.98	1.28	2.61	0.86	4.96	1.5

Stands the obtained measured results reported in tab. and graphically represented in Figure 66 and Figure 67, we improved the performances of the data glove based on bend sensors with respect to the ones reached in literature. Let's consider, for instance, the measures concerning Tests *A* and *B*, for which we registered an average R_K=4.84°±1.34° and *SD*=1.6°±0.28° values, very interesting if compared to the meaning reported values R_K=6.63°±1.86°, *SD*=2.10°±0.56° [Gentner, 2009] and R_K=8.42°±1.35°, *SD*=2.78°±0.25° (Dipietro et al., 2003). Again an improvement was registered regarding the Tests *C* and *D* measurements since we obtained the values of R_K=2.08°±0.5°, *SD*=0.56°±0.16° compared to R_K=3.29°±1.29°, *SD*=1.07°±0.42° (Gentner and Classen, 2009).

If we consider a more stringent filtering procedure, eliminating more than only our 5% of values as previous work suggests (Simone et al., 2007), we obtain for Tests *A* and *B* the values of R_K=4.76°±1.34° and *SD*=1.58°±0.3° and for

Tests *C* and *D* the values of R_K=2.0°±0.65°, *SD*=0.5°±0.17° so even with a small further improvement.

With respect to the average, slightly different was the behavior of subject 3 (man), who obtained results just a little worst than the others. This was due to his hand size a bit larger than our standard *M* glove size, so he experienced some difficulties in closing the hand, when fingers assumed high angular bending degrees.

Differing from previously reported results (Dipietro et al., 2003), we experienced no meaningful differences between men and women tests, being the *SD* averaged value for men 0.98 and for women 1.29.

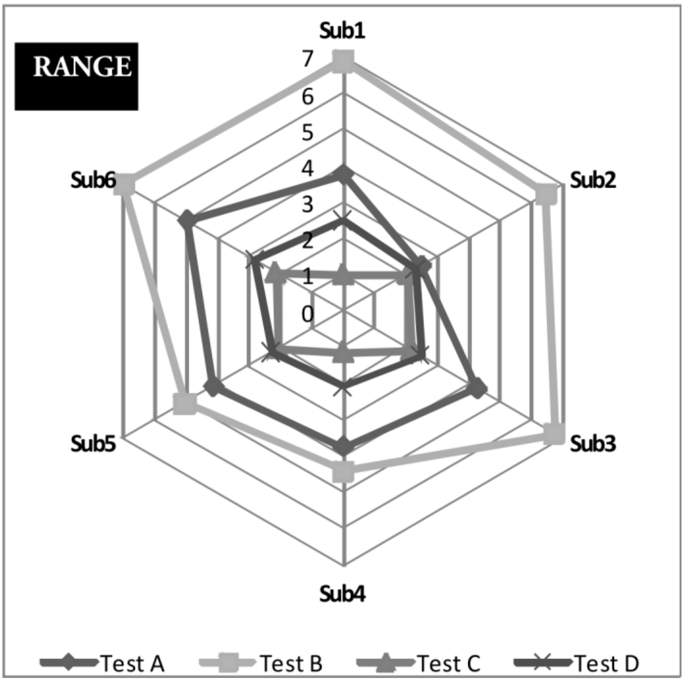

Figure 66. *RANGE:* c*omparison between results and tests*

Analyzing the Figure 66 it appears evident how the Test *B* had relatively worst results, while the data glove performances were better for Test *C*. This can demonstrate how our rail system repositioned quite well the array to flat arrangement with the hand returning to flat posture.

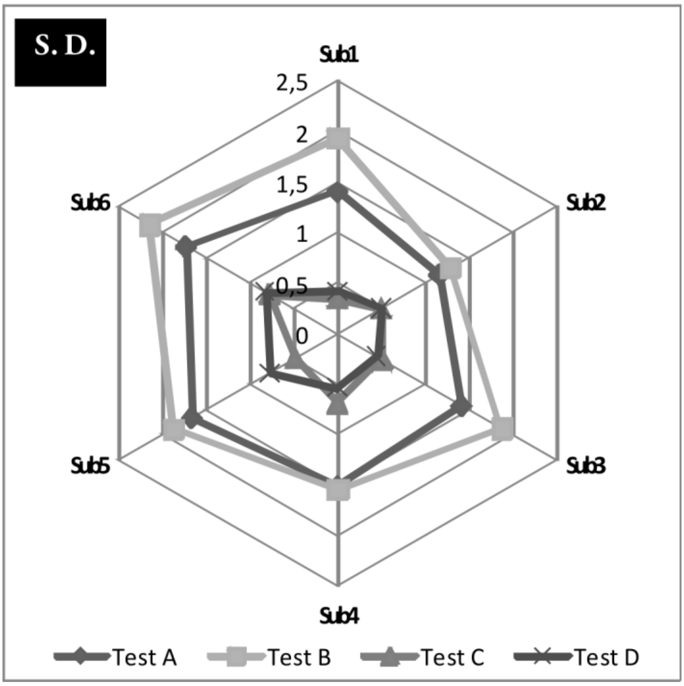

Figure 67. *S.D.:* **c***omparison between results and tests*

Referring to Figure 68, the results can be further improved if we do not consider the thumb values. In fact we adopted the array configuration with three sensors even for this finger, but this is not the ideal occurrence. Probably it would be better to adopt an array made of two sensors plus one sensor in a different position, but this aspect will be investigated in future.

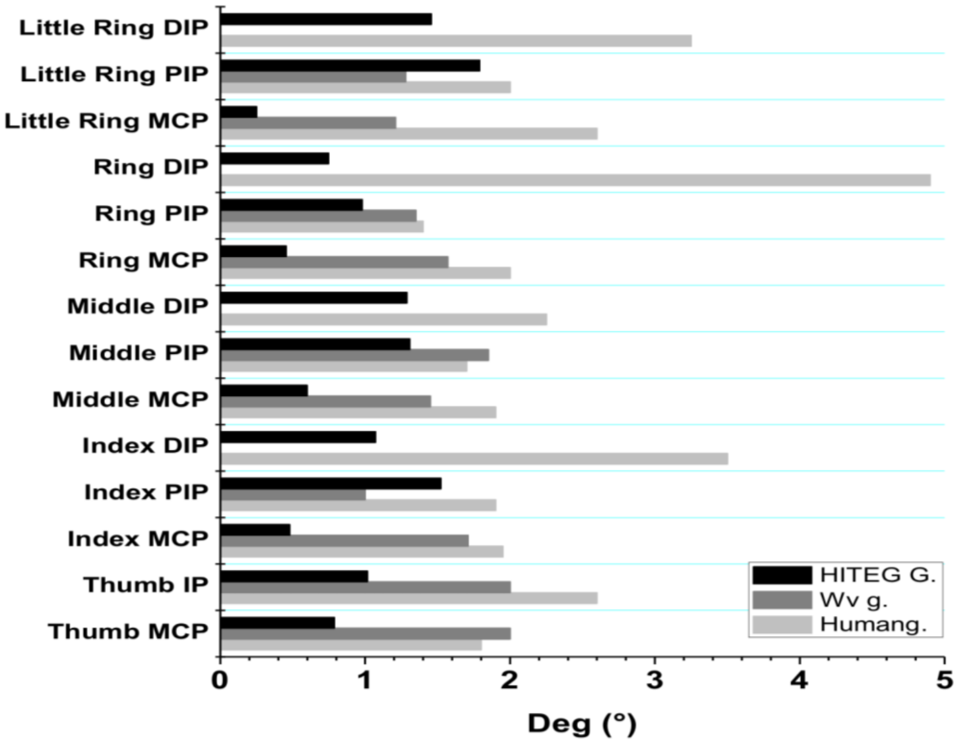

Figure 68. *Comparison between HitegGlove and the others two best presented gloves for every human hand joint (excepted thumb joints)*

4.6.3 Conclusions

It was demonstrated how the novel sensor array here proposed can be successfully exploited to realize data gloves with improved performances. The introduction of the array configuration demonstrated to represent an interesting improvement in accuracy and repeatability of data glove measurements. This is mostly due to the already discussed advantages which the array configuration can assure with respect to the standard single sensor layout. In particular the single substrate for the three sensors placed on the three joints of one finger guarantees the avoid misalignment among sensors while the rail configuration assures always array-finger alignment maintenance. Our work attests also an high correlation between R_k and *SD* parameters as just previously reported (Wise et al., 1990; Gentner and Classen, 2009).

As a final nice consideration, since the array realizes a tidier data glove, according to the Birkhoff's (1933) curious speculative work, we can state to have increased the aesthetic value of our previous works (Saggio et al., 2009).

Chapter 5

Applications: Virtual Reality

5.1 Introduction

Virtual reality (VR) is a technology which allows a user to interact with a computer-simulated environment, whether that environment is a simulation of the real world or an imaginary world.

Humans perceive external reality through the five senses of hearing, sight, taste, touch and smell. If one or more of these sensed inputs is replaced by a machine generated input then that person will to some degree enter an artificial reality. So watching a cinema or TV film, or using a machine such as an aircraft training simulator, has some degree of artificial reality even though most sensed inputs come from normal reality. However, both research and fiction have suggested that a person receiving most of their inputs from machines would enter an artifical reality, and coined the phrase "virtual reality" (VR) to describe this state.

So one possible definition of VR is "The illusion of participation in a synthetic environment rather than external observation of such an environment. VR relies on three dimensional (3D), stereoscopic, head tracked displays, hand/body tracking and binaural sound. VR is an immersive, multisensory experience". Another one defines it as "I cubed, immersion, interaction and imagination"[33].

5.2 Glove-Based Systems

Everyday our hands allow us to interact with external environment and to manipulate objects transmitting information thanks to the tactile sense. So you can imagine that are and there will be a lot of scientists and researchers with the aim to acquire dates from hand movements. In the previous Chapter 4 I presented a specific discussion about several aspects of a glove-based system. I focused on three fundamental parts:

- Bending sensors architecture;
- Hardware acquisition;
- Software implementation.

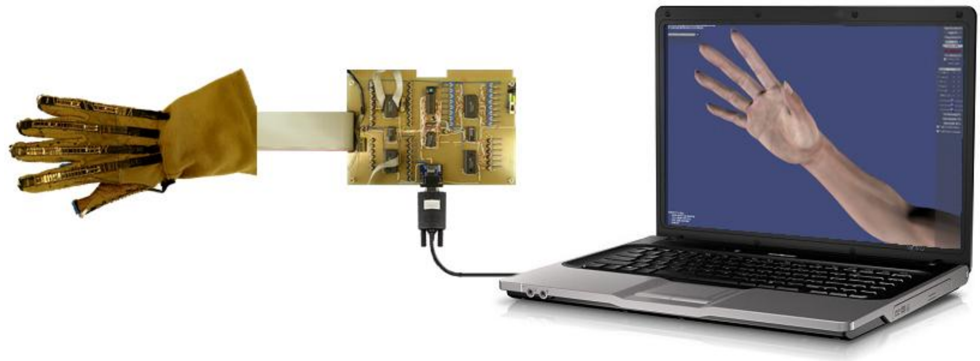

Figure 69. *Hiteg glove-based system*

To date, several sensors architectures were already presented. Now the analysis concerns the other two fundamental parts.

5.2.1 Hardware Acquisition

The number of adopted bend sensors was 19 in order to record an equal numbers of finger's degree of freedom (DOF).

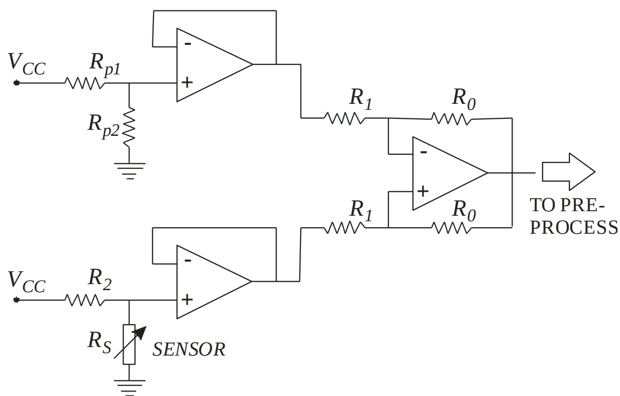

Figure 70. *HW acquisition electrical circuit: the signal is set to pre-process level*

Resistance values recorded from the sensors were converted into voltage signals and then feed into two 16 bit TI CD4067B multiplexers, followed by a Microchip MCP3202 A/D converter. A Microchip PIC16F690 microcontroller, receiving data from the A/D converter via SPI protocol, provides to address the multiplexers in order to determine which sensor's response accept and furnish data to a wireless system and then to a personal computer.

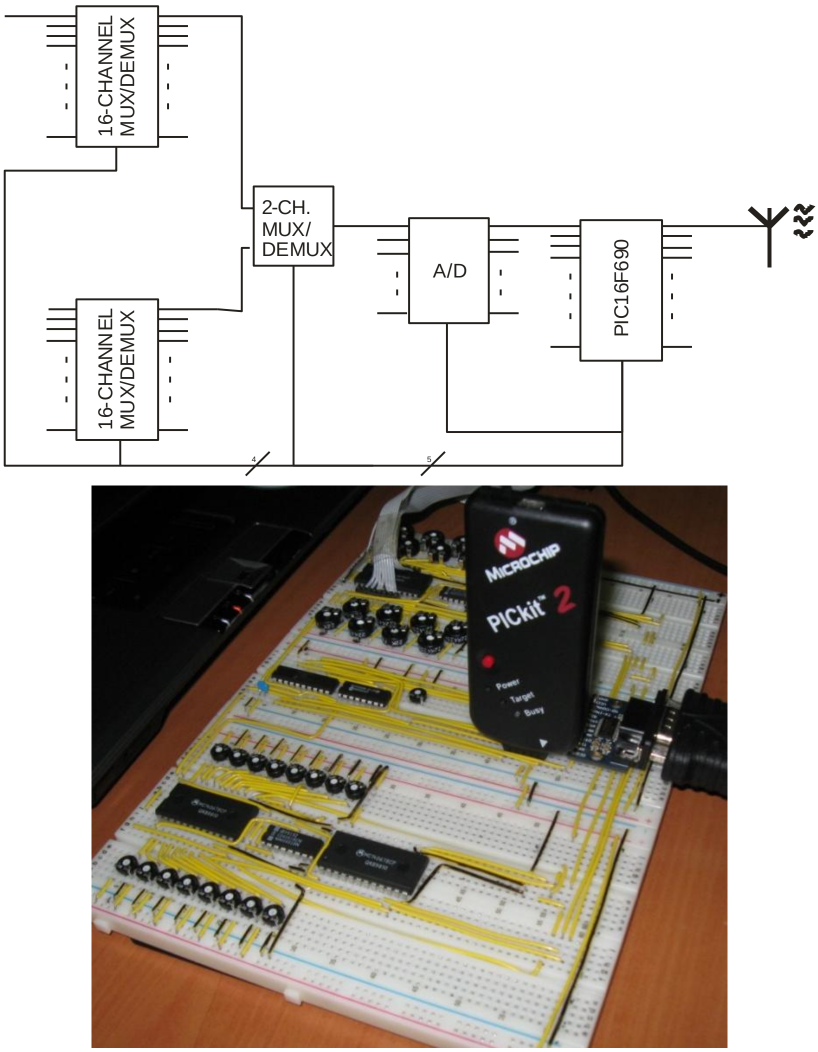

Figure 71. *HW electrical circuit: it is composed by 3 mux/demux, 1 A/D converter and 1 PIC*

The PIC16F690 microcontroller is an 8BIT FLASH MCU, DIP20, 256 byte SRAM, presents an EUSART module for the serial communication, a SSP module to connect SPI, I2C interfaced peripherals and was programmed via the Microchip© PICkit™ 2.

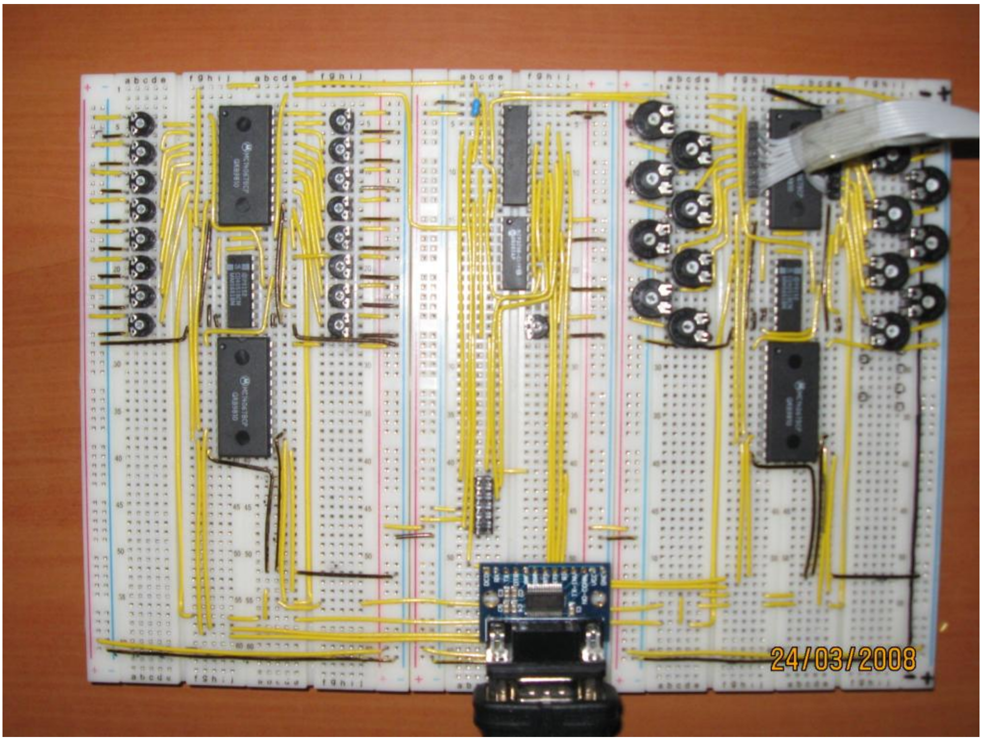

Figure 72. *Top view of hardware electronic circuit*

In order to communicate with the pc, we started with a standard serial interface. It allows to obtain a simple and fast communication with the PIC. Today the port provides 192 kbit/second. The communication is an asynchronous type in order to guarantee a real time exchange between the pc and the controller. The initial string for starting communication is shown with three typical tokens.

After several optimization, today the electronic circuit is very small and lgiht, using a dsPIC 33FJ256GP710 with 100 pin I/O. The next Figure 73 show the dsPic with the correspondent bus (3 cms * 1 cm); in the Figure 73 is reported the electronic circuit connected to a prototypal glove.

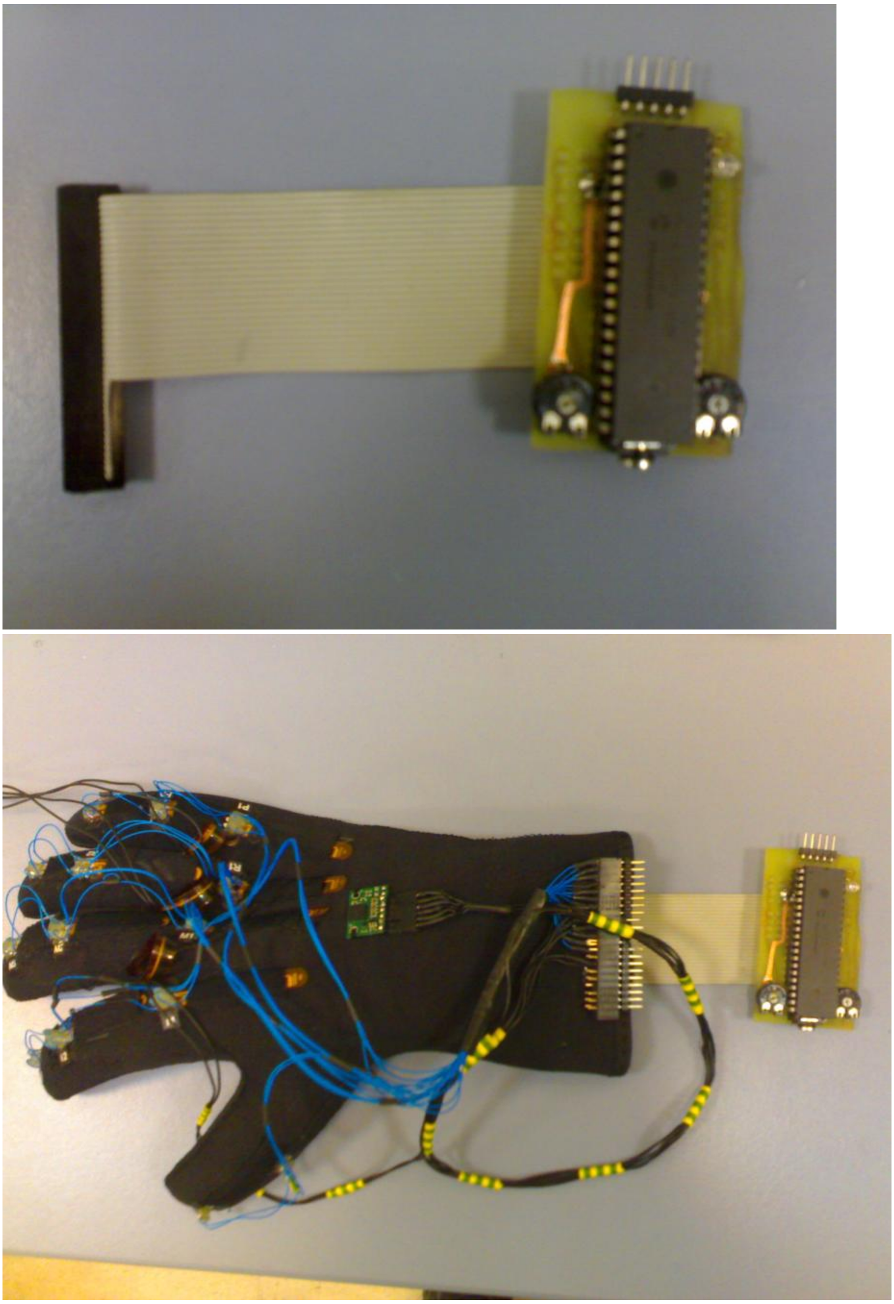

Figure 73. *Last version of the circuit: all electronic components are inserted in a DSPic 3cm*1 cm.*

5.2.2 Transmission System

To implement a wearable and comfortable instrumented glove that can provide a continuous stream of data for several hours during ordinary everyday life, it is mandatory to have a wireless connection between the sensors of the glove and a receiver apparatus that is located in the close proximity or in the same room of the person who wear the glove.

The wireless system was required to assure at least 24 hours of battery autonomy. Therefore, short-range and low power consumption transmission system must be considered in the design of the wireless connection.

Next table shows the main commercial products that are available for the deployment of a Wireless Personal Area Network, which means short range (till about 10 meters) and low consumption ad-hoc wireless network in the Industrial Scientific Medical (ISM) band for data transmission [35][36]. In the same Table I, we have also included a new air interface that is currently proposed as a solution for Wireless Body Area Networks (WBANs) and it is not commercially available. This air interface is based on the combination of Frequency Modulation Ultra WideBand (FM-UWB) at the physical layer and IEEE 802.15.4 at the medium access control layer [37].

In the following, we derive the main requirements (data rates and energy consumption) that will drive the choice of the air interface for the wireless connection and also the network configuration and topology that are more appropriate for the specific application.

First of all, let us recall some of the main characteristics of the prototype of glove that will be implemented:

- The glove is monitored by using a minimum of 19 sensors.
- Because of the natural constraints on the movement of the fingers, a number of N_1=5 sensors per glove (large range sensors) can provide a maximum angle measurement of $\alpha_1=120^0$, while a number of N_2=14 sensors per glove (small range sensors) can provide a maximum angle measurement of $\alpha_2=90^0$. Furthermore, the maximum rate of movement of a hand (from opening to closure) is R_{max}=6 Hz.
- The measure of the angle of each sensor must be converted to digital format with a maximum quantization error which we imposed of at most $\alpha_R=1^0$.

I optimized the design of the wireless system separately for the large range and small range sensors.

Taking into account the requirements on the quantization error, the analog signal provided by the large range sensors must be converted to a digital data expressed with n_1 bits, while the analog signal provided by the small range sensors must be converted to a digital data expressed with n_2 bits, where:

$$n_1 = \left\lceil \log_2 \frac{\alpha_1}{\alpha_R} \right\rceil = 7, \qquad n_2 = \left\lceil \log_2 \frac{\alpha_2}{\alpha_R} \right\rceil = 7 \qquad \textbf{Eq 16}$$

The sampling rate R_1 of the data provided by each large range sensor and the sampling rate R_2 of the data provided by each small range sensor, can be computed on the basis of the maximum rate of movement of a hand:

$$R_1 = \frac{\alpha_1}{\alpha_R} R_{\max} = 720 \text{ Hz}, \qquad R_2 = \frac{\alpha_2}{\alpha_R} R_{\max} = 540 \text{ Hz} \qquad \textbf{Eq 17}$$

and, hence, the data rate B_1 provided by each large range sensor and the data rate B_2 provided by each small range sensor, are given by:

$$B_1 = R_1 n_1 = 5{,}040 \text{ bit/s}, \qquad B_2 = R_2 n_2 = 3{,}780 \text{ b}$$

The aggregated data rate B_{tot} provided by one glove and which must be delivered to a server via wireless links was:

$$B_{tot} = B_1 N_1 + B_2 N_2 = 78{,}120 \text{ bit/s} \qquad \textbf{Eq 18}$$

It is worth noting that this data rate was computed for a single glove. To choose the proper topology of the sensor networks, we have to recall that the final objective of the prototype was to monitor simultaneously two or more gloves in the same area. The wireless network should only support the transmission from the sensors to the monitoring server (uplinks) and there was no need for data exchange between sensors. Therefore, the chosen air interface should only support a star topology. Furthermore, the allocation of the channel resources was very easy since the service request from each sensor is known a priori and was constant during the provision of the service.

wireless technology	ZigBee	Bluetooth	WiMedia	FM-UWB/802.15.4
topology	star, peer-to-peer (or mesh)	star (piconet), interconnected stars (scatternet)	peer-to-peer (or mesh)	star, peer-to-peer (or mesh)
maximum number of nodes	255	8(in a piconet)		255
maximum link data rate	250 kbps	723 kbps	480 Mbps	100 kbps
Energy consumption	very low	low	medium	very low

Taking into account the previous discussion about the requirements of the wireless network in terms of energy consumption, topology, data rate and number of nodes, we selected the ZigBee network as the most suitable choice. In fact, ZigBee can effectively satisfy the requirements on the data rate and the maximum number of nodes while assuring a very low energy consumption.

By using the information provided by the datasheet of the Chipcon CC2420/ZigBee, we can compute the power P_d dissipated by a single Tx/Rx device, that is:

$$P_d = V_o I_t = 3.6 \times 17.4 \times 10^{-3} = 0.062 \text{ W} \quad \textbf{Eq 19}$$

where I_t is the current consumption in the Tx mode and V_o is the operating voltage. Assuming the utilisation of a battery PP3 (9V) battery with a capacity C_b of 500 mAh (equivalent to 16200 J) and a constant discharge, the maximum duration T_l of the battery charge is:

$$T_l = C_b / P_d = 16200 / 0.062 = 72 \text{h} \quad \textbf{Eq 20}$$

Therefore, assuming a continuous monitoring, the expected battery lifetime is 3 days, which can be considered a suitable value for our purposes.

5.3 Virtual Glove

I experienced great advantages from the utilization of our 3D virtual model of the hand. During the pre-processing data phase, the model has been utilized as an helpful tool to verify the measurement repeatability. During the real-time visualization phase, the model allowed the hand visualization from different point of views, a continuous monitoring of the coherence in data stream, a rapid re-calibration if necessary. During the post-processing data phase, thanks to the model, it was possible to replay all the finger's movements in slow / rapid / frame-by-frame motion, it was possible to isolate only one finger at time, removing the others from the view, in order to focus the operator's attention only into some important details.

5.3.1 Virtual Model

The basic model of the virtual hand was realized starting from *Blender*, which is an open source multiplatform software for 3D graphical applications. It has a robust feature set and has the interesting capabilities of texturing, skinning, animating, rendering. The 3D scene for the hand model was built by a mesh i.e. a point set that compose a spotted matrix. The pointed mesh represents the esoskeleton of the hand, so all the movements are performed through a mesh careful disposition.

The mesh can be visualized as an envelope covering the underlying structure made by several parts (bones) inter connected one each other, exactly in a similar way of a human skeleton. Every bone has got a pivot around which it can spatially rotate. The skeleton repositioning corresponds then to rotate every single junction, replacing all the mesh vertexes.

Every bone was described by two matrixes: a local one (local transform) and a combined one (combined transform). The local matrix describes translations and rotations with respect to its pivot. Obviously the bones are connected one to each other, so translation and rotation of a bone influences all the others in a cascading way. It means that for every junction movement the combined matrix of all the junctions is recomputed in a recursive way:

$$C_i = L_i \cdot C_{i-1}$$

The combined matrix of the i-th junction is computed multiplying its local matrix by the combined matrix of the "father junction".

Differing from previously reported simplified kinematics model of human hand [31] and from some graphical results [34], we considered all finger joint's degree of freedom, including flex-extension and addu-abduction movements, obtained graphical results with a very good likeness with a real human hand. Just for the addu-abduction movements, we adopted the *DirectX*, i.e. a collection of application program interfaces for handling tasks related to multimedia. The DirectX software development kit (SDK) consists of runtime libraries in redistributable binary form and it works with a format called "x" just compatible with Blender output.

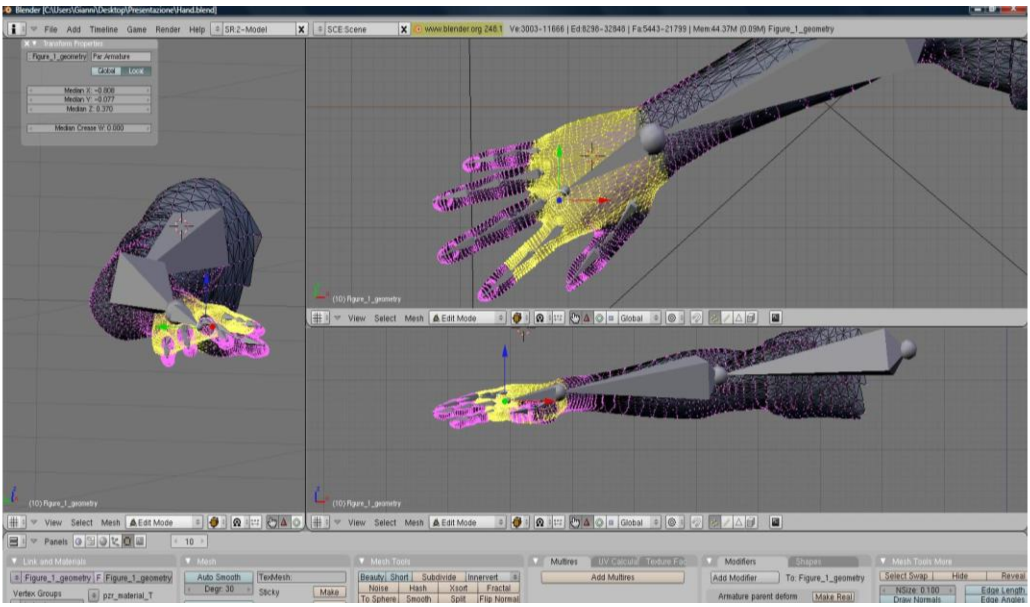

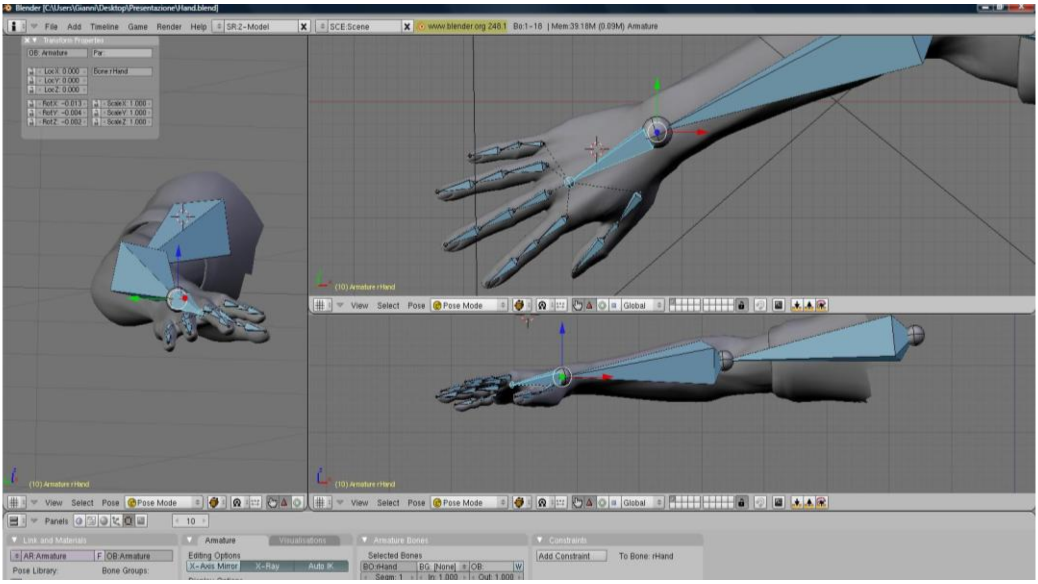

Figure 74

The virtual glove is controlled by C++ language routines. The calibration process is very simple because it is sufficient to define the minimum values (flat palm finger) and the maximum values (closed fist) of all the sensors, then recurring to the intermediate values previously recorded during the characterization procedure.

Finally, the Graphic User Interface (GUI) was realized with Windows Application Program Interfaces (API) and it is programmed by C++ language.

Obviously not all movements are allowed. The antagonization between insertion extensor / flexor tendons produces limited range of motions for each joint of each finger that, with a simplified schematization useful for our purposes, can be summarized as: 0°-120° for proximal inter-phalangeal (PIP) and 0°-90° for both metacarpo-phalangeal (MPC) and distal-interphalangeal (DIP) joints, being hyper-extension movements here neglected. In the same manner for abduction / adduction movements a motion range of 0°-25° was considered. This is schematized in Figure 75.

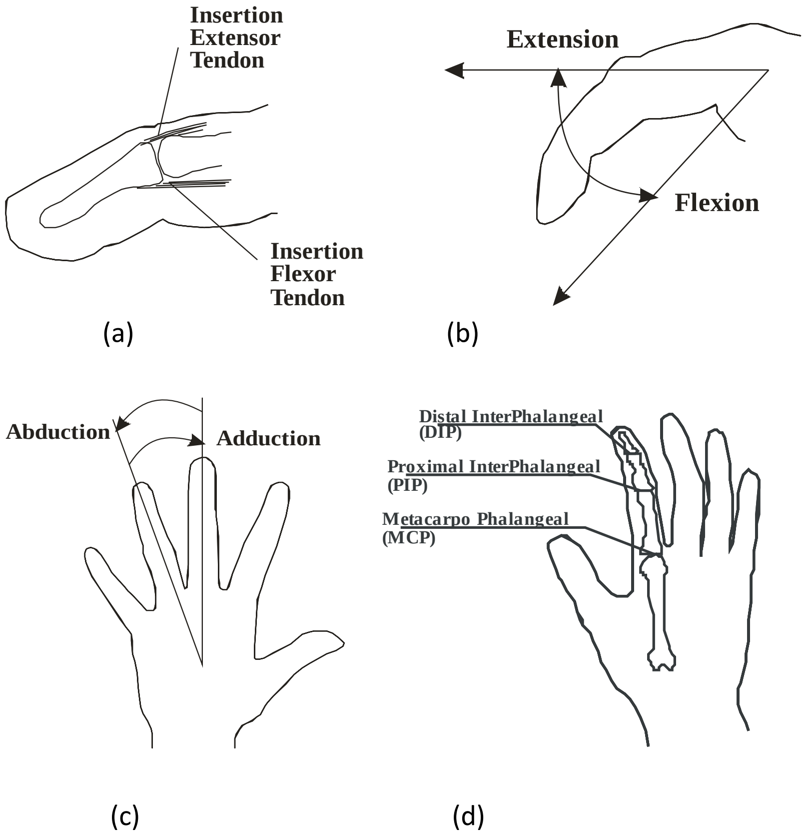

Figure 75. *Summary of allowed fingers movements: 0°-120° for proximal inter-phalangeal (PIP) and 0°-90° for both metacarpo-phalangeal (MPC) and distal-interphalangeal (DIP) joints*

The program interface includes several controls, such as a recorder option so to recall the data stream upon request, zoom in/out, play/pause, save/open options. Then it is reported an error message if senseless measured input data are received and the single wrong acquisition value was changed according to an interpolation algorithm between the previous and the following measured data.

5.3.2 Graphical Interface I

Acquired, conditioned and wireless transmitted data can finally be recorded for a real-time and/or for a post process implementation of virtual reality. To this aim we developed a computer graphic scenario which accurately replicates every DOFs in finger movements. As an example Figure 76 represents index finger closing gesture. The graphical part was based on Blender which is an open source, cross platform suite of tools for 3D creation. A pointed mesh represents the hand exoskeleton and all the movements are performed through a mesh accurate disposition. The obtained graphical result shows a very good likeness with a real human hand. Finger movements were performed via C++ software language and the program interface presents standard control buttons: save/open, play/pause, zoom in/out. Error or warning messages occur in the case of senseless received data.

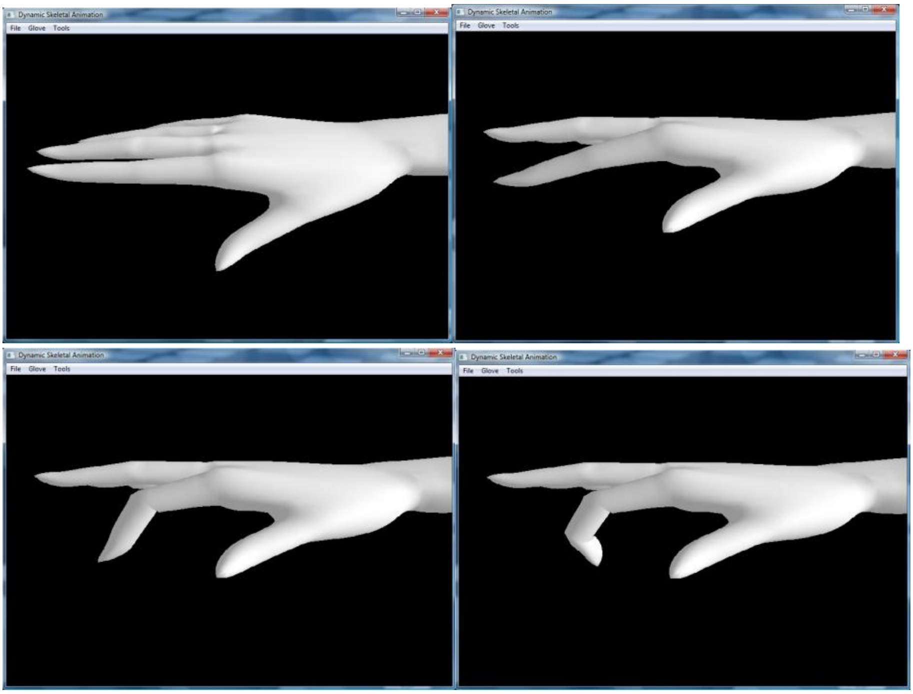

Figure 76. *First graphical interface: a simple hand without controls*

5.3.3 Graphical Interface II

The second evolution shows an incredible virtual model comparable with the human hand.

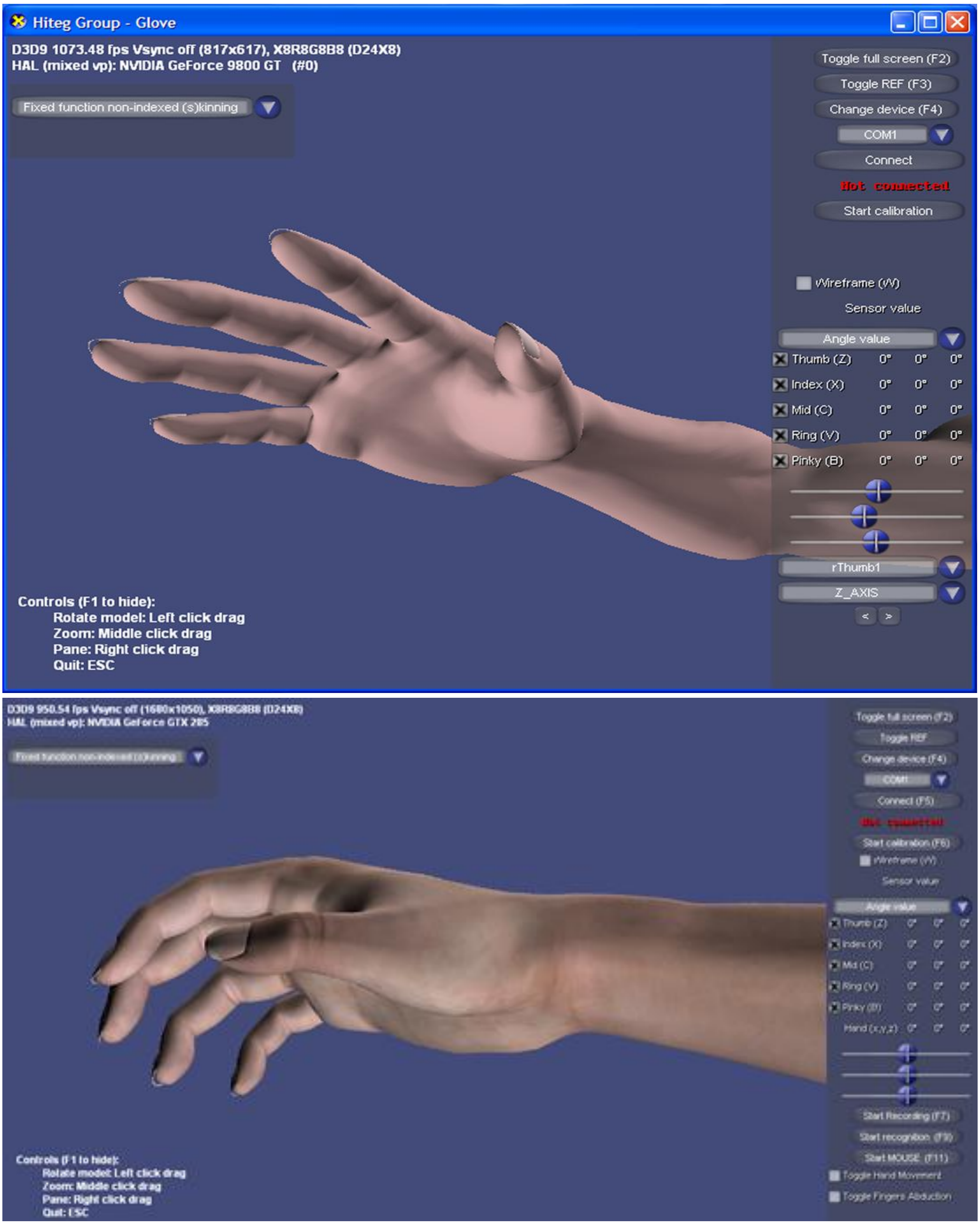

Figure 77. *Last Graphical interface: an incredible real effect is reached. On the right, there is a very complete list of controls*

In the right part of the panel, there is a vertical menu. This lets customize quickly several optional possibilities and controls:

- Full monitor (F2)
- Hardware acceleration (F3)
- Serial port (combo box)
- Change device (F4)
- Connect/disconnect (F5)
- Calibration start (F6)
- Wireframe drawing(W)
- Thumb settings
- Index settings
- Middle settings
- Ring settings
- Little ring settings
- Start Recording (F7)
- Start Recognition (F9)
- Start Mouse mode (F11)
- Start Wrist rotation;

5.4 Applications

Hiteg instrumental glove including virtual reality represents a lot of opportunity for several significant fields: social, as sign language recognition and as alternative support to actual general purpose pc input devices; medical, for functional analysis, for rehabilitation follow up on patients with damaged upper/lower limbs and for medical staff training; working, for staff training in dangerous conditions or gesture recognition; sport, in order to recording movement and posture monitoring during activity or effect of external parameters evaluation on physical performances; entertainment, as games, multimedia or music.

To date, I have tested the glove with several interesting aspects:

- Hand movements recognition;
- Wireless totally-adaptable Mouse;
- Wireless totally-adaptable Keyboard;
- Data Recording;
- Surgical rehabilitation and training
- Games Support.

5.4.1 Movements Recognition

The presented menu shows the direct possibility to select "Start Recognition" (F9). Compared to several very complex solutions, I tried to understand a numerical sequence of values. In particular, I selected the representation of 0 to 9 numbers with right hand alone.

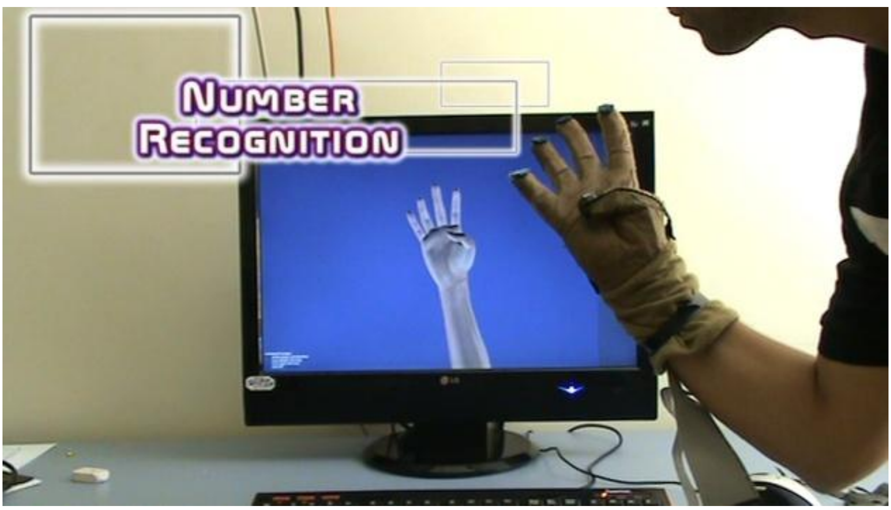

In general, the wrist rotation is utilizable in order to obtain another free degree of freedom. When the software recognize a symbol, it is able to reproduce a corresponding sound (number or word) and to show the associated writing.

The final aim is to realize a complete language totally obtained thanks to the sensors mounted on the glove.

5.4.2 Wireless totally-adaptable Mouse

One of the more suggestive applications is a wireless mouse. A specific software in order to obtain a driver for the mouse is implemented. A bending of PIP index joint is the left button of the mouse. The right button is obtained with a PIP middle joint bending. The shifting is related to the accelerometer mounted on the wrist.

Velocity and acceleration are totally adaptable to own demands.

5.4.3 Wireless totally-adaptable Keyboard

In the daily use of a personal computer there are some commands combinations of the keyboard that is very useful in order to improve the work. So I thought to establish a specific procedure for several utilities.

For example, ALT-TAB combination (switch between several opened applications) is obtained with thumb and little ring unbending and a rotation of the wrist.

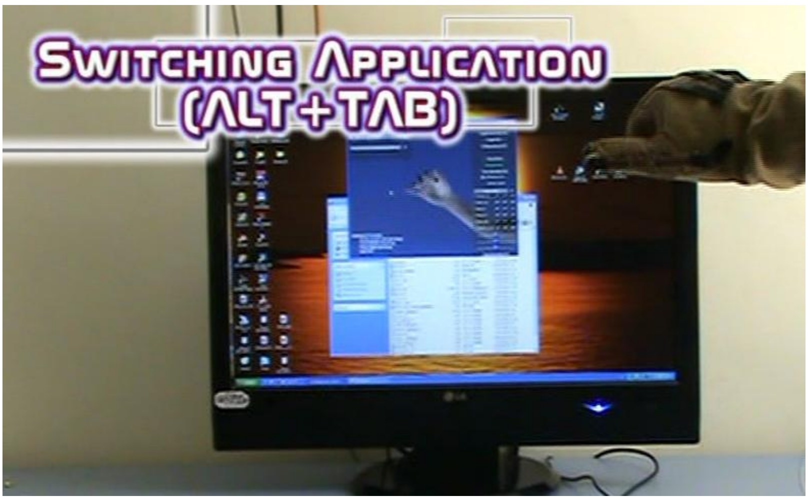

Moreover a graphical interface shows a virtual keyboard in the monitor. Every command is so selectable pushing with the PIP index bending. In the next Figure there is the simple visualized keyboard.

5.4.4 Surgical Rehabilitation

The first glove application is the surgical rehabilitations in patients with hand problems. The glove has the possibility to monitoring every little improvement in the movements until 1°. There is the possibility to safe all data in an appropriate file. The glove guarantee a continue monitoring of the activity and it is light and comfortable to wear for the patients.

Data can be used in an off line modality to reproduce in a second moment all the patient movements. A complete rehabilitation process can be observed and filed.

5.4.5 Videogames.

With the advancements in video game systems, personalized operation is becoming more desirable. Original video games allowed any user to operate the game at different skill levels which were selected at the start of the game. Each user, however, was treated the same during operation of the game. It would be desirable to allow each user to have a personality which interacts with the game, such that video game have the ability to “recognize” a user and adjust game operation accordingly.

Video game systems typically include one or more controllers for controlling the operation of a video game. These controllers are connected to a central processing unit through a communication bus cable. The video game user, therefore, is restricted in possible operating locations. That is, a user cannot play a game from a relatively remote location.

Wii and other consoles are able to reproduce human hand movements with accelerometers and gyroscopic sensors. The glove extends this possibility in order to obtain a total control of own experience. There aren’t push buttons e the hand is free to move in all directions.

The obtained sensation is fantastic and the senses immersion is total: to drive a motorcycle or to pilot an helicopter or to kill terrorists becomes unique experience.

5.4.6 Surgical Training

Learning and assessment are focused in the clinical setting. Development is incremental and requires the set standards to be reached in the domains of specialty based knowledge, clinical judgment, technical and operative skills, and professional skills and behavior to ensure progression. Trainees' progress is measured by an integrated framework of work-place assessments, annual reviews of competence progression, assigned educational supervisors' structured placement report and examinations.

Hiteg Glove offers to young doctors or surgeons a real possibility to obtain an excellent education for the future medical steps. In this case, Hiteg Software takes charge of show real-time approaches, methods, techniques with great optical performances.

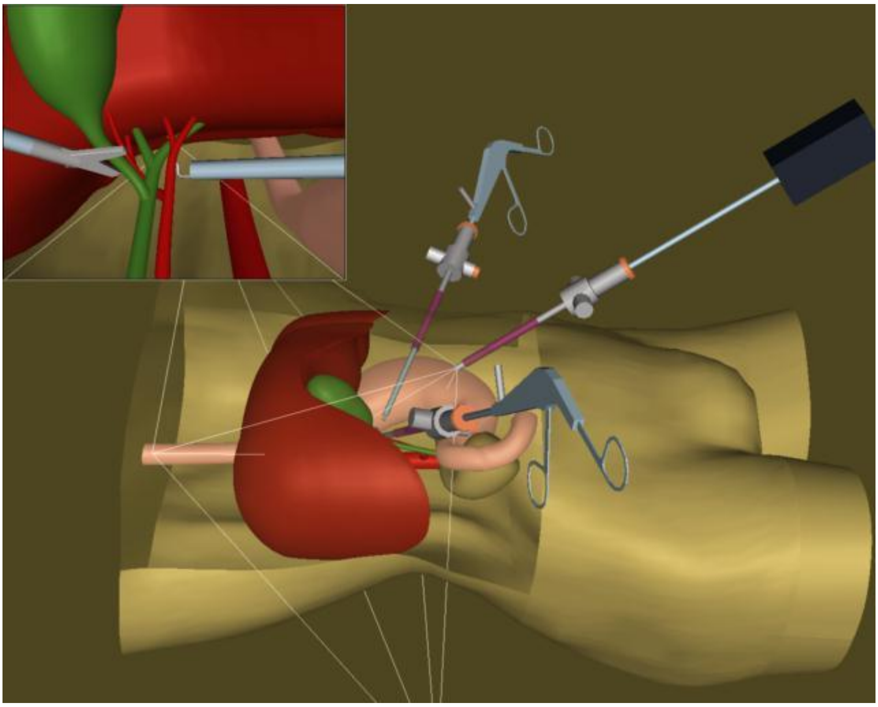

5.4.7 Universal Platform: Wireless Control

Thanks to the supported wireless technology, Hiteg Glove can be utilized in order to realize an universal platform. This platform allows to control several actuators and in the other side is totally customizable based on the subject purposes.

We could turn on the light, open a door, change television or pull the blind up simply using a light and wearable glove. The project is reported in the next figure; I initially think that the system is perfectly customizable for a person with motor disabilities. The user transmits the command to the host with the glove thanks to the bending of a specific joint or in combination with a vocal command. An RS232/Wireless-Lan adapter is used for the communication between the host and the PIC (Programmable Interface Control). The PIC is then programmable in order to actuate the desiderated control, in this case a simple lamp but in general everything that you want.

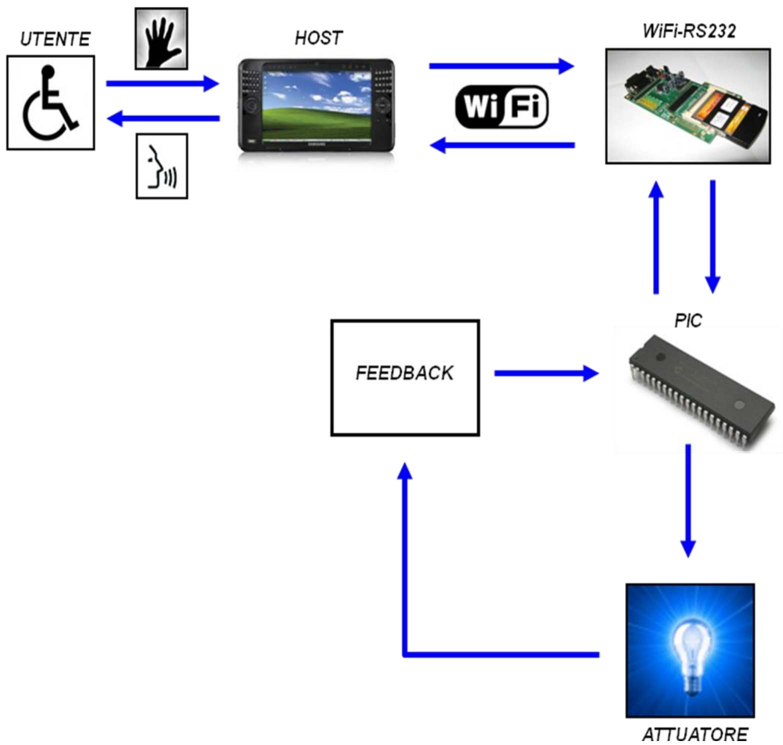

5.4.8 Training Simulation

Operator Training Simulators (OTS) train operators on fundamental plant operations and improve their ability to optimize plant performance with the same simulation tool. Its accurate and realistic simulations allow engineers to stretch the limits of a plant's capability and identify operational and physical constraints in a safe, theoretical environment. It facilitates a thorough, scientific investigation of problems and opportunities for intelligent and fully-supportable decision making. And the same advanced simulation accuracy that makes it the world's best optimization test bed also makes it the world's best training simulator! OTS mirrors the exact look and feel of a plant, captures operator best practices, and enables operators to exercise best practices.

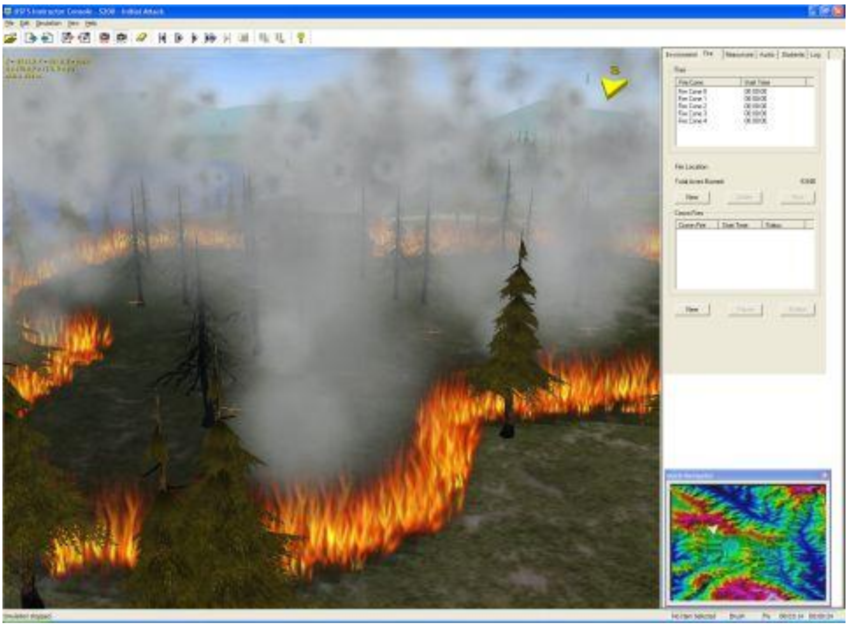

5.4.9 Total Body

Now the glove, tomorrow all the body. The acquired experience on the glove inspires the possibility to extend the sensor architecture to all human body and to modify the virtual software in order to have a real time visual of all the human body. In the sense, I and my group tried to draw a first prototype of the virtual body, reported in the next figure.

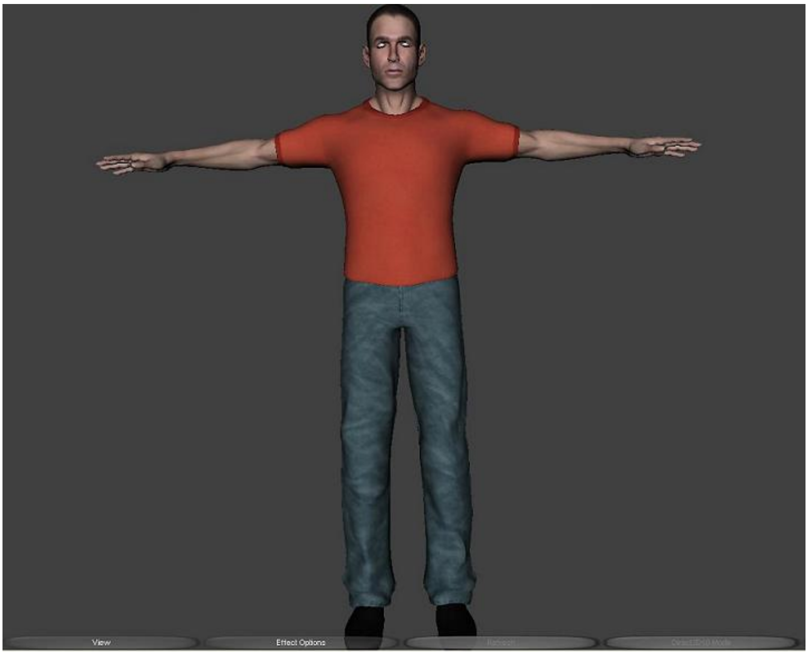
View
Effect Options

Conclusions

This work is focused on the realization of piezoresistive sensor based on PEDOT:PSS. These devices change their electrical resistance when they are bent. The substrate is totally flexible, low cost, customizable, based on Poly (Trimellitic-anhydride-chloride copolymerized with 4,4-methylenedianiline) in *N*-methylpyrrolidone.

An ad-hoc measurement was realized in order to obtain an electrical resistance sensor measure. The idea is to replicate as really as possible the human finger flexion/extension movements. The set-up consists of three hinges controlled by three step-by-step motor to measure an array up to three different sensors. All the system is remotely controlled by Labview NI Interface and the resistive response of the sensor is read by a 5.5 digits 34405A Agilent digital multimeter.

Among several possibilities to adopt these sensor, my first aim is a glove-based system realization. An instrumented-glove (called *Hiteg Glove*) is the ensemble of mechanical to electrical transducers, a support (usually Lycra based), conditioning electronics plus power supply, transmission system, all useful to measure the 23 degree of freedom [3] of finger joint movements. Thanks to their lightness, cheapness and the fact that I experienced a novel way of their application which, the bend sensors was utilized ad transducers. Each sensor was mounted on the glove in correspondence of one human hand joint so to permit the flexion/extension movements registering. Moreover ad-hoc projected sensors were utilized for the abduction/adduction movements.

The last step of this works provides to realize a 3D Virtual Model of the glove. The basic model of the virtual hand was realized starting from *Blender*, which is an open source multiplatform software for 3D graphical applications. It has a robust feature set and has the interesting capabilities of texturing, skinning, animating, rendering. Virtual Hand permits a real-time replay of the hand movements obtained with the glove.

The instrumental glove including virtual reality represents a lot of opportunity for several significant fields: social, as sign language recognition and as alternative support to actual general purpose pc input devices; medical, for functional analysis, for rehabilitation follow up on patients with damaged upper/lower limbs and for medical staff training; working, for staff training in dangerous conditions or gesture recognition; sport, in order to recording movement and posture monitoring during activity or effect of external parameters evaluation on physical performances; entertainment, as games, multimedia or music.

References

[1] H. Shirakawa, E.J. Louis, A.G. MacDiarmid, C.K. Chiang, A.J. Heeger, Synthesis of electrically conducting organic polymers: halogen derivatives of polyacetylene (CH)*x*, J. Chem. Soc. Chem. Commun. (1977) 578–580.

[2] T. Skotheim, Handbook of Conducting Polymers, Marcel Dekker, New York, 1986.

[3] D.J. Sturman "Whole-Hand Input" Ph.D. dissertation, Massachusetts Institute of Technology, Cambridge, 1992. Available: http://xenia.media.mit.edu/~djs/thesis.ftp.html

[4] G. Placidi "A smart virtual glove for telerehabilitation" Computers in Biology and Medicine 37 (2007) 1100-1107

[5] L. DiPietro, A.M. Sabatini, P. Dario "Evaluation of an instrumented glove for hand-movement acquisition" Journal of Rehabilitation Research and Development, Vol.40, No. 2, March/April 2003, pp. 179-190

[6] N. Karlsson, B. Karlsson, P. Wide "A glove equipped with finger flexion sensors as a command generator used in fuzzy control system" IEEE Trans. Instrum. Meas., vol.47, no. 5, pp. 1330-1334, Oct. 1998

[7] N.W. Williams, J.M. Penrose, C.M. Caddy, E. Barnes, D.R. Hose, P. Harley "A goniometric glove for clinical hand assessment" *Journal of Hand Surgery* (British and European Volume, 2000) 25B: 200-207

[8] L.K Simone, E. Elovic, U. Kalambur, D. Kamper "A low cost method to measure finger flexion in individuals with reduced hand and finger range of motion" Proceedings of the 26th Annual International Conference of the IEEE EMBS, San Francisco, CA, USA, September 2004, pp. 4791-4794

[9] E. Becker, R. Parashkov, G. Ginev, D. Schneider, S. Hartmann, F. Brunetti, T. Dobbertin, D. Metzdorf, T. Riedl, H.-H. Johannes,W. Kowalsky, All-organic thin-film transistors patterned by means of selective electropolymerization, Appl. Phys. Lett. 83 (2003) 4044–4046.

[10] W. Jeffrey Hurst, Electronic Noses & Sensor Array Based Systems: Design & Applications, CRC Press, 1999, ISBN 1566767806.

[11] G.A. Sotzing, S.M. Briglin, R.H. Grubbs, N.S. Lewis, Preparation and properties of vapor detector arrays formed from poly(3,4-ethylenedioxy) thiophenepoly(styrenesulfonate)/insulating polymer composites, Anal. Chem. 72 (2000)

[12] U. Lang, P. Rust, J. Dual, Towards fully polymeric MEMS: fabrication and testing of PEDOT/PSS strain gauges, Microelectron. Eng. 85 (2008) 1050– 1053.

[13] H.S. Nalwa (Ed.), Handbook of Organic Conductive Molecules and Polymers, Wiley, New York, 1997.

[14] W.A. Daoud, J.H. Xin, Regioregular poly(3-alkylthiophenes): synthesis, characterization and application in conductive fabrics, J. Appl. Polym. Sci. 93 (2004) 2131–2135.

[15] G.Latessa et at. Piezoresistive behaviour of flexible PEDOT:PSS based sensors, Sens&Act B 139 (2009) 304-309

[16] "Sensori e Rivelatori", A. Nannini, P. Bruschi

[17] PhD Thesis, "Strain sensing applications with carbon nanotubes based devices", Regoliosi P.

[18] A. Reale, P. Regoliosi, L.Tocca, P.Lugli, S.Orlanducci, M.L.Terranova and G.Bruni, "Evaluation of the Gauge Factor for membranes assembled by single-walled Carbon nanotubes", Appl. Phys. Lett. Volume 85 No. 14 pp. 2812-2814 (2004).

[19] Papakostas et at, "Influence of substrate on the gauge factor of polymer thick-film resistors" J. Phys. D: Appl. Phys. **33** (2000) L73–L75

[20] Dipietro L., Sabatini A., "A Survey of Glove-Based Systems and Their Applications" IEEE transactions on Systems, man and cybernetics, part C: Applications and reviews, vol 38,num4,2008

[21] R. Degeorges, J. Parasie, D. Mitton, N. Imbert, J.-N. Goubier, F. Lavaste "Three-dimensional rotations of human three-joint fingers: an optoelectronic measurement. Preliminary results" *Surg. Radiol. Anat.* (2005) 27: 43-50

[22] G. Placidi "A smart virtual glove for telerehabilitation" Computers in Biology and Medicine 37 (2007) 1100-1107

[23] L. DiPietro, A.M. Sabatini, P. Dario "Evaluation o fan instrumented glove for hand-movement acquisition" Journal of Rehabilitation Research and Development, Vol.40, No. 2, March/April 2003, pp. 179-190

[24] N.W. Williams, J.M. Penrose, C.M. Caddy, E. Barnes, D.R. Hose, P. Harley "A goniometric glove for clinical hand assessment" *Journal of Hand Surgery* (British and European Volume, 2000) 25B: 200-207

[25] L.K Simone, E. Elovic, U. Kalambur, D. Kamper "A low cost method to measure finger flexion in individuals with reduced hand and finger range of motion" Proceedings of the 26th Annual International Conference of the IEEE EMBS, San Francisco, CA, USA, September 2004, pp. 4791-4794

[26] P. Coiffet and G. C. Burdea, *Virtual Reality Technology*. NewYork: Wiley, 2003.

[27] D. J. Sturman and D. Zeltzer, "A survey of glove-based input," *IEEE Comput. Graph. Appl.*, vol. 14, no. 1, pp. 30–39, Jan. 1994.

[28] J. J. LaViola, "A survey of hand posture and gesture recognition techniques and technology," Brown Univ., Providence, RI, Tech. Rep. CS-99-11, Jun. 1999.

[29] H. Eglowstein, "Reach out and touch your data," *Byte*, vol. 15, no. 7, pp. 283–290, Jul. 1990

[30] R.Gentner, J.Classen, "Development and evaluation of a low-cost sensor glove for assessment of human finger movements in neurophysiological settings", Journal of Neuroscience Methods 178 (2009) 138–147

[31] Noamann et at, "Design and Implementation DHM Glove using variable resistors sensors", J.Artif.Intell.1 (1): 44-52, 2008

[32] Wise et at., "Evaluation of a fiber optic glove for semi-automated goniometric measurements" Journal of Rehabilitation Researchand Development Vol . 27 No. 4, 1990 Pages 411-424

[33] Spear, "Virtual Reality: Patent Review", World Patent Information 24 (2002) 103–109

[34] C.S. Fahn, H. Sun "Development of a Sensory Data Glove Using Neural-Network-Based Calibration" *ICAT 2000*

[35] IEEE Std. 802.15.4-2003, Standard for Telecommunications and Information Exchange Between Systems—Local Area Metropolitan Area Networks—Specific Requirements — Wireless Medium Access Control (MAC) and Physical Layer (PHY) Specifications for Low Rate Wireless Personal Area Networks (WPAN).

[36] IEEE Std. 802.15.3-2003, Standard for Telecommunications and Information Exchange Between Systems—Local Area Metropolitan Area Networks—Specific Requirements — Wireless Medium Access Control (MAC) and Physical Layer (PHY) Specifications for High Rate Wireless Personal Area Networks (WPAN).

[37] John F.M. Gerrits, Michiel H.L. Kouwenhoven, Paul R. van der Meer, John R. Farserotu, John R. Long, Principles and Limitations of Ultra Wideband FM Communications Systems, EURASIP *Journal on Applied Signal Processing*, Special Issue on UWB-State of the Art, Volume 2005, Number 3, pp. 382 - 396, March 2005.

List of publications

August 2008
Sensor and actuator B: chemical
"Piezoresistive Behavior of flexible PEDOT:PSS based sensors"
G.Latessa, F.Brunetti, G.Saggio, A.Reale, A. Di Carlo

May 09
Wireless Vitae 09: wireless communication and network
Aalborg (Denmark)
"Long term measurements of human movements for health care and rehabilitation purposes"
G.Saggio, G. Latessa, F. De Santis, M. De Sanctis, E. Cianca, F. Giannini

May 09
Wireless Vitae 09: wireless communication and network
Aalborg (Denmark)
"Characterization of piezoresistive sensors for goniometric glove in hand prostheses"
L. Giovannini, G. Orengo, G. Latessa, G.Saggio

June 2009

IEEE Intern WoWMoM Workshop on Interdisciplinary Res on E-Health Services& Systems

Kos Island (Greece)

"A NOVEL MEASUREMENT SET-UP FOR THE CHARACTERIZATION OF BEND SENSORS APPLIED IN EVALUATION OF CONTROL MOTION DISEASES"

G.Latessa, G.Saggio, L.Bianchi, M.Marciani, F.Giannini

June 2009

IEEE Intern WoWMoM Workshop on Interdisciplinary Res on E-Health Services& Systems

Kos Island (Greece)

"MECHANICAL MODELING OF BEND SENSORS EXPLOITED TO MEASURE HUMAN JOINT MOVEMENTS

G.Latessa, G.Saggio, S.Bocchetti, P.Bisegna

June 2009

IEEE Intern WoWMoM Workshop on Interdisciplinary Res on E-Health Services& Systems

Kos Island (Greece)

"VIRTUAL REALITY IMPLEMENTATION AS A USEFUL SOFTWARE TOOL FOR E-HEALTH"

G.Latessa, G.Saggio, F. De Santis, L. Bianchi, F. Giannini, M.G.Marciani

Conferences

June 2007 - Eindhoven (Holland)

ICOE07: INTERNATIONAL CONFERENCE ON ORGANIC ELECTRONICS

"PIEZORESISTIVE BEHAVIOUR OF POLYMER-CARBON NANOTUBES COMPOSITES AND THEIR INTEGRATION IN ACTIVE SENSORS BASED ON OTFTS"

September 2007 - Ventotene (Italy)

ISOPHOS07: INTERNATIONAL SCHOOL ON ORGANIC PHOTOVOLTAICS

October 2007 - Varenne, Como (Italy)

ECOER07: European Conference on Organic Electronics and Related Phenomena

"PIEZORESISTIVE BEHAVIOUR OF POLYMER-CARBON NANOTUBES COMPOSITES AND THEIR INTEGRATION IN ACTIVE SENSORS BASED ON OTFTS"

April 2009 - Santa Margherita Ligure (GE)
ISSBB09: Italian Society for Space Biomedicine and Biotechnology
"*SENSOR'S* DESIGN AND CHARACTERIZATION FOR BIOMEDICAL APPLICATIONS"

Submitted Papers

January 2010
"IMPROVING PEFORMANCES OF DATA GLOVES BASED IN BEND SENSORS"
Journal of Neuroscience Methods

January 2010
"DESIGN CONSIDERATION AND MECHANICAL CHARACTERIZATION OF WEARABLE SENSORS FOR MEASURING RELATIVE FINGERE MOVEMENTS"
Sensor & Actuator A

Acknowledgments / Ringraziamenti

I 3 anni di Dottorato di Ricerca rimarranno per sempre impressi nella mia mente e nel mio cuore. Con essi, poche ma fondamentali persone che non dimenticherò mai in tutta la mia vita e delle quali manterrò un nitido e piacevole ricordo.

In primis, e non potrebbe essere così perché altrimenti (diciamoci la verità) mi picchia, un sentito "grazie" va a mio fratello Francesco, semplicemente perché senza di lui non sarebbe la stessa cosa. Da più di un anno oramai viviamo sotto lo stesso tetto e, esclusa qualche lussazione, qualche cicatrice e un po' di costole incrinate, direi che ce la stiamo cavando alla grande.

Pur se adesso ci hanno divisi, non posso poi che ringraziare mio cuginetto (anche se sta facendo vecchio, rimane sempre il mio cuginetto) Mario: l'ho visto nascere e crescere, siamo stati a contatto per ore e ore, giorni e giorni, eppure, e non mi spiego perché, è diventato un banale romanista.

Un grazie speciale al mitico Andrea Reale e a Francesca Brunetti, persone vere e leali da cui ho imparato molto, moltissimo e non mi riferisco al solo ambito lavorativo; al leader maximo, l'uomo della Trinità, il Mosè del 2000, alias Aldo Di Carlo, a cui devo più di un grazie (speriamo …).

C'è poi un miscuglio di gente, amici più che colleghi, gay più che etero: l'uomo dalle mani fatate, l'idolo delle adolescenti, il mio trapanatore preferito: Stefano Dear! il genio (poco) e sregolatezza (tanta), l'uomo-virtuale, colui che ha contribuito a rompere la quotidiana tranquillità del Hiteg Lab: Carlo Alberto! il trio delle meraviglie, il Ma-Gi-Ca dei giorni nostri, i 3 in grado di fare tutto e il

contrario di tutto, gli inscindibili: Stefano, Riccardo, Eleonora! Il solitario, il bello e tenebroso, l'uomo dall' ex sinistro fatato: Stefano Bellocchio! Il rimorchiatore (di casini) e il rimorchiatore (di donne): (senza specificare chi/cosa) Luigi Salamandra e Peppe Romano! L'uomo passato in pochi giorni dall'essere grande trombeur de femme a neo-paparino (e mo?): Enrico! La ragazza che è arrivata in lab grassa e brutta e ne è uscita sorridente (!) e carina: Angela!

Qui un rullo di tamburi …. Trtrtrtrtrtr … la persona che nemmeno sa quanto è stata importante e quanto ancora è importante per il mio equilibrio psichico, con la sua dolcezza, la sua serenità e i suoi modi gentili (che cozzano con la mia rudezza)…non ve lo dico! Scherzo… un grosso bacio Vale!

Infine, i miei amici universitari, coloro che mi hanno sopportato non solo di giorno, ma spesso anche di sera, vicino ad una coca-cola (ehm) o ad una birra, all'uni così come a calcetto (e qui ne ho date di lezioni): Enzo, Danilo (gay), Mimmo, Gigi, Danilo (etero)..ogni giorno che passa mi chiedo sempre: "ma cumm c sim accucchiat"!

In chiusura, grazie di tutte le emozioni che mi dai:

Vola Mio Magico Napoli

Peppe